SAE Aerospace
An SAE International Group

AEROSPACE INFORMATION REPORT

SAE AIR5687

Issued 2011-09

Inlet / Engine Compatibility – From Model to Full Scale Development

RATIONALE

The intent of this document is to capture the experience and lessons learned since approximately 1967 necessary to ensure that model-scale inlet total-pressure recovery and distortion data faithfully represent the corresponding full-scale inlet recovery and distortion characteristics.

FOREWORD

The SAE S-16 Committee, Turbine Engine Inlet Flow Distortion, is pleased to dedicate this document to Mr. Gregg Turley. Gregg was a member of the Committee from 2001 until his untimely death in 2006. Gregg will be remembered for his quiet, understated approach and bringing his knowledge, perceptions, and range of experiences to tasks at hand including this document. This document is a collection of lessons learned since the late 1960s by practitioners of this discipline including those of Gregg while working at Northrop Grumman Corporation. These will be a resource to both new and experienced inlet/engine compatibility practitioners for decades to come.

This document has been cleared for public release per Case Number 88ABW-2010-2038.

The SAE S-16 Committee welcomes input from both industry and government organizations relative to the contents of this document. Please feel free to address any comments on this document to the Chairman, SAE S-16 Committee.

TABLE OF CONTENTS

1. SCOPE 4
1.1 Purpose 4
1.2 Application 4

2. REFERENCES 4
2.1 Applicable Documents 4
2.1.1 SAE Publications 4
2.2 Applicable References 4
2.3 Additional References 6
2.4 Symbols and Abbreviations 8

3. INTRODUCTION 11

4. BACKGOUND 12
4.1 Evolution of Inlet Development, Test, and Evaluation Practices Prior to the F-111 13
4.2 The F-111 Inlet/Engine Compatibility Experience 16

5. CASE STUDIES 19
5.1 Case Studies Offering Correlations 19
5.1.1 RA-5C Case Study 19
5.1.2 YF-12 Case Study 24
5.1.3 F-15 Case Study 28

TO PLACE A DOCUMENT ORDER: Tel: 877-606-7323 (inside USA and Canada)
Tel: +1 724-776-4970 (outside USA)
Fax: 724-776-0790
Email: CustomerService@sae.org
SAE WEB ADDRESS: http://www.sae.org

SAE values your input. To provide feedback on this Technical Report, please visit
http://www.sae.org/technical/standards/AIR5687

5.1.4 B-1 Case Study 35
5.1.5 F-18E/F Case Study 45
5.1.6 F-22 Case Study 53
5.2 Case Studies Offering Key Observations 68
5.2.1 F-16 Case Study 68
5.2.2 B-2 Case Study 70

6. SIMILARITIES AND TEST TECHNIQUES 73
6.1 Geometric Similarities 73
6.1.1 Moldline and Scaling 73
6.1.2 Subscale Model 73
6.1.3 Full-Scale Wind Tunnel Hardware 75
6.2 Flow Similarities 76
6.3 CFD Simulation Techniques 77
6.4 Test and Evaluation Techniques 78
6.4.1 Wind Tunnel Test Techniques 78
6.4.2 Flight Test Techniques 86

7. LESSONS LEARNED AND RECOMMENDATIONS 92
7.1 Lessons Learned 92
7.2 Recommendations 93
7.2.1 Recommendations For Research To Correct Discrepancies Noted In Lessons Learned 93
7.2.2 Recommendations For Future Programs 93

LIST OF FIGURES

FIGURE 1 INLET INSTALLATION OF THE BELL P-59 14
FIGURE 2 P-59 INLET APERTURE AND DIVERTER 14
FIGURE 3 P-80 INLET INSTALLATION 15
FIGURE 4 F-89 INLET/DIVERTER INSTALLATION 15
FIGURE 5 F-100F INLET INSTALLATION 15
FIGURE 6 F-101 INLET CONFIGURATION WITH EXTERNAL DIVERTER AND SIDEPLATE 16
FIGURE 7 INLET SYSTEM FOR THE F-111 17
FIGURE 8 RA-5C INLET SYSTEM 20
FIGURE 9 RA-5C INLET WIND TUNNEL MODELS 21
FIGURE 10 VARIATION OF TOTAL-PRESSURE RECOVERY WITH REYNOLDS AND MACH NUMBERS, AND SCALE 22
FIGURE 11 VARIATION OF DYNAMIC CIRCUMFERENTIAL DISTORTION WITH REYNOLDS NUMBER 23
FIGURE 12 YF-12 INLET AND INSTALLATION 24
FIGURE 13 YF-12 INLET MODEL DETAILS 25
FIGURE 14 YF-12 INLET MODEL INSTRUMENTATION DETAILS 26
FIGURE 15 YF-12 PERFORMANCE AND DISTORTION, MACH 2.8 27
FIGURE 16 YF-12 PERFORMANCE AND DISTORTION, MACH 2.1 27
FIGURE 17 F-15 INLET CONFIGURATION 28
FIGURE 18 F-15 INLET TEST ARTICLES 29
FIGURE 19 EFFECT OF ENGINE PRESENCE ON PEAK DISTORTION 31
FIGURE 20 EFFECT OF ENGINE PRESENCE ON INLET PERFORMANCE PARAMETERS 32
FIGURE 21 REPRESENTATIVE EFFECT OF REYNOLDS NUMBER AT MACH 0.6, α = 4 DEG, β = 0 DEG 33
FIGURE 22 EFFECT OF FILTER FREQUENCY ON INLET DATA AT MACH 1.8, α = -2 DEG, β = 0 DEG 34
FIGURE 23 B-1 AIRCRAFT AND INLET DETAILS 36
FIGURE 24 0.1-SCALE B-1A IN AEDC TUNNEL 16S 37
FIGURE 25 0.20-SCALE B-1A INSTALLED IN AEDC TUNNEL 16S 37
FIGURE 26 FULL-SCALE B-1A IN AEDC TUNNEL 16T 38
FIGURE 27 DETAILS OF B-1A INLET WIND TUNNEL MODELS 39
FIGURE 28 EFFECT OF REYNOLDS NUMBER AND SCALE AT M = 0.85 41
FIGURE 29 EFFECT OF REYNOLDS NUMBER AND SCALE AT M = 2.0 42
FIGURE 30 COMPARISON OF FLIGHT TO WIND TUNNEL TEST 43
FIGURE 31 ENGINE EFFECTS AT M = 0 44
FIGURE 32 ENGINE EFFECTS AT M = 2.2 44

FIGURE 33 F/A-18E INLET WIND TUNNEL MODEL 404 AND FLIGHT-TEST AIRCRAFT E2 45
FIGURE 34 INLET RECOVERY AT TRANSONIC CRUISE CONDITIONS 47
FIGURE 35 INLET RECOVERY VARIATION WITH UNIT REYNOLDS NUMBER 48
FIGURE 36 PEAK CIRCUMFERENTIAL DISTORTION DURING MANEUVERS AT TRANSONIC SPEEDS 48
FIGURE 37 PEAK RADIAL DISTORTION DURING MANEUVER AT TRANSONIC SPEEDS 49
FIGURE 38 PEAK TOTAL-PRESSURE PATTERNS DURING MANEUVER AT TRANSONIC SPEEDS 49
FIGURE 39 PLANAR WAVE CONTENT AT TRANSONIC SPEEDS 50
FIGURE 40 INLET RECOVERY AT SUPERSONIC FLIGHT CONDITIONS 50
FIGURE 41 PEAK CIRCUMFERENTIAL DISTORTION AT SUPERSONIC SPEEDS 51
FIGURE 42 PEAK RADIAL DISTORTION AT SUPERSONIC SPEEDS 51
FIGURE 43 PLANAR WAVE CONTENT AT SUPERSONIC SPEEDS 52
FIGURE 44 PEAK TOTAL-PRESSURE PATTERNS AT SUPERSONIC SPEEDS 52
FIGURE 45 FULL-SCALE F-22 INLET WITH FIXED AND VARIABLE BLEED 54
FIGURE 46 SUBSCALE F-22 INLET TESTED IN THE AEDC 16-FT TRANSONIC AND SUPERSONIC WIND TUNNELS 54
FIGURE 47 WIND TUNNEL INLET RAKE GEOMETRY 56
FIGURE 48 F119-PW-100 FLIGHT TEST ENGINE-FACE RAKE 57
FIGURE 49 FLIGHT TEST INLET RAKE GEOMETRY 57
FIGURE 50 REYNOLDS NUMBER CORRECTION 59
FIGURE 51 STATISTICAL IMPACT OF SCREENING ONE SECOND VERSUS FIVE SECONDS OF DATA TO DETERMINE WORST CASE DISTORTION INTENSITY 61
FIGURE 52 WIND TUNNEL AND FLIGHT TEST CORRELATIONS AT 1-G TRIM FLIGHT, LOW ALTITUDES AND LOW-SUBSONIC FLIGHT CONDTIONS 63
FIGURE 53 WIND TUNNEL AND FLIGHT TEST CONDITIONS AT 1-G TRIM FLIGHT, MID-ALTITUDE AND HIGH-SUPERSONIC FLIGHT 65
FIGURE 54 DISTORTION SUMMARY AT LOW-SUBSONIC SPEEDS WITH NEGATIVE AND POSITIVE AOA 66
FIGURE 55 DISTORTION SUMMARY, MID-TO HIGH-SUPERSONIC, NEGATIVE AND POSITIVE AOA 66
FIGURE 56 F-16 INLET MODEL WITH SIMULATED PROBES 70
FIGURE 57 F-16 INLET BUZZ TEST DATA 70
FIGURE 58 EFFECT OF INLET BREAK ON CONSUMPTION OF FAN STABILITY PRESSURE RATIO 72
FIGURE 59 FULL-SCALE F-15 INLET WITH MODIFIED FOREBODY 75
FIGURE 60 TYPICAL INLET WIND TUNNEL MODEL 79
FIGURE 61 AIP RAKE IN MODEL 80
FIGURE 62 TYPICAL FLOW-PLUG ARRANGEMENT 81
FIGURE 63 TAPE TRANSITION DOTS 83
FIGURE 64 DISTORTION SCREENS FOR DIRECT-CONNECT ENGINE TESTING 84
FIGURE 65 INLET DISTORTION SCREEN INSTALLATION 84
FIGURE 66 DISTORTION SCREEN SWIRL PATTERN 85
FIGURE 67 TYPICAL MILITARY FIGHTER AIRCRAFT INCREMENTAL ENVELOPE EXPANSION VS. A LIMITED SURVEY FOR WIND TUNNEL COMPARISON 86
FIGURE 68 TYPICAL LOW-SPEED ENVELOPE EXPANSION APPROACH SHOWING INTEGRATION OF PROPULSION AND FLYING QUALITY MANUEVERS 89
FIGURE 69 EXAMPLE OF F-18 HARV FLIGHT TEST INSTRUMENTATION FOR INLET/ENGINE COMPATIBILITY TESTING 90

LIST OF TABLES

TABLE 1 EARLY AIRCRAFT PROGRAMS OFFERING INSIGHT INTO THE EVOLUTION OF INLET/AIRFRAME INTEGRATION TECHNOLOGY 12
TABLE 2 AIRCRAFT PROGRAMS OFFERING WIND TUNNEL TO FLIGHT CORRELATIONS OF INLET RECOVERY AND DYNAMIC TOTAL-PRESSURE DISTORTION 13
TABLE 3 F-15 TEST CONDITIONS 30
TABLE 4 TOLERANCES FOR TRIM AND MANEUVER FLIGHT CONDITIONS 88

1. SCOPE

This document reviews the state of the art for data scaling issues associated with air induction system development for turbine-engine-powered aircraft. In particular, the document addresses issues with obtaining high quality aerodynamic data when testing inlets. These data are used in performance and inlet-engine compatibility analyses. Examples of such data are: inlet recovery, inlet turbulence, and steady-state and dynamic total-pressure inlet distortion indices. Achieving full-scale inlet/engine compatibility requires a deep understanding of three areas: 1) geometric scaling fidelity (referred to here as just “scaling”), 2) impact of Reynolds number, and 3) ground and flight-test techniques (including relevant environment simulation, data acquisition, and data reduction practices). The Model-to-Full Scale Subcommittee of the S-16 Turbine Engine Inlet Flow Distortion Committee has examined archives and has obtained recollections of experts regarding air induction system development experience to produce this document.

1.1 Purpose

The primary objective of this document is to provide a consolidated record of what is known regarding the effectiveness of wind-tunnel scale-model testing in the prediction of full-scale flight characteristics such as inlet recovery, inlet turbulence, and steady-state and dynamic total-pressure inlet distortion. Discussion is offered regarding these findings in light of our current knowledge and understanding. Based on this discussion material, the SAE S-16 Committee has been able to achieve consensus on lessons learned and to provide recommendations.

1.2 Application

This document focuses on turbine-engine-powered military air vehicles, including some recent advanced aircraft air-induction systems. No information is provided for commercial transport high-bypass turbofan installations, small turbo-jet/turbofan aircraft, turboprop aircraft, turbine-engine-powered missiles, ground vehicle installations, or auxiliary power units. However, many of the lessons learned and recommendations made in this document are applicable to these installations as long as the user recognizes and understands the limitations of the information that he/she is attempting to use. This statement is based on anecdotal discussions with engineers who work or have worked on such installations and who have judiciously and successfully applied these lessons and recommendations.

2. REFERENCES

The following publications form a part of this document to the extent specified herein. The latest issue of SAE publications will apply. The applicable issue of other publications will be the issue in effect on the date of the purchase order. In the event of conflict between the text of this document and references cited here, the text of this document takes precedence. Nothing in this document, however, supersedes applicable laws and regulations unless a specific exemption has been obtained.

2.1 Applicable Documents

2.1.1 SAE Publications

Available from SAE International, 400 Commonwealth Drive, Warrendale, PA 15096-0001, Tel: 877-606-7323 (inside USA and Canada) or 724-776-4970 (outside USA), www.sae.org.

ARP1420 Gas Turbine Engine Inlet Flow Distortion Guidelines

AIR1419 Inlet Total-Pressure-Distortion Considerations for Gas-Turbine Engines

AIR5866 An Assessment of Planar Waves

AIR5686 A Methodology of Assessing Inlet Swirl Distortion

2.2 Applicable References

2.2.1 Aerodynamics Research Branch, NACA Headquarters, “Bibliography of NACA and Other Reports on Air Inlets and Internal Flows,” NACA RM No. 8J05, October 1948.

2.2.2 Surber, L.E., and Robinson, C.P., “Survey of Inlet Development for Supersonic Aircraft,” AIAA 83-1164, June 1983.

2.2.3 Smith, Robert, Jr., “Marrying Airframes and Engines in Ground Test Facilities – An Evolutionary Revolution,” AIAA 95-0950, September 1995.

2.2.4 Davis, W.F. and Sherrer, R., “Aerodynamic Principles for the Design of Jet-Engine Induction Systems,” NACA RM A55F16.

2.2.5 Alford, J.S., GER-1404, General Electric, “Inlet Flow Distortion Index,” International Days of Aeronautical Sciences, Paris, France, May 1957.

2.2.6 Schweikhard, W.G., and Dennon, S.R., “Review and Evaluation of Recent Developments of Melick Inlet Dynamic Flow Distortion Prediction,” NASA CR 4061, May 1987, p. 78.

2.2.7 Air Force Aero Propulsion Laboratory, “Proceedings of the Air Force Airframe – Propulsion Compatibility Symposium,” AFAPL TR-69-103, June, 1970.

2.2.8 Burcham, F.W., and Hughes, D., “Analysis of Inlet-Flight Pressure Fluctuations Leading To Engine Compressor Surge of an F-111A Airplane for Mach Numbers to 2.17,” AIAA Paper No. 70-624, June, 1970.

2.2.9 Behal, J.A., Belga, M.H., and Simons, D.E., “Wind Tunnel/Flight Data Correlation, Final Report Vol. I, II, III, and IV,” AFFDL TR-71-105, October 1971.

2.2.10 Stevens, C.H., Spong, E.D., Nugent, J., and Neumann, H.C., “Reynolds Number, Scale, and Frequency Content Effects on F-15 Instantaneous Distortion,” AIAA 79-0104, January 1979.

2.2.11 Smeltzer, D.B., Smith, R.H., and Cubbison, R.W., “Wind Tunnel and Flight Performance of the YF-12 Inlet System,” AIAA 74-621, July 1974.

2.2.12 Stevens, C.H., Spong, E.D., and Hammock, M.S., “F-15 Inlet/Engine Test Techniques and Distortion Methodologies Studies, Vol. I, Technical Discussion,” NASA CR 144866, June 1976.

2.2.13 Farr, A.P., “Evaluation of F-15 Inlet Dynamic Distortion,” AIAA 73-784, August 1973.

2.2.14 Farr, A.P., and Schumacher, G.A., "System for Evaluation of F-15 Inlet Dynamic Distortion," Progress in Astronautics and Aeronautics, Vol. 34, Instrumentation for Airbreathing Propulsion, Fuhs, A. E. and Kingery, M., Editors, The MIT Press, 1974, pp. 59-76.

2.2.15 Imfeld, W.F., “The Development Program for the F-15 Inlet,” AIAA 74-1060, October 1974.

2.2.16 Webb, L.D., Whitmore, S.A., and Jannsen, R.L., “Preliminary Flight and Wind Tunnel Comparisons of the Inlet/Airframe Interaction of the F-15 Airplane,” AIAA 79-0102, January 1979.

2.2.17 Webb, L.D., Andryich, V., and Whitmore, S.A., "Flight and Wind Tunnel Comparisons of the Inlet/Airframe Interaction of the F-15 Airplane," NASA TP 2374, November 1984.

2.2.18 Johnson, R.H., “Inlet Distortion Scaling of Wind Tunnel Model Results,” NASA CR-143840, December 1976.

2.2.19 Johnson, R.H., “Comparison of Inlet Distortion from Flight and Wind Tunnel Tests,” NASA CR-144864, April 1978.

2.2.20 Haagenson, W.R., and Randall, L.M., "Inlet Development for the B-1 Strategic Bomber,” AIAA-74-1064, October 1974.

2.2.21 Graham, F.J., “Results of a 0.1-Scale B-1 Inlet Model at Transonic and Supersonic Mach Numbers,” AEDC-TR-71-219, October 1971.

2.2.22 Riddell, J.F., “Results of a 0.2-Scale B-1 Inlet Verification Model Test at Transonic and Supersonic Mach Numbers,” AEDC-TR-72-156, October 1972.

2.2.23 Mace, J., Turley, G., and Ball, R., “Wind Tunnel to Flight Correlations of F/A-18E/F Inlet Performance,” AIAA Paper 2009-5459, August 2009.

2.2.24 Hall, G.R. et al., “Development of the F/A-18 E/F Air Induction System,” AIAA-93-2152, June 1993.

2.2.25 Kidman, D.S., Reagan, P.V., and Malloy, D.J., “Comparison of Inlet Compatibility Results from Subscale Wind Tunnel and Full-Scale Flight Tests of the F/A-22 Aircraft with the F119-PW-100 Engine,” ISABE-2005-1169, September 2005.

2.2.26 Shepard, D., “A Two-Dimensional Interpolation Function for Irregularly-Spaced Data,” Proceedings of the 1968 23rd ACM National Conference, January 1968, pp. 517-524.

2.2.27 McCallum, B.N., "F-16 Inlet Stability Investigation," AIAA-89-2465, 1989.

2.2.28 McDonald, T. and Barter, S., “F-16 Conformal Fuel Tank Initial Envelope Expansion,” Society of Experimental Test Pilots 45th Meeting, September 2001.

2.2.29 Hurwitz, W.M. and Whitcomb, K.G., “Flight Test Validation of B-2 Inlet/Engine Compatibility: A Risk Management Approach,” AIAA 97-3157, July 1997.

2.2.30 Gridley, M.C. and Cahill, M.J., “ACIS Air Induction System Trade Study,” AIAA-1996-2646, July 1996.

2.2.31 Braslow, A.L. and Knox, E.C., “Simplified Method for Determination of Critical Height of Distributed Roughness Particles for Boundary-Layer Transition of Mach Numbers from 0 to 5,” NACA TN 4363, 1958.

2.2.32 Braslow, A.L., Harris, R.V., Jr., and Hicks, R.M., “Use of Grit-Type Boundary-Layer-Transition Trips on Wind Tunnel Models,” NASA TN D-3579, 1966.

2.2.33 Arend, D.J., “Evaluation of an Innovative Supersonic Boundary Layer Transition Device – Phase I Results,” AIAA Paper No. 98-3422, July 1998.

2.2.34 Rae, W.H., Jr. and Pope, A., “Low-Speed Wind Tunnel Testing,” John Wiley and Sons, New York, New York, 1984.

2.2.35 Beale, D.K., Cramer, K.B., and King, P., “Development of Improved Methods for Simulating Aircraft Engine Inlet Distortion in Turbine Engine Ground Tests,” AIAA Paper No. 2002-3045, June 2002.

2.2.36 Brimelow, B., Collins, T.P., and Pfefferkorn, G.A., “Engine Testing in a Dynamic Environment,” AIAA Paper No. 74-1198, October 1974.

2.2.37 Steenken, W.G. et al., “Factors Affecting Inlet-Engine Compatibility During Aircraft Departures at High Angle of Attack for F/A-18 Aircraft,” National Aeronautics and Space Administration Report TM-1999-206572, February 1999.

2.3 Additional References

The following publications are provided for information purposes only and are not a required part of this SAE Aerospace Technical Related Publications

2.3.1 Amin, N.F. and Hollweger, D.J., "F/A-18 Inlet/Engine Compatibility Flight Test Results," Journal of Aircraft, Vol. 20, Number 8, August 1983.

2.3.2 Arend, D.J. and Saunders, J.D., "An Experimental Evaluation of the Performance of Two Combination Pitot Pressure Probes," AIAA Paper 2009-1073, January 2009, p. 16.

2.3.3 Beaulieu, W. D., Boyd, Jr., H. E., Kostin, L. C., and Martin, A. W., "Propulsion System Flow Stability Program (DYNAMIC), Phase II Final Technical Report, Part VI Inlet Turbulence Scaling," AFAPL-TR-69-113, Part VI, February 1970.

2.3.4 Martin, A.W., "Propulsion System Flow Stability Program (DYNAMIC), Phase II Final Technical Report, Part I Summary," AFAPL-TR-69-113, Part I, February 1970.

2.3.5 Yuhas, A.J., Ray, R.J., Burley, R.R., Steenken, W.G., Lechtenberg, L., and Thornton, D., "Design and Development of an F/A-18 Inlet Distortion Rake: A Cost and Time Saving Solution," October 1995.

2.3.6 Blackwell, J.A., Jr., "Preliminary Study of Effects of Reynolds Number and Boundary-Layer Transition Location on Shock-Induced Separation," NASA TN-5003, 1969.

2.3.7 Bowditch, D.N. and Coltrin, R.E., "A Survey of Inlet/Engine Distortion Compatibility," NASA TM-83421, June 1983.

2.3.8 Brunner, D.W., Marshall, F.L., Marrs, K.J., Edwards, W.E., Pascoe, R.A., and Forner, J.A., "Development of the Integrated Propulsion System for the AGM-86A Air Launched Cruise Missile," AIAA 76-916, September 1976.

2.3.9 Burcham, F.W. and Bellman, D.R., "A Flight Investigation of Steady-State and Dynamic Pressure Phenomena in the Air Inlets of Supersonic Aircraft," AGARD CP-91-71, Paper No. 24, September 1971.

2.3.10 Burcham, F.W. and Bellman, D.R., "A Flight Investigation of Steady-State and Dynamic Pressure Phenomena in the Air Inlets of Supersonic Aircraft," NASA TMX-67495.

2.3.11 Cawthon, J.A., Truax, P.P., and Steenken, W.G., "Supersonic Inlet Design and Airframe-Inlet Integration Program (Project Tailor-Mate)," AFFDL-TR-71-124, Vol. III, May 1973.

2.3.12 Colbourne, D.E. and Flitcroft, J.E., "Prediction and Measurement of Time-Variant, Three-Dimensional Flows in Military Aircraft Intakes," Paper No. 4, AGARD CP-301, May 1981.

2.3.13 Coulam, Robert F., "Illusions of Choice — Robert MacNamara; The F-111; The Problems of Weapons Acquisition," ISBN 0-691-07583-2, Princeton University Press, 1977.

2.3.14 Cox, R.A. "Low Speed, Flat Plate, Carborundum Grit Trip Strip," AIAA International Meeting & Technical Display, AIAA Paper No. 80-0868, May 1980.

2.3.15 Cubbison, R.W., Meleason, E.T., and Johnson, D.F., "Performance Characteristics from Mach 2.58 to 1.98 of an Axisymmetric Mixed-Compression Inlet System with 60-Percent Internal Contraction," NASA TM X-1739, February 1969.

2.3.16 Hall, G., Hurwitz, W.M., Tiebens, G., Norby, W.P., Singshinsuk, P., and Wilt, C.E., "Development of the F/A-18E/F Air Induction System," AIAA 93-2152, June 1993.

2.3.17 Hodder, B.K., "An Investigation of Engine Influence on Inlet Performance," NASA CR 166136, January 1981.

2.3.18 Huges, D.L., Holzman, J,K., and Johnson, H.J., "Flight-Determines Characteristics of An Air Intake System on an F-111A Airplane," NASA TND-6679.

2.3.19 Younghans, J.L. et al., "Low Speed Effects of Reynolds Number and Lip Geometry on High Bypass Ratio Inlet Performance," AIAA 82-0059, June 1982.

2.3.20 Wasserbauer, J.F., Meleason, E.T., and Burstadt, P.L., "Experimental Investigation of the Performance of a Mach 2.7 Two-Dimensional Bifurcated Duct Inlet with 30 Percent Internal Contraction," NASA TM 106728, May 1996.

2.3.21 Surber, L.E. and Stava, D.J., "Supersonic Inlet Performance and Distortion During Maneuvering Flight," AGARD CP-91-71, Paper No. 25, September 1971.

2.3.22 Leamer, P.C. and Kennon, I.G., “Experimental Investigation of a 0.15-Scale Model of an Underfuselage Normal Shock Inlet,” NASA CR 3049.

2.3.23 MacMiller, C.J., and Haagenson, W.R., “Unsteady Distortion Characteristics with the B-1B,” NA-86-1490A, 68th Specialists Meeting of the AGARD Propulsion and Energetics Panel on Engine Response to Distorted Inflow Conditions, Munich, Germany, September 1986.

2.3.24 MacMiller, C.J., and Haagenson, W.R., “Unsteady Inlet Distortion Characteristics with the B-1B,” Paper No. 16, AGARD CP-400, March 1987.

2.3.25 Motycka, D.L., “Comparison of Model and Full Scale Inlet Distortion for Subsonic Commercial Transport Inlets,” AIAA 84-2487, 1984.

2.3.26 Norby, W.P., "Small Scale Inlet Testing for Low Cost Screening Applications," AIAA-90-1926, July 1990.

2.3.27 Reukauf, P.J., Schweikhard, W.G., and Arnaiz, H., “Flight-Test Techniques for Obtaining Valid Comparisons of Wind-Tunnel and Flight Results From Tests on a YF-12 Mixed-Compression Inlet,” AIAA 74-1195, October 1974.

2.3.28 Wasserbauer, J.F., Shaw, R.J., and Neumann, H.E., “Design of a Very-Low-Bleed Mach 2.5 Mixed-Compression Inlet with 45 Percent Internal Contraction,” NASA TMX-3135, March 1975.

2.3.29 Robins, P.J., “Research into the Effects of Scale and Fan Influence on Intake Performance. Report 1. Test on a Full Scale ‘S’ Duct,” Rolls-Royce IAR 00017, September 1972.

2.3.30 Robins, P.J., “Research into the Effects of Scale and Fan Influence on Intake Performance. Report 2. Test on a Full-Scale Pod Intake,” Rolls-Royce IAR 00018, September 1972.

2.3.31 von Doenhoff, A.E. and Horton, E.A., “A Low-Speed Experimental Investigation of the Effect of a Sandpaper Type of Roughness on Boundary-Layer Transition,” NACA TN 3858, 1956.

2.3.32 Schweikhard, W.G. and Montoya, E.J., “Research Instrumentation Requirements for Flight/Wind Tunnel Tests of the YF-12 Propulsion System and Related Flight Experience,” Progress in Astronautics and Aeronautics, Vol. 34, Instrumentation for Airbreathing Propulsion, Fuhs, A.E. and Kingery, M., Editors, The MIT Press, 1974, pp.19-39.

2.3.33 Schweikhard, W.G. and Cubbison, R.W., “Preliminary Results From Wind Tunnel and Flight Tests of the YF-12 Propulsion System,” NASA TMX-56016, 1973.

2.3.34 Sherman, D.A, Motycka, D.L., and Oates, G.C., “Experimental Evaluation of a Hypothesis for Scaling Inlet Turbulence Data,” AIAA 71-669, June 1971.

2.4 Symbols and Abbreviations

AEDC	Arnold Engineering Development Center
AFB	Air Force Base
AFSC	Air Force Systems Command
AIP	aerodynamic interface plane
AIR	Aerospace Information Report
AOA, α	angle of attack
AOS, β	angle of sideslip
APC	Airframe Propulsion Compatibility

ARP	Aerospace Recommended Practice
BLC	boundary layer control
CFD	computational fluid dynamics
D	diameter
EAID	engine auxiliary inlet door
ECS	environmental control system
FLT	full-scale flight-test vehicle
FM	frequency modulation
FOD	foreign object damage
FSCP	full-scale with cold pipe
FSE	full-scale with engine
GE	General Electric
H	height of diverter
HARV	High Angle-of-Attack Research Vehicle
ICD	Interface Control Document
IEC	inlet/engine compatibility
KC	distortion descriptor sensitivity coefficients
L	length
LEX	leading edge extension
m	massflow rate
M	Mach number
MDC	McDonnell Douglas Corporation
NACA	National Advisory Committee for Aeronautics
NASA	National Aeronautics and Space Administration
NATF	Navy Advanced Tactical Fighter
P	pressure
$\bar{P}$	time average pressure
P_t	total pressure
PRS	fan/compressor stability pressure ratio

PRSM	fan/compressor stability pressure ratio margin
P&W	Pratt & Whitney
q	dynamic pressure
R	gas constant for air
R_x, R_L	Reynolds number based on length
R_k	Reynolds number based on surface roughness
RPM	revolutions per minute
S	Strouhal number
SAE	Society of Automotive Engineers
SAFS	secondary airflow system
SPO	system program office
STOVL	short takeoff / vertical landing
T	temperature
$\overline{T}$	time average temperature
T_t	total temperature
TFX	Trigraph for Joint Air Force – Navy Project resulting in F-111A/B
Tu	turbulence
V	velocity
WAT	corrected mass flow
Y_{DIV}	boundary layer diverter offset
ΔPC	ARP 1420 circumferential distortion descriptor
ΔPR	ARP 1420 radial distortion descriptor
ΔPRMS	root mean square pressure variation
ΔPRS	fan/compressor stability pressure ratio change
Δx	boundary layer transition length
θ	circumferential angular position
γ	specific heat ratio of air
f	frequency
δ’	boundary layer displacement thickness
k	surface roughness height

μ	viscosity
ν, ν_k	kinematic viscosity
τ	time scale
u, u_k	velocity in boundary layer

Subscripts

0, ∞	freestream
2	aerodynamic interface plane (AIP) measurement station
cb	centerbody
FS	full scale
max	maximum
min	minimum
MS	model scale
st	shock trap

Distortion Descriptors

IDC	GE circumferential distortion index
IDL	GE combined descriptor
IDR	GE radial distortion index
IDT	GE total distortion index
K_θ, K_{theta}	Pratt & Whitney circumferential descriptor
K_{a2}	Pratt & Whitney combined descriptor

3. INTRODUCTION

Since the introduction of turbine engines into aircraft, practices used for developing, testing, and evaluating inlets have evolved, largely due to three influences. The first influence is the expanding speed, maneuver, and survivability envelopes of aircraft. The second is the improved understanding of the effects that highly turbulent flows, in particular, have on engine operability. Finally, the third is the desire to reduce technical, schedule, and cost risks. This evolution has occurred over the time span of a single generation of engineers. The SAE S-16 Committee deemed it prudent to capture the background and lessons learned leading to current practices used for wind-tunnel testing, computational techniques, and flight testing of inlet systems.

The design process leading to a final configuration of an inlet system is iterative in balancing technical and programmatic goals or requirements. During these iterations, the evolution of the inlet and its integration into the airframe relies heavily on wind-tunnel testing and computational fluid dynamic (CFD) analyses. Currently, wind-tunnel testing of subscale inlet models remains the primary tool for acquiring dynamic total-pressure data at the aerodynamic interface plane (AIP), and is the primary source for inlet data used for judging the compatibility of the propulsion system before flight. Inlet/engine compatibility deficiencies can be identified and modifications proposed based on subscale inlet test data.

Practices for inlet development, test, and evaluation are constantly being improved to fit within this evolving, iterative design process. During the early design stages of a program, the design proceeds using empirical databases and CFD tools to assess the need for alterations to the inlet's moldline and its integration with the airframe. These analyses are typically done using full-scale geometry and flight conditions. As the design proceeds and the moldlines are sufficiently matured, the practice of testing subscale inlet models in wind tunnels is introduced. In doing so, there is an assumption based on fluid dynamic theory that data obtained using a subscale model in the tunnels is correlated with the corresponding data of the full-scale vehicle in flight. Experiences garnered and reported on by this generation of engineers have shown that this assumption is largely correct.

In early reports, "scaling" had two distinct meanings. The first meaning referred to the geometric relationship between the subscale model and its components, and the corresponding full-scale geometry. The second meaning referred to the mathematical relationship between the data obtained on the subscale model in the tunnel and data obtained on the full-scale flight vehicle. Both relationships are examined in this report. That is to say, techniques are examined for scaling the geometry to obtain similar flow conditions about the subscale and full-scale geometries. And the correlations of data taken with subscale models in wind tunnels to data taken with corresponding full-scale vehicles at flight conditions are examined.

Information in this document is arranged to provide insight into the state of the art, and outlines the path that practitioners followed to arrive at this state. Inlet/airframe integration practices took a dramatic turn with the development of the F-111 aircraft. The next section reviews the practices before the F-111. It also examines the pivotal events surrounding the F-111's inlet development. Case studies of inlet systems developed after the F-111, from the timeframe of the RA-5C to the F-22, are presented. The intent is to portray the evolution of scaling practices for developing, testing, and evaluating inlet systems. Current scaling practices are reviewed along with lessons learned by this generation of engineers.

4. BACKGOUND

The understanding of inlet dynamic distortion as a consideration for inlet/engine operability in gas turbine powered aircraft has been improving since the late 1960s. In the mid-1970s, as the destabilizing effects of inlet dynamic distortion in gas turbine engines were better recognized, the SAE S-16 Committee on Turbine Engine Inlet Flow Distortion established guidelines for its characterization and formulated a methodology for correlating the resulting effect on turbine-engine compression-system aerodynamic stability. The resulting recommendations outlined in ARP1420 and AIR1419 have been adopted in various forms in essentially every major aircraft turbine-engine installation design since then. Although the specific methodology used in each program has varied in practice, the essential components and inherent assumptions have been the same.

Aircraft systems developed prior to the F-111 had no insight that an inlet's dynamic total-pressure distortion had a destabilizing effect on engine operability. At most, there was recognition that steady-state total-pressure distortion was important (e.g., steady-state distortion methodology was applied in the development of the B-58 (Reference 2.2.1)). Examining these early systems listed in Table 1 provides insight into the evolution of inlet integration for early military aircraft, and specifically boundary-layer management approaches. For additional insight, an excellent survey of inlet development is provided in Reference 2.2.2.

TABLE 1 - EARLY AIRCRAFT PROGRAMS OFFERING INSIGHT INTO THE EVOLUTION OF INLET/AIRFRAME INTEGRATION TECHNOLOGY

Aircraft	Engines	First Flight Date
P-59	I16-GE	1942
P-80	J33-A-21	1944
F-89	J35-A-35	1948
F-100	J57-P-21A	1953
F-101	J57-P-55	1954

During and after the development of the F-111 aircraft, researchers focused on understanding and developing methods to assess the effect that inlet dynamic total-pressure distortion had on engine operability. This work included the development of methodologies for simulating dynamic distortion using subscale models tested in wind tunnels and measuring such distortion in flight test. Most military aircraft programs initiated after the F-111 development benefited from this research. A reduced number of these programs have had both wind-tunnel and flight-test elements, thus allowing an evaluation of our understanding and ability to correlate inlet total-pressure-recovery and dynamic-distortion data between subscale models tested in wind tunnels and full-scale aircraft tested in flight. Some of these aircraft programs that have readily accessable data are listed in Table 2 and are examined in Section 5.

TABLE 2 - AIRCRAFT PROGRAMS OFFERING WIND TUNNEL TO FLIGHT CORRELATIONS OF INLET RECOVERY AND DYNAMIC TOTAL-PRESSURE DISTORTION

Aircraft	Engines	First Flight Date
F-111	TF30-P-103	1964
RA-5C*	J79-GE-10	1958
YF-12	J58	1963
F-15	F100-PW-100	1972
B-1A	F101-GE-100	1974
F-16	F110-GE-100	1989 (Re-engine activity)
B-2	F118-GE-100	1989
F/A-18 E/F	F414-GE-400	1998
F-22	F119-PW-100	1990

*The RA-5C aircraft was developed before the F-111. It was, however, used as a flight-test vehicle for inlet dynamic distortion research after the F-111 experiences and before subsequent aircraft developments.

4.1 Evolution of Inlet Development, Test, and Evaluation Practices Prior to the F-111

Development of inlet systems used in early turbine-powered aircraft did not involve the use of subscale inlet testing (Reference 2.2.3). Instead, generic inlet shapes were tested by NACA and industry in wind tunnels at relatively large scale to establish pressure loss and airflow data. These were isolated inlet models in contrast to integrated inlet/forebody models. Total-pressure distortion did not appear to be a consideration. Inlets used on these early aircraft were first tested during full-scale flight tests. Based on historical references, correlation of subscale inlet data (when subscale inlet models were employed) was not considered necessary in the calculation of installed engine performance. Any performance or operability problems that arose were solved on the full-scale vehicle. A combination of factors resulted in these early practices being successful, including low-diffusion (small cross-sectional area changes) diffusers, subsonic flight speeds, and benign maneuverability envelopes. Also, many early turbine engines used centrifugal compressors that, when compared with axial compressors, are relatively insensitive to total-pressure distortion.

An example of solving inlet problems during full-scale development of these early aircraft is inferred from the P-59 aircraft (Figure 1). Little information regarding the development of this aircraft (circa 1943–1945) has survived. Examination of the remaining example of this aircraft, in the National Museum of the United States Air Force at Wright-Patterson AFB, suggests addition of an internal boundary-layer diverter system after the aircraft's initial fabrication (Figure 2).

MSG07-053206-083.ppt
AIR5687

FIGURE 1 - INLET INSTALLATION OF THE BELL P-59

MSG07-053206-084.ppt
AIR5687

FIGURE 2 - P-59 INLET APERTURE AND DIVERTER

The appearance of the internal diverter in the P-59, seen in Figure 2, suggests that this was added to the full-scale hardware to alleviate some problem (Reference AIR5866). Pilots of these early aircraft reported a disconcerting phenomenon that came to be known by the descriptive term “duct rumble.” This phenomenon is now believed to be associated with self-sustained flow oscillations. Evidently, designers thought that the diverter would remove the forebody boundary layer and solve the problem. The evidence of developmental problems associated with the forebody boundary-layer management seems to be a harbinger of installations where sub- to-full-scale solutions would have to be developed (i.e., the scaling of the boundary-layer diverter). And it illustrates a problem repeatedly underestimated by inlet designers over the years.

Pilots encountered a similar forebody boundary-layer problem during flight tests of the P-80 seen in Figure 3. They reported “rumble” (Reference 2.2.4) in the P-80 bifurcated inlet duct before an effective fuselage boundary-layer diverter was developed. It was reported that this “rumble” was due to a side-to-side flow imbalance between the two branches of the bifurcated duct. [This phenomena is now referred to as twin-duct instability.] Again, it is not clear whether wind-tunnel tests of subscale inlets were ever involved, but designers came to understand that inlet/engine compatibility could be compromised by viscous-flow interactions. They realized as well that the best way to avoid operability problems, especially as they moved into supersonic flight, was to prevent (or at least minimize) boundary-layer entry into the inlet.

FIGURE 3 - P-80 INLET INSTALLATION

Soon, aircraft developers began to include boundary-layer diverters with side-mounted inlet installations in the initial design rather than wait until the full-scale design was well established (e.g., F-89 seen in Figure 4). In these configurations, they adopted the use of external boundary-layer diverters that employed wedges or “plows” to divert the fuselage boundary layer more efficiently than had been possible with internal diverters.

MSG07-053206-086
AIR5687

FIGURE 4 - F-89 INLET/DIVERTER INSTALLATION

Many of these early turbine-powered aircraft incorporated inlets whose performance would not have been affected significantly, if at all, by the presence of the airframe. As a case in point, the F-100 aircraft (Figure 5) incorporated a simple nose inlet where the primary effect of the airframe design would be associated with duct length and the resultant buildup of boundary layer in the diffuser. Otherwise, the inlet performance would be adequately determined from the available NACA and industry test data on isolated subscale inlet models in wind tunnels.

MSG07-053206-087
AIR5687

FIGURE 5 - F-100F INLET INSTALLATION

Later, with the introduction of supersonic aircraft such as the F-89, F-101, F-102, and F-105, external diverters employed splitter plates to avoid interaction of the inlet's normal-shock wave with the fuselage boundary layer. An example of this is the F-101 aircraft (Figure 6). Eventually, when wind-tunnel tests of integrated inlet/forebody subscale models became the norm for side-mounted installations, the standoff distance of the splitter plate and diverter from the fuselage was not geometrically scaled on subscale models. Instead, the standoff distance was scaled by the thickness of the local fuselage boundary-layer to avoid its ingestion at all anticipated test conditions. This process, in general, was assumed to work best for large-scale (approximately 1/4-scale) models in which the viscous effects within the inlet itself were not far removed from those found at full scale.

MSG07-053206-088
AIR5687

FIGURE 6 - F-101 INLET CONFIGURATION WITH EXTERNAL DIVERTER AND SIDEPLATE

4.2 The F-111 Inlet/Engine Compatibility Experience

During the 1940s and early 1950s, the approach to inlet/engine compatibility could best be described as an art rather than as a science. In 1956, NACA published the document, "Aerodynamic Principles for the Design of Jet-Engine Induction Systems" (Reference 2.2.4). This document was considered the "bible" for air-induction-system design and inlet/engine compatibility. The document included an extensive list of references and, in addition, an extensive bibliography. If the document itself did not have specific guidance for a given application, something useful usually could be found in the references or the bibliography. However, there were only one or two references that described some sort of numerical methodology relative to inlet distortion at the compressor face other than the simple relationship of maximum-minus-minimum pressure divided by the average pressure.

This document served the industry in the late 1950s and early 1960s. However, many instances of inlet/engine operability or compatibility problems were encountered, as were discussed in Section 4.1. By 1958, General Electric had defined a numerical inlet distortion methodology (Reference 2.2.5) for the GE J79 turbojet engine. This methodology was used extensively (and successfully) in the development of the inlets for the General Dynamics B-58A supersonic aircraft. Up to this time, low-response compressor-face probes measured the pressures used in the numerical distortion methodology, although several instances of concern about unsteadiness of the inlet flow were mentioned.

The F-111 program represented a turning point in the field of inlet/engine compatibility. The Requests for Proposals for the dual service TFX (later the F-111) were issued October 1961. Other important dates for the F-111 program are listed below for reference in the discussion that follows:

- General Dynamics announced as winner—November 1962.
- First flight—December 1964.
- Production contract —April 1965.
- First production aircraft delivery—July 1967.
- Production completed—November 1976.

The F-111 (Figure 7) incorporated significant advances in aircraft/propulsion configuration complexity as noted in the following list:

- First afterburning turbofan engine.
- Largest range of afterburner thrust modulation to date—50% to 100%.
- Twin-spool engine for military aircraft.
- Low pressure rotor—three-stage fan plus six-stage low-pressure compressor.
- High pressure rotor—seven-stage high-pressure compressor.
- Airframe—twin engine.
- Variable sweep wing.
- Armpit inlet location—1/4th axisymmetric with translating centerbody, double-cone, second-cone variable angle.
- Primary mission design points: Mach 1.2 dash at sea level, Mach 2.2 at altitude, 16 degrees angle-of-attack at Mach 2.2, and over-speed to Mach 2.5.

FIGURE 7 - INLET SYSTEM FOR THE F-111

The engine for the F-111 was the Pratt & Whitney TF-30. By the time the program started, Pratt & Whitney had defined a numerical inlet distortion methodology (KD2, Reference 2.2.6) for the engine. The validity of the methodology was verified using distortion screen testing in ground test cells. Wind-tunnel tests of the inlet with forebody showed that the steady-state distortion levels were acceptable; thus, no engine stalls were predicted. The wind-tunnel tests used steady-state probes located at the compressor face.

Note that engine stalls did occur during a full-scale wind-tunnel test of the inlet/engine system. This test hardware had a partial forebody and wing designed to provide the correct local Mach number and flow angles at the inlet and was tested with an operating engine at static and supersonic conditions. However, the wind-tunnel tests were performed at higher altitudes than were in the vehicle flight envelope. As a result, the wind-tunnel Reynolds number was lower than what the actual flight Reynolds number would be, possibly producing nonrepresentative test conditions. Because of this and because the steady-state distortion levels were acceptable, the consensus judgment was that there would not be any engine-related issues with flight tests.

Early flight testing of the F-111 was, however, plagued with engine stalls. The stalls resulted from dry power throttle transients, afterburner lights, afterburner zone changes, aircraft angle of attack changes, and inlet spike and cone angle off-schedule conditions. High-response instrumentation installed on the flight-test vehicles showed high levels of flow turbulence (total-pressure RMS levels) at the compressor face, but low-response instrumentation showed acceptable total-pressure distortion levels. Thus began a series of tests and changes to the engine and the inlet configuration that lasted for several years.

The period from 1965 to 1969 was a time of intensive investigation to determine the causes of engine stall and to develop an approach for predicting these stalls. Many theories were postulated. There were many analysis and test programs by industry, universities, Air Force, Navy, and NASA Laboratories. Included among these programs was an experimental investigation conducted at the Air Force Arnold Engineering Development Center (AEDC) in which an XB-70 inlet simulator and YJ93 engine were tested in the supersonic tunnel of the Propulsion Wind Tunnel Facility (Reference 2.2.7). During these tests, the engine appeared to drift into stall during conditions that were otherwise thought to have sufficient stability margin. Flight tests of the XB-70 aircraft had also encountered engine stalls. The project conducted further ground tests to study the effects of inlet-generated turbulence and distortion on YJ93 engine flow instabilities. These tests showed that high levels of turbulence, albeit with low levels of distortion, resulted in the engine drifting into stall, even after as much as 8 minutes on test condition.

This time period of investigation culminated in the “Aircraft-Propulsion System Compatibility Symposium” held in Miami Beach, Florida, on June 24 through 26, 1969. The various papers given at this symposium are collected in Reference 2.2.7. The keynote address at this symposium by Mr. Joe Jones, Deputy Assistant Secretary of the Air Force, Research and Development, included this quote, which summarizes the history of this time period:

“Yet, on the first attempt to exploit the potentials of the turbofan engine in an afterburning configuration for the supersonic multi-mission F-111 fighter aircraft, severe stability and installation difficulties were encountered that had not been anticipated. Possibly the general success in adapting the turbofan to the relatively simple pod-mounted installations on subsonic transport-type aircraft had tended to mask certain of the problem potentials of the more sophisticated supersonic installation. The significant engineering challenges in the missile and space programs and the general success being achieved may also have in itself contributed a lulling effect. Additionally, the Government and industry engineering management environment of that period, coupled with new fixed price incentive contractual relationships, created an additional obstacle to a broad scale and rapid attack on the fundamental engineering problems at the outset. Internally, within the Air Force, the technical laboratories had become sufficiently separated from the SPO [Systems Project Office] organizations that they lacked a proper understanding or sense of responsibility for the technical problem being encountered. Finally, the engine and airframe contractors, operating under the terms and conditions of their individual contracts with their own specifications, performance guarantees, correction of deficiency clauses, and schedule problems, were not prone to become involved in each other’s efforts anymore than was absolutely necessary. As a result of this general environment, when confronted with serious inlet/engine stability and nozzle/airframe backend problems on the F-111, we found ourselves with too little fundamental knowledge and with the various engineering groups constrained by an awkward management and contractual relationship. Even more recently, many of the same constraints were initially prevalent in developing a solution for the F-4E/J-79 installation problems. Fortunately, the system did finally awaken and reveal its resiliency. Once the seriousness of these problems was recognized and appreciated, ad hoc arrangements were made and the military laboratories, SPO technical personnel, NASA, and airframe and engine contractor teams rose to the challenge and initiated the necessary collaborative effort to effect solutions. But, the time lag had been costly.”

Plourde and Brimelow found that time-dependent patterns lasting on the order of one rotor revolution produced the same loss of stabiltiy margin as a steady-state pattern (Reference 2.2.7). This insight was found by putting a turbulence generator with a plug in front of a TF30 engine. In the later parts of the F-111 flight-test program, data were collected using this general approach, but the time scale was different than the one rotor revolution. Later, the time scale was changed to correspond to the Plourde and Brimelow criteria even before the paper was published. Their initial test data suggesting this approach was gathered in the spring 1968 and was passed on to the F-111 program. Application of this approach in the later stages of the F-111 flight-test program contributed significantly to solving most of the engine stall problems.

The Society of Automotive Engineers Committee S-16 was formed at the request of the Air Force in 1971. Its charter was to develop a single methodology to address the inlet/engine compatibility problem using the knowledge that had evolved in this period of extensive research. The Committee was composed of members from the airframe and engine industries, the military, and the NASA Laboratories.

After several meetings (some of which were very contentious), a general consensus was reached that the Plourde and Brimlow approach was valid and should be the basis of the methodology. This consensus was supported by F-111A flight-test data reported by Burcham and Hughes (Reference 2.2.8). After considerable additional debate (supported by analysis), the S-16 Committee agreed that a simple universal methodology for all engines was not possible (much to the disappointment of the military and airframe community). It was at this point that a more general approach was adopted, allowing the Committee to develop descriptors applicable to all engines, while recognizing that various coefficients and constants would have to be determined for specific engines.

Progress was slow even though the Committee was meeting four times a year during this initial time period. The Committee's first document, ARP1420, was published in March 1978 after approximately 20 meetings. The ARP1420 approach requires the airframe manufacturer to gather high-response total-pressure data at the AIP on their inlet models and calculate distortion descriptors consistent with the specific numerical approach for a given engine. The location of the AIP, and its associated set of instrumentation, within an inlet is mutually agreed upon by the airframe and engine manufacturers following the guidelines in ARP1420.

The correlation of model- to full-scale high-response data gathered consistent with ARP1420 seems to be adequate to ensure successful airframe development programs with few (if any) compatibility problems (fidelity of the model scale to full scale is required). This approach, which was derived from military aircraft with engines having inlet guide vanes, continues to serve the industry well as demonstrated in Section 5, Case Studies. Applications of the basic ARP1420 methodology to vehicles that have significant configuration differences from those that formed the basis for this methodology should address the fundamental tenets of that methodology.

5. CASE STUDIES

A number of military aircraft programs have conducted subscale wind-tunnel tests and corresponding full-scale flight tests to develop the inlet system and verify its performance. Some of these programs documented their wind-tunnel and flight data such that correlations between the two were examined. This affords the Committee an opportunity to examine how well inlet recovery and dynamic distortion obtained in the wind tunnel corresponds to that eventually measured in flight. Another set of programs, while not providing correlations directly, provided insight or lessons for use in future development programs. Both types of programs are presented in this section as case studies.

5.1 Case Studies Offering Correlations

The following case studies provide findings associated with correlating inlet performance and dynamic pressure distortion measured in wind tunnels with that found in flight tests. This section is organized in chronological order, proceeding from the earliest known examination of model- to full-scale data correlations through more recent experiences. This approach is taken because it highlights an improved understanding of inlet-engine compatibility and test techniques. The results of these case studies are discussed, where available, as they relate to geometric scaling fidelity, Reynolds number effects, ground/flight-test techniques, and correlating wind-tunnel to flight inlet recovery and total-pressure distortion data. Finally, a relevant summary, as reported by the original authors, is presented along with observations by this Committee having the benefits of 30 years of hindsight.

5.1.1 RA-5C Case Study

The RA-5C case study is presented not because it had an inlet/engine compatibility issue, but because it was selected as a testbed aircraft to examine, for the first time, issues associated with scaling inlet dynamic-distortion data from ground to flight tests. The Air Force Systems Command (AFSC) formed the Airframe-Propulsion Compatibility (APC) Committee as an ad hoc group with members drawn from the Air Force's Aero Propulsion Laboratory, Flight Dynamics Laboratory, and Aeronautical Systems Division to work the F-111 inlet/engine compatibility issues. Later, members of the APC Committee, as ordered by the AFSC Commander, initiated research and development programs to provide a technology base of inlet/engine compatibility information for future systems. One of these programs, conducted during 1969–1971, used the RA-5C aircraft as a test vehicle. Its primary objective was to develop techniques for correlating wind-tunnel and flight-test inlet performance data (Reference 2.2.9). Both scaling and Reynolds number effects were independently studied. This program is the first known to report on these issues.

The twin-engine RA-5C had two inlet apertures, each mounted on opposite sides of the fuselage ahead of the wing. A diverter was employed to standoff the inlet aperture from the forebody boundary layer. The external-compression inlets were two-dimensional, variable horizontal-ramp geometries and operated at a Mach 2 design point with two oblique shock waves followed by a normal shock wave. Each duct had a small amount of offset and a ratio of length to engine-face diameter of 6.6. A photograph of the aircraft and schematic of the inlet geometry is provided in Figure 8.

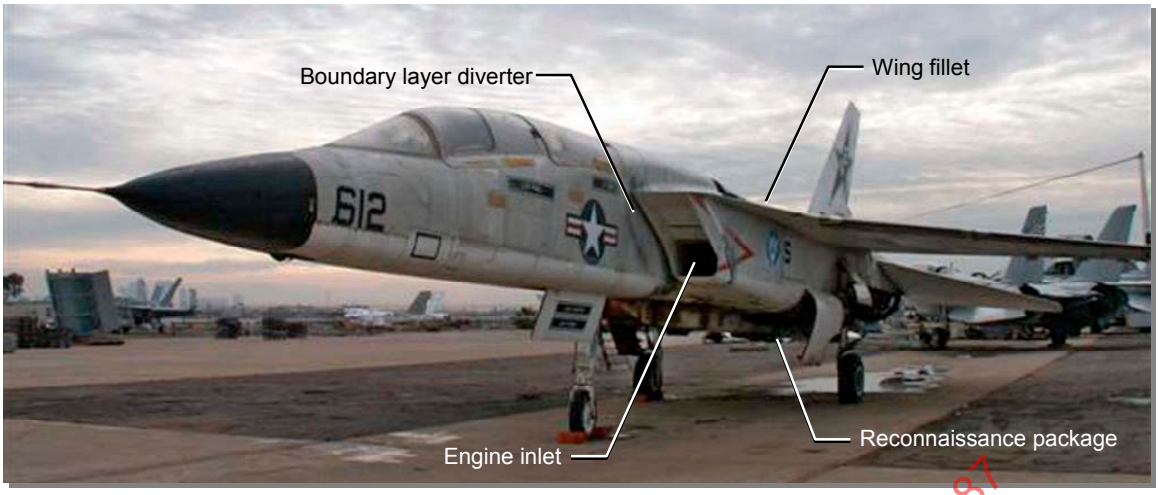

(A) RA-5C AIRCRAFT AND INLET/AIRFRAME INTEGRATION

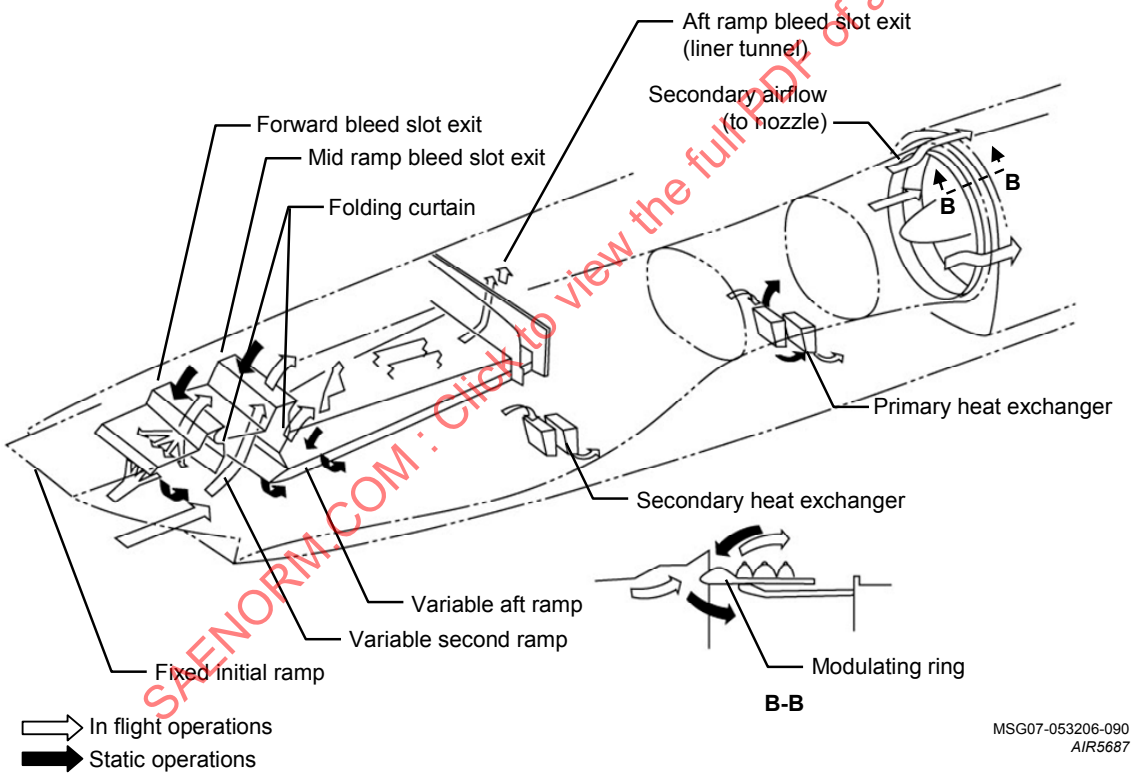

(B) RA-5C INLET DETAILS

FIGURE 8 - RA-5C INLET SYSTEM

5.1.1.1 Test Item Configuration

The RA-5C program was unique in that data from two subscale models and the full-scale flight vehicle were obtained allowing the influence of model scale and Reynolds number to be examined. The wind-tunnel test series included two models of different scales; specifically, a 0.125-scale model and a 0.228-scale model were tested. Photographs of the wind-tunnel models are provided in Figure 9. Geometric similarity of the forebody, ramps, duct, engine bullet-nose, secondary flow apertures, and protuberances were maintained for the port (left) inlet of each model. The starboard (right) inlets were faired over and only a small span of the port wing was included. The height of the full-scale diverter, $H_{div\ FS}$, was set to a computed local boundary-layer thickness, δ_{FS}, at Mach 2 and 50,000-foot altitude, i.e., $H_{div\ FS} / \delta_{FS} = 1$. The diverter height for each subscale model, $H_{div\ MS}$, was such that the ratio $H_{div\ MS} / \delta_{MS} = 1$ where δ_{MS} was the local boundary-layer thickness computed at Mach = 2 and nominal tunnel conditions. No information was available regarding the use of boundary-layer transition grit on the wind-tunnel models.

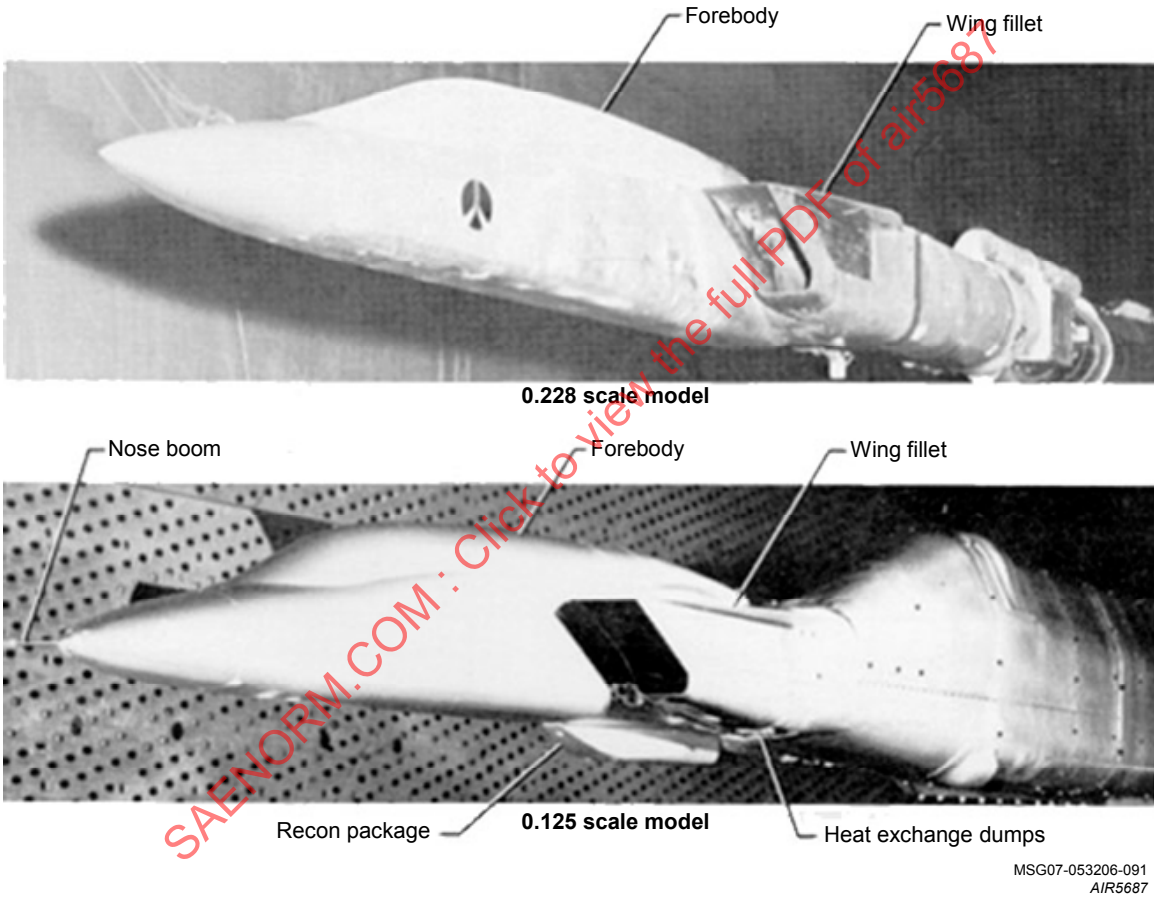

FIGURE 9 - RA-5C INLET WIND-TUNNEL MODELS

5.1.1.2 Test Conditions

The ground tests were conducted in the AEDC's 16-foot transonic and 16-foot supersonic propulsion wind-tunnel facilities at Mach numbers ranging from 0.65 to 2.0. The 0.125-scale model was strut mounted while the larger 0.228-scale model was sting mounted. At the Mach numbers reported here, the inlets were operated as flowthrough systems. Data were obtained over an angle-of-attack and sideslip range of –4 degrees to +18 degrees and –10 degrees to +10 degrees, respectively. Flight tests were conducted from the North American Rockwell, Columbus Division facility, in Columbus, Ohio.

5.1.1.3 Data Acquisition, Processing, and Analysis

The measured database included steady-state and dynamic total pressures from the two subscale models and the flight-test aircraft. The AIP of each model was instrumented with 30 high-response transducers mounted in rakes at similar locations and orientations. The probes at the AIP were arranged with five per rake and located on centers of equal area. Pressure measurements for the 0.125-scale model were made using a concentric steady-state and dynamic pitot probe with a 0.125-inch outer-diameter and a length-to-diameter ratio of about 10. The larger 0.228-scale model used a unique probe with a 0.083-inch outer-diameter pitot probe of length-to-diameter ratio of about 3. Additionally, each probe consisted of a single tube for measuring the total pressure. Then, within the rake housing, the single tube branched with one leg measuring the steady-state pressure while the other leg was routed to the dynamic pressure transducer also located inside the rake housing.

The flight-test vehicle also employed a 30-probe arrangement similar to the subscale models. The flight-test measured steady and dynamic pressures using concentric pitot probes similar to those used during the testing of the 0.125-scale model in the wind tunnel. However, each pitot probe was a 0.500-inch outer-diameter tube of length-to-diameter ratio of about 2.

The dynamic-data acquisition system used at AEDC was capable of measuring pressures at frequencies up to 8 kHz. At each test point, the dynamic data were recorded for about 20 seconds and stored using a 72-channel FM multiplex tape system. During the post-test data analysis, the dynamic data were digitized and filtered such that the resultant data had cutoff frequencies of 4 kHz for the 0.228-scale model and 8 kHz for the 0.125-scale model.

The flight-test steady-state data were recorded at 120 samples per second using a pulse code modulator. The dynamic data were FM multiplexed onto an onboard tape recorder. Both the steady and dynamic data were then sent to the flight-test ground station using telemeter links. The record length used in flight tests to obtain dynamic data was 7.5 seconds.

5.1.1.4 Results and Discussion

These data provided insight into the effects of model scale and Reynolds number on total-pressure recovery. Each scale (0.125, 0.228, and full scale) was tested over a range of Reynolds and Mach numbers. The Reynolds number length scale, L, was the distance from the leading edge of the inlet ramp to the diffuser exit. The data presented here (Figure 10) are reported as “match airflow” and presumed to be at engine airflow for sustained flight at that Mach number. For any constant scale and Reynolds numbers, the recovery is seen to decrease with increasing Mach number largely due to losses across the inlet’s shock waves (follow Curve A in Figure 10). For any constant scale and Mach number, recovery increases with Reynolds number presumably due to thinning boundary layers (follow Curve B in Figure 10). Of note though, for any constant Mach and Reynolds number, recovery generally decreases with model scale with an exception at Mach 1.8 for the wind-tunnel models (follow Curve C in Figure 10).

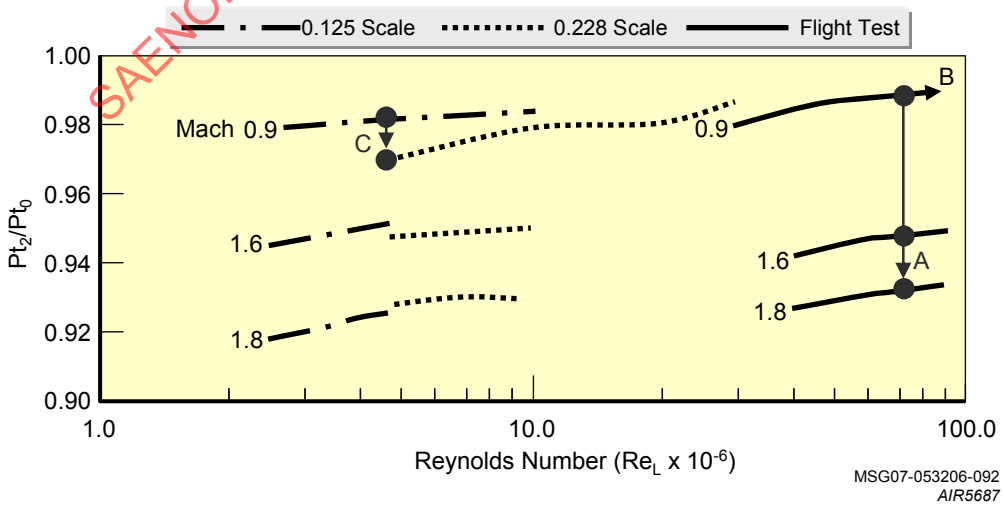

FIGURE 10 - VARIATION OF TOTAL-PRESSURE RECOVERY WITH REYNOLDS AND MACH NUMBERS, AND SCALE

This database also provided insight into the behavior of dynamic pressure distortion with changes in scale, Mach and Reynolds numbers. Several distortion indices were computed and screened, but the index K_{theta} is selected for review here since circumferential distortion generally is stressed for engine operability. See Reference 2.2.10 for a description of the K_{theta} distortion index. For any constant scale and Reynolds numbers, the distortion is seen (Figure 11) to increase with Mach number, probably due to interactions of boundary layers with the inlet's shock waves. For constant scale and Mach number, distortion generally decreases with Reynolds number probably due to thinning boundary layers. There were exceptions, however, for which the causes were not reported. Changes in scale with constant Mach number reportedly produced surprising trends. At Mach 0.9, distortion generally increased with model scale and Reynolds number. At supersonic flight speeds, however, distortion was lowest for the 0.228-scale model regardless of Reynolds number.

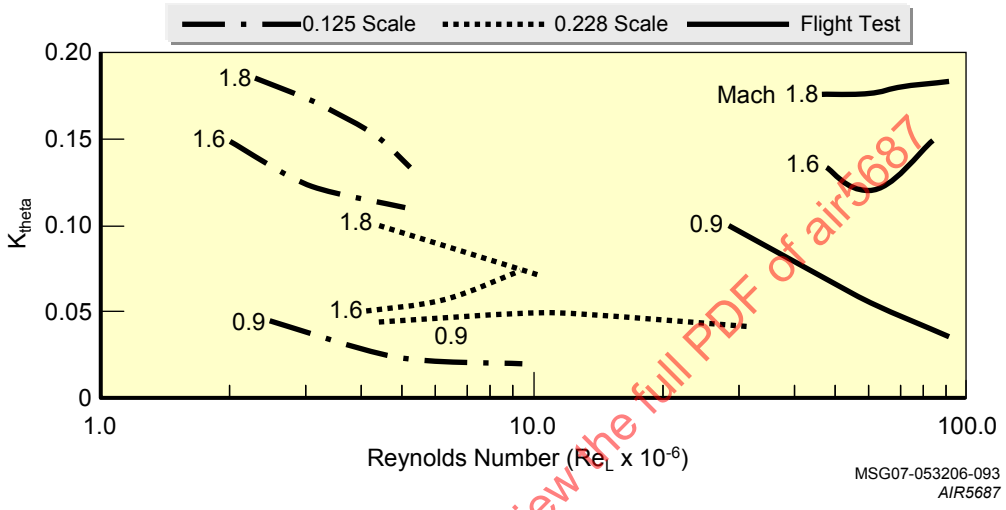

FIGURE 11 - VARIATION OF DYNAMIC CIRCUMFERENTIAL DISTORTION WITH REYNOLDS NUMBER

5.1.1.5 Findings of the Original RA-5C Study

At the time, relevant findings from this program were summarized as:

- Recovery increased with Reynolds number.
- 0.125-scale model was of sufficient size to obtain recovery and dynamic-distortion data.
- A record length of 7.5 seconds provided stabilized data in flight test.

5.1.1.6 S-16 Committee Observations of RA-5C Data

Today, several key observations are noted pertaining to wind-tunnel to flight correlation for recovery and distortion. These data produced results that generally follow expected trends based on aerodynamic similarity rules. Recovery measured using the 0.125-scale model at Reynolds number used in wind tunnels could be used to estimate flight recovery. No reason is seen to use a larger scale wind-tunnel model. At similar Mach numbers, a recovery improvement of up to 1% may be expected for a Reynolds number correction from wind-tunnel to flight test.

The measurements indicate that, except at supersonic speeds, dynamic circumferential distortion decreased with increasing Reynolds number for constant Mach number and scale. Other observations of dynamic distortion from this database are less clear. For example, while similar levels of distortion were measured on the 0.125-scale model and the full-scale vehicle, the 0.228-scale model yielded noticeably lower distortion. Several factors are offered to explain this. First, the 0.228-scale model used probes having a small length-to-diameter ratio to measure the dynamic pressure data; this might have introduced a bias in the measurements. Second, the small length-to-diameter ratio of the flight probes might have introduced a bias.

5.1.2 YF-12 Case Study

The YF-12 program allows comparison of inlet data from a 1/3-scale wind-tunnel model, a full-scale nacelle wind-tunnel model with and without engine, and full-scale flight tests (Reference 2.2.11).

5.1.2.1 Test Item Configuration

The YF-12 had an axisymmetric mixed-compression inlet (Figure 12) designed for a cruise Mach number of 3.2. The inlet had a translating centerbody spike with a 26-degree included angle; the spike also provides throat area control. Boundary-layer bleed, using porous surfaces, was located upstream of the inlet throat on the centerbody. Boundary-layer bleed on the cowl was in the form of a shock trap slot at the throat station. Forward bypass doors controlled the position of the normal-shock wave, while the aft bypass doors provided airflow matching with the engine. The inlets were wing mounted, with slight inward and downward cant (3.24 and 6.82 degrees, respectively). This placed a slight bend in the subsonic diffuser.

MSG07-053206-094
AIR5687

FIGURE 12 - YF-12 INLET AND INSTALLATION

All wind-tunnel models had the same scaled contours for the translating spike centerbody and diffuser moldlines. Both the 1/3-scale inlet model and the full-scale inlet model with cold-pipe were terminated with a massflow plug. The full-scale inlet model and flight-test inlet had fixed louvered exits for the centerbody bleed and forward bypass, while the 1/3-scale inlet model had ducted exits with variable area that were used to match bleed massflow ratio to full scale. The full-scale inlet with engine and the flight hardware routed the shock trap bleed and aft bypass to an ejector for engine cooling. The full-scale inlet without engine and the 1/3-scale inlet model controlled this flow with variable valves. Finally, the full-scale and flight hardware had 32 internal tubes to pass the shock trap bleed flow aft, while the 1/3-scale inlet model had 8 area-scaled tubes external to the model. These model differences are shown in Figure 13. The forebody of the flight configuration introduced some nonuniformity on the inlet approach flowfield. Mach number variation at the cowl plane was about 2.5%, and sideslip variation was as much as 4 degrees. The upwash angle at the cowl plane was not significantly affected.

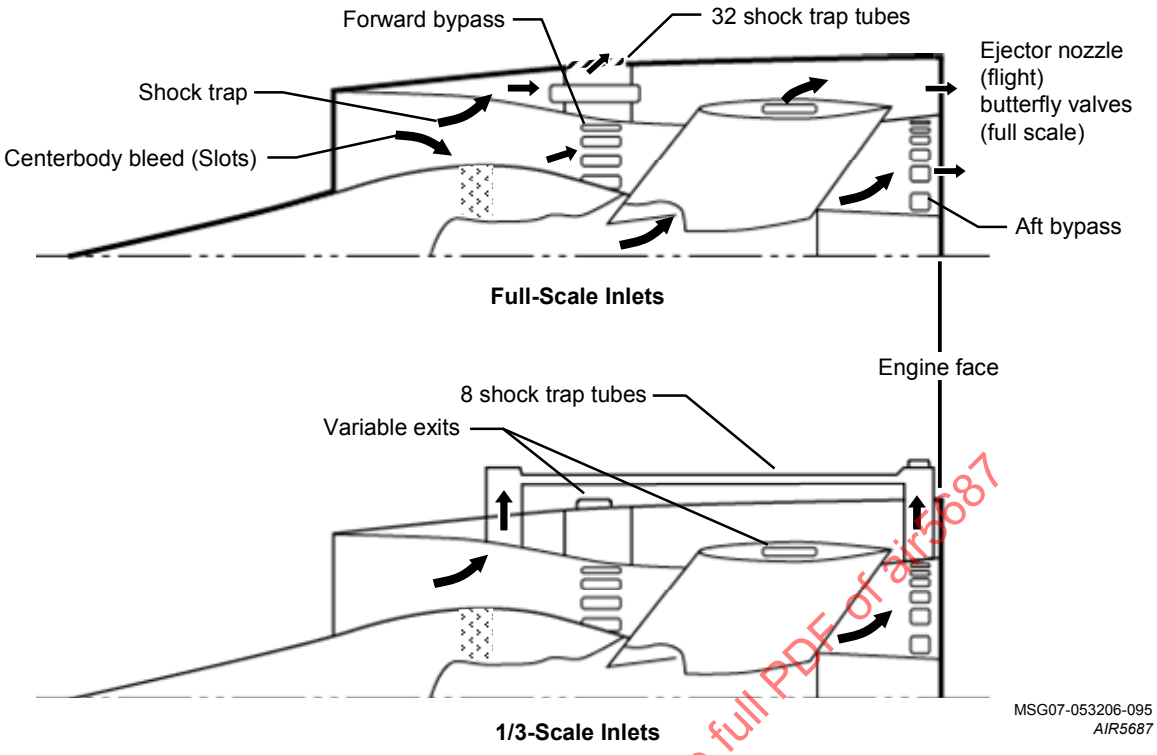

FIGURE 13 - YF-12 INLET MODEL DETAILS

5.1.2.2 Test Conditions

Test articles for the YF-12 included wind-tunnel models at 1/3-scale and full-scale, as well as the full-scale flight-test aircraft. The full-scale wind-tunnel model was tested with and without an engine. The 1/3-scale model was tested at the NASA Ames 8- by 7-foot wind tunnel and in both the 9- by 7-foot and 11- by 11-foot Unitary Plan wind tunnels. The full-scale inlet, with and without an engine, was tested at the NASA Lewis 10- by 10-foot wind tunnel. All ground test models were isolated inlets.

5.1.2.3 Data Acquisition, Processing, and Analysis

Pressure instrumentation for each model varied (Figure 14). Of particular note is the difference in number of dynamic total-pressure probes on the engine-face rakes (denoted by Column F in Figure 14). The 1/3-scale inlet model had 40 dynamic probes (8 rakes, 5 rings) clocked 15 degrees from top dead center, while the full-scale inlet model and flight tests had 24 dynamic probes (6 rakes, 4 rings) clocked 5 degrees from top dead center. No information was found concerning the data processing.

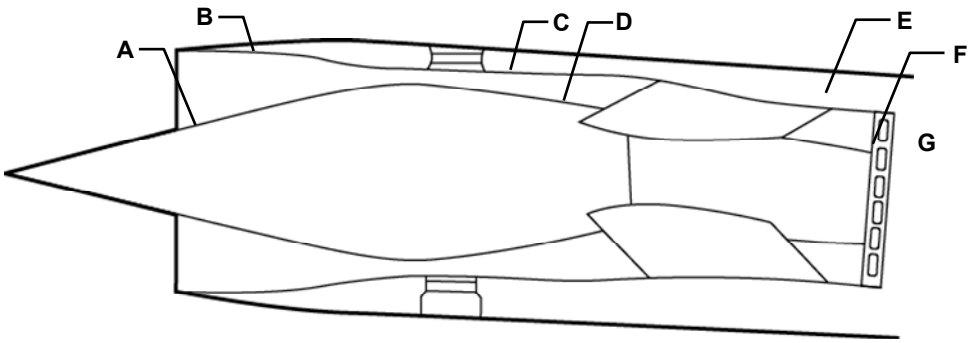

NASA Research Center	Scale	Type	Location of Pressure Sensors							
			A	B	C	D	E	F	G	Total
			Number of Sensors							
Ames	1/3	Steady State	73	32	84	44	47	40	-	320
		Dynamic	12	6	16	12	1	40	-	87
Lewis	Full	Steady State	75	58	128	94	45	52	-	402
		Dynamic	-	11	27	-	12	24	-	74
Flight	Full	Steady State	9	17	43	22	7	50	3	151
		Dynamic	4	4	8	8	5	46	5	80

MSG07-053206-096
AIR5687

FIGURE 14 - YF-12 INLET MODEL INSTRUMENTATION DETAILS

5.1.2.4 Results and Discussion

This section discusses the geometric scaling fidelity, Reynolds number effects, and ground test techniques.

Comparison of the inlet performance and distortion at Mach 2.8 is shown in Figure 15. The data show variation of total-pressure recovery, various massflow rates, and steady-state distortion as a function of engine massflow ratio (m_2/m_∞) for three models at similar Reynolds numbers. These data were obtained by varying the forward bypass doors. The variation of pressure recovery with engine massflow ratio correlates very well between the three models, although the flight-test inlet remained started to a higher total-pressure recovery than the wind-tunnel models. There are discrepancies in the shock trap (m_{st}/m_∞) and centerbody bleed (m_{cb}/m_∞) massflow ratios, which were attributed to differences in bleed passage geometry in the 1/3-scale inlet wind-tunnel model and leakage in the flight-test inlet. Total-pressure distortion was increased when measured on full-scale hardware compared to that obtained on the 1/3-scale model.

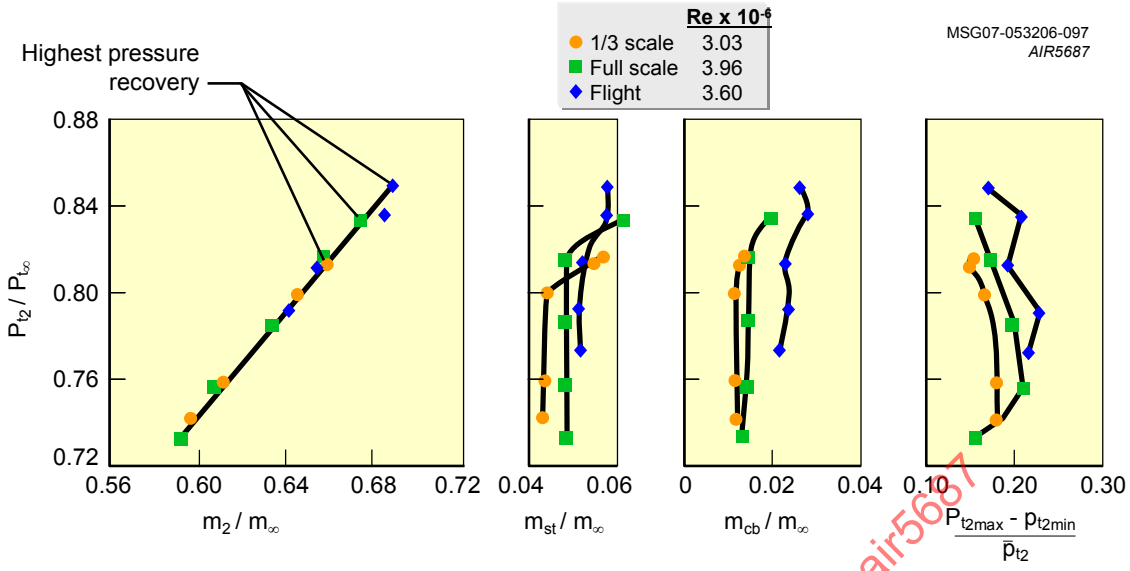

FIGURE 15 - YF-12 PERFORMANCE AND DISTORTION, MACH 2.8

Inlet performance and distortion at Mach 2.1 is compared in Figure 16. For this Mach number, the inlet was operating at reduced massflow ratio compared to the Mach 2.8 data. In this case, the correlation of total pressure was not as good, with the flight-test inlet operating at higher massflow ratios. It was noted that the flight-test data were obtained with the inlet operating at a higher corrected airflow than the ground test data. Massflow ratios of the shock trap and centerbody bleed systems were similar to the Mach 2.8 data. The distortion between the three models was similar except for the highest airflow conditions where differences were found.

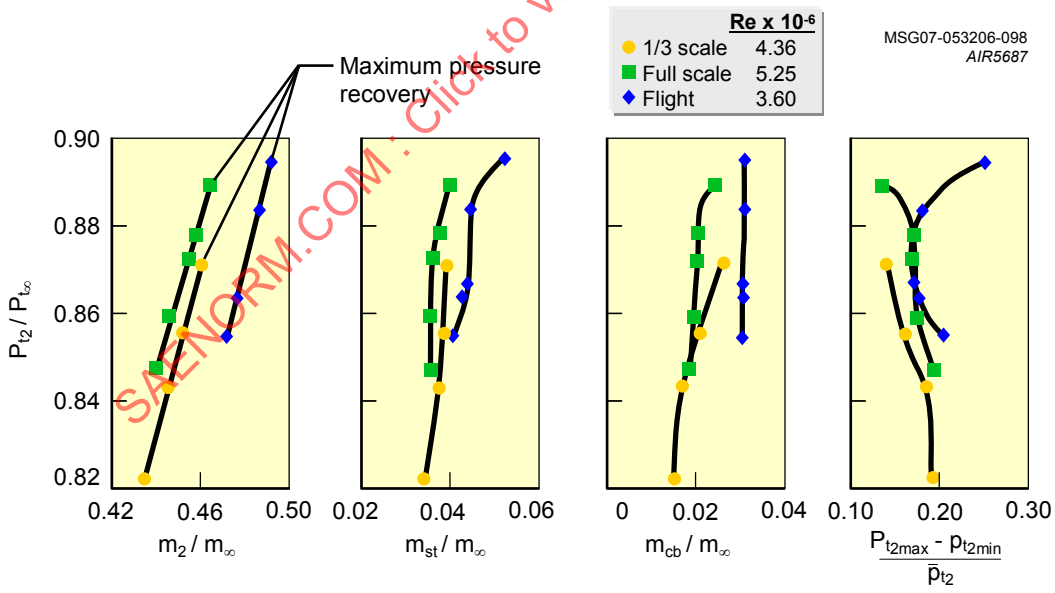

FIGURE 16 - YF-12 PERFORMANCE AND DISTORTION, MACH 2.1

5.1.2.5 Findings of the Original YF-12 Studies

The results of the original YF-12 research indicated:

- Wind-tunnel results were a satisfactory indication of flight performance when inlet operating conditions were matched.
- Testing at less than flight Reynolds numbers did not affect data comparisons.
- Nonuniform flow at flight conditions did not have a detrimental effect on inlet performance.

In general, comparison of steady-state data between ground and flight test was of sufficient quality that expectations were that similar comparisons would be found using inlet dynamic data.

5.1.2.6 S-16 Committee Observations of YF-12 Data

The results of the YF-12 case study highlight the need to ensure consistent inlet operating conditions for mixed-compression inlets. Seemingly insignificant geometry or secondary massflow control variations can result in substantial differences in total-pressure recovery and distortion. It is felt, however, that when geometric and aerodynamic similarity is maintained, then satisfactory correlation between ground and flight-test inlet data will be found. No references presenting the dynamic total-pressure data have been found.

5.1.3 F-15 Case Study

NASA sponsored an effort with McDonnell Douglas Corporation (MDC), currently The Boeing Company, to determine if time-variant distortion data taken from a subscale inlet model could be used to accurately predict the distortion levels for the full-scale vehicle (Reference 2.2.12). F-15 subscale inlet data obtained by MDC during the F-15 development program were compared with F-15 flight-test inlet data obtained by NASA during an F-15 inlet/engine compatibility flight-test program. Other researchers (References 2.2.13 to 2.2.17) documented the F-15 development and compared the full-scale inlet flight data with both full-scale and subscale wind-tunnel data.

5.1.3.1 Test Item Configurations

The F-15 inlet configuration was a two-dimensional external compression, overhead variable capture area design with three horizontal compression ramps and an internal diffuser ramp. This inlet is seen in Figure 17. Boundary-layer bleed systems included the porous surfaces on the second and third ramps, a throat slot bleed, and inboard/outboard sidewall bleeds. The throat slot flow exits through a bypass door for inlet/engine airflow matching. The inlet was offset from the fuselage with a boundary-layer diverter to preclude the ingestion of the fuselage boundary layer.

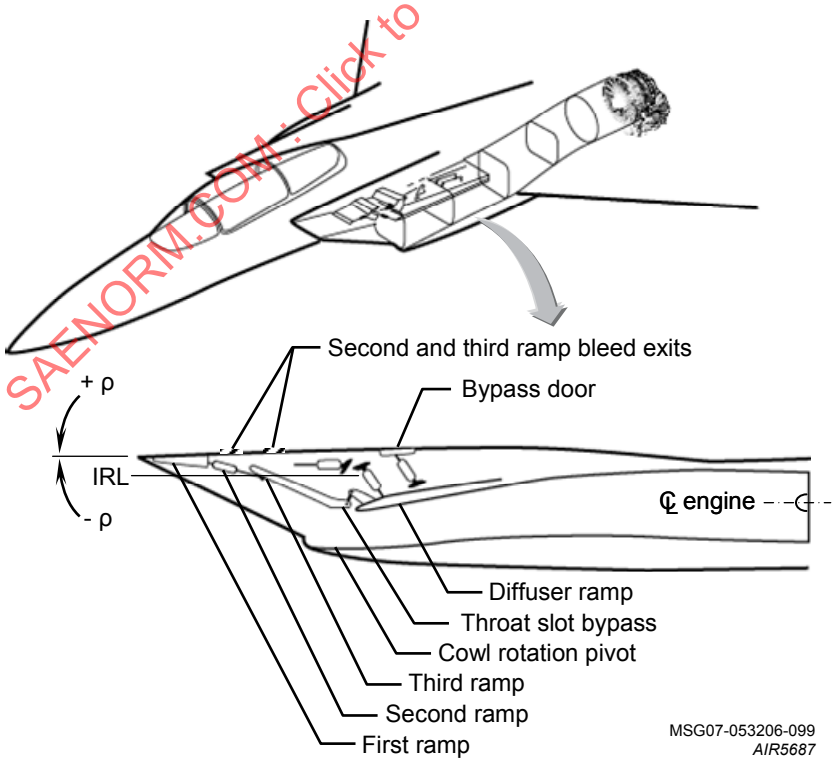

FIGURE 17 - F-15 INLET CONFIGURATION

Test articles included a 1/6th-scale forebody-inlet wind-tunnel model, a full-scale inlet model with partial forebody, and a full-scale flight-test aircraft. The full-scale inlet model with partial forebody was tested with and without a full-scale engine. These test articles, referred to as the subscale model (1/6th scale), full-scale with engine (FSE), full-scale with cold pipe[1] (FSCP), and the full-scale flight-test vehicle (FLT) are shown in Figure 18.

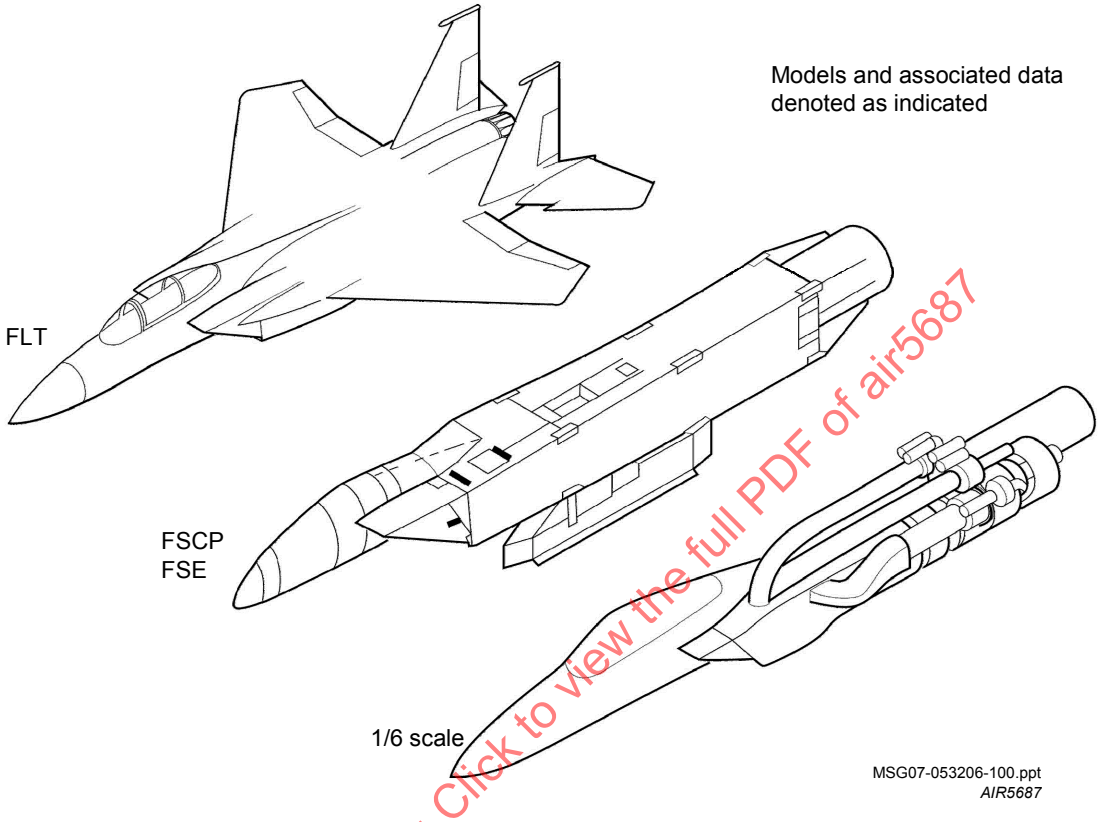

FIGURE 18 - F-15 INLET TEST ARTICLES

The 1/6th-scale model consisted of a fuselage forebody assembly, a remotely controlled left inlet with true aerodynamic configuration up to the AIP. The duct aft of the AIP station included a remotely-actuated massflow plug. The boundary-layer bleed systems were scaled identical to the air vehicle, but airflow was controlled using ducts with massflow plugs. A modification of the boundary-layer diverter offset, Y_{Div}, for the 1/6th-scale model was made to account for Reynolds number and scale difference between model scale and full scale using the following scaling relationship

$$\frac{(Y_{Div} - \delta)_{FS}}{(Y_{Div} - \delta)_{MS}} = \frac{D_{FS}}{D_{MS}}$$

where δ is the boundary-layer thickness on the fuselage at the leading edge of the compression ramp, and D was the diameter of the AIP. The full-scale boundary-layer thickness was estimated using a flat plate at Mach 2.2 at 40,000-foot altitude; a similar procedure was used to estimate the boundary-layer thickness for a model-scale flat plate at Mach 2.2 at test Reynolds numbers.

The full-scale inlet wind-tunnel models (FSE and FSCP) were constructed of full-scale flight weight hardware and represented the true aerodynamic configuration and control system. The full-scale model could not be tested with the complete forebody because of tunnel blockage limitations. Partial forebodies were designed to simulate the local transonic and supersonic inlet-approach flowfields using data from an F-15 forebody flowfield development test. For the FSE, an XF100-PW-100 ground test engine was used. This engine had the same basic aerodynamic configuration as production F100 engines. The FSCP hardware consisted of a straight pipe with a mass flow-metering device mounted in place of the engine.

[1] Cold pipe refers to testing large or full-scale models without the presence of an engine or propulsion simulator.

The flight-test aircraft (tail number AF 71-0281) was used during the F-15 propulsion-system development flight-test program. The left engine nacelle was instrumented with an AIP rake having 48 high-response pressure sensors. The flight-test aircraft was powered by two Pratt & Whitney F100-PW-100 turbofan engines.

Reference 2.2.13 contains substantial discussion of the steps taken to match inlet configurations, test conditions, airflow rates, and time record length in order to have valid scaling comparisons. For the references cited above, the full-scale wind-tunnel models and the flight-test aircraft had the same inlet configuration (e.g., inlet ramp positions and the bypass door position) that were tested during the 1/6th-scale test.

5.1.3.2 Test Conditions

The test conditions (quasi-steady) included Mach number, angle-of-attack, and angle-of-sideslip, and are shown in Table 3.

TABLE 3 - F-15 TEST CONDITIONS

Parameter	Minimum	Maximum
Mach	0.4	2.5
Angle of attack	–10 deg	12 deg
Angle of sideslip	0 deg	10 deg
Percentage airflow	47.3	108.6
Reynolds number/FT (million)	0.2	3.6

5.1.3.3 Data Acquisition, Processing, and Analysis

An exact match of scaled inlet corrected airflow rates was not possible because the maneuvering flight-test conditions required maximum throttle position. Hence, only one flight airflow rate was available for comparison with the wind tunnel. If the wind-tunnel articles did not test at the corresponding flight corrected airflow rate, then the wind-tunnel data was interpolated between the two corrected airflow rates bracketing the flight-test corrected airflow rate. The interpolation technique assumed linear relationship of the Pratt & Whitney distortion descriptor parameters (both circumferential and radial components) with corrected airflow rate. In the data which follow, flagged symbols indicate interpolated data. The Pratt & Whitney distortion descriptors are defined in Reference 2.2.10.

During the flight test, it was not possible to hold the aircraft in extreme maneuver conditions and maintain Mach number and altitude. The flight-test data record lengths ranged from 0.6 to 2.8 seconds, resulting in equivalent data analysis time for the 1/6th-scale wind-tunnel model test of 0.1 to 0.5 seconds, respectively. According to Reference 2.2.10, the time variant data were random and statistically stationary. The frequency scaling of the dynamic distortion data were nominally filtered at 170 Hz for full scale (the cutoff frequency for the F100-PW-100 1/rev fan speed), while the 1/6th -scale data were filtered at 1040 Hz. (Note that the frequency scaling was not exact due to limitations of the filtering equipment.)

For the F-15 development program, the AIP total-pressure instrumentation had 48 low-response and 48 high-response total-pressure probes located on equal-area centers in an eight-leg and six-ring configuration. The same engine-face rake was used for both the full-scale wind-tunnel tests and the flight tests. The 1/6th-scale test engine-face rake was scaled to the full-scale configuration.

5.1.3.4 Results and Discussion

The effects of scaling and testing techniques were determined for the following (1) geometric scaling, (2) presence of engine, (3) Reynolds number, and (4) cutoff frequency effects. These are described below.

5.1.3.4.1 Engine Presence

The effect of engine presence on the distortion levels was obtained for supersonic freestream conditions using the data from the FSE and the FSCP. The parameters examined included steady-state and instantaneous total-pressure patterns, total-pressure recovery, turbulence levels, and fan distortion descriptors. The instantaneous total-pressure contours are compared in Figure 19. The contour patterns demonstrated satisfactory agreement with the low- and high-pressure in the same location, and a similar angular extent of the low pressure region. Total-pressure recovery, turbulence levels, and fan distortion descriptor (P&W parameter K_{a2}) are shown in Figure 20. The presence of the engine had a small favorable effect on these parameters. Note the turbulence levels were relatively low.

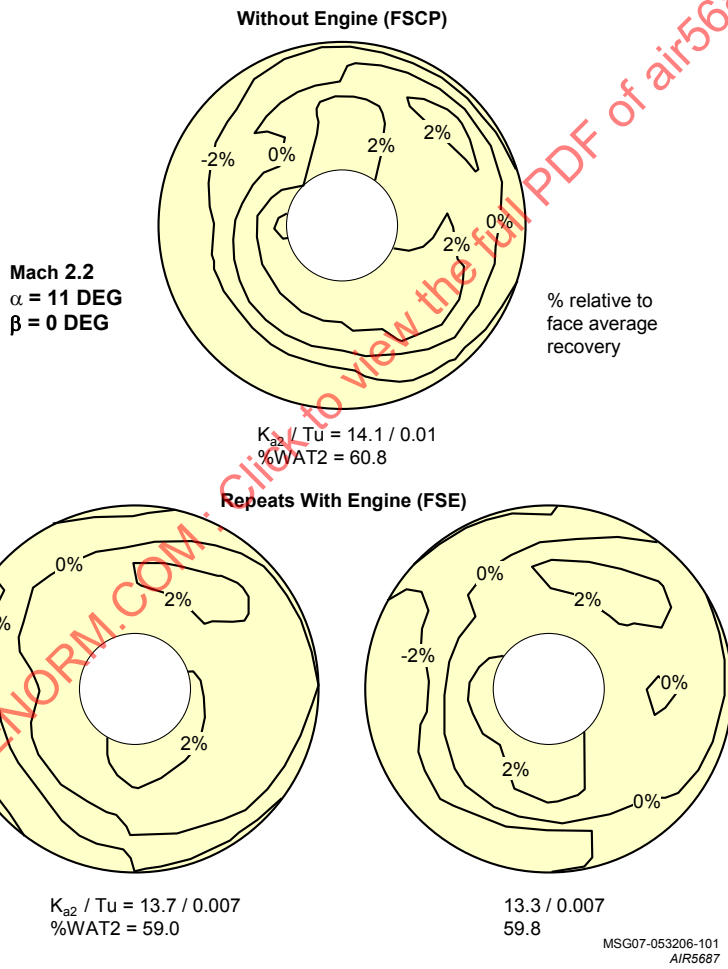

FIGURE 19 - EFFECT OF ENGINE PRESENCE ON PEAK DISTORTION

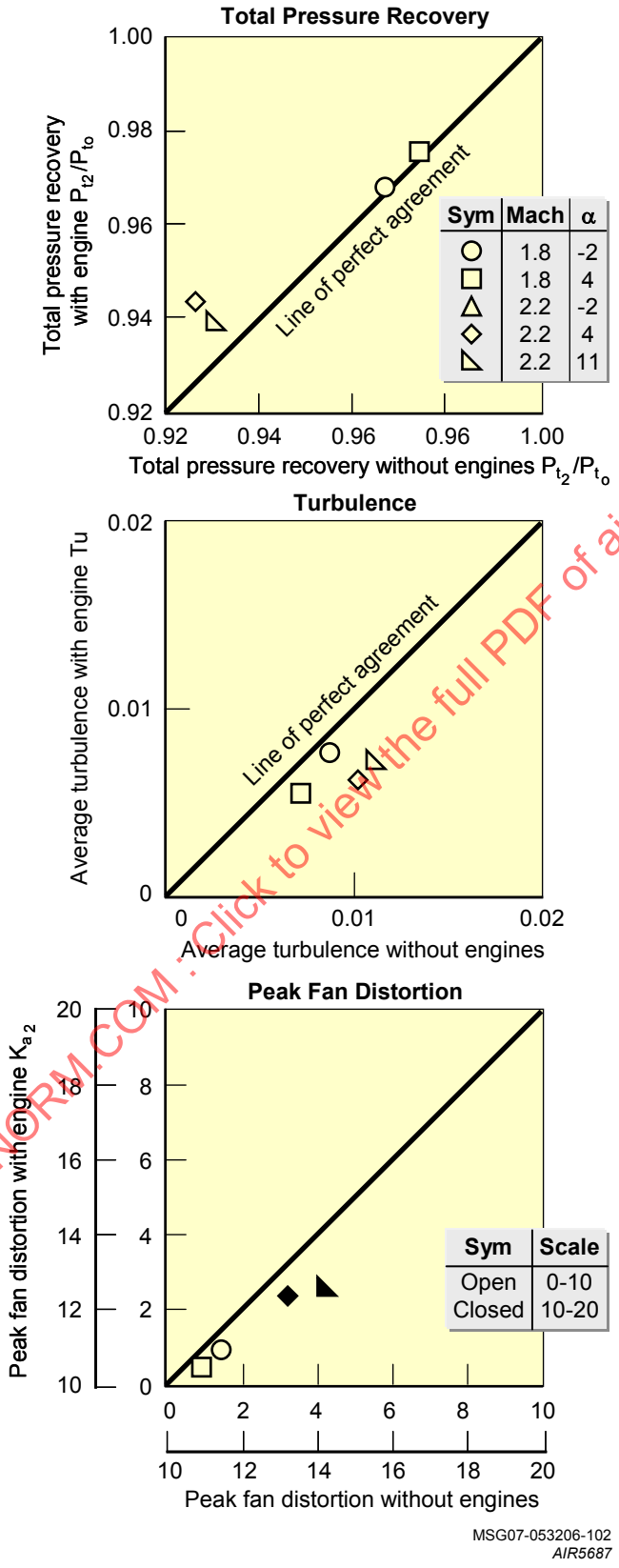

FIGURE 20 - EFFECT OF ENGINE PRESENCE ON INLET PERFORMANCE PARAMETERS

5.1.3.4.2 Scaling and Reynolds Number

A representative set of comparisons for total-pressure recovery, turbulence levels, and fan distortion values as a function of Reynolds number are shown in Figure 21. The Reynolds number was based on a reference length of 1-foot for full scale and 1/6-foot for model scale. The steady-state data exhibited the same trends as the corresponding peak dynamic data. The data in Reference 2.2.10 indicated, that with few exceptions, the expected trends of increasing total-pressure recovery and decreasing turbulence and peak dynamic distortion with increasing Reynolds number. Note again the turbulence values were low and that flagged symbols indicated interpolated data.

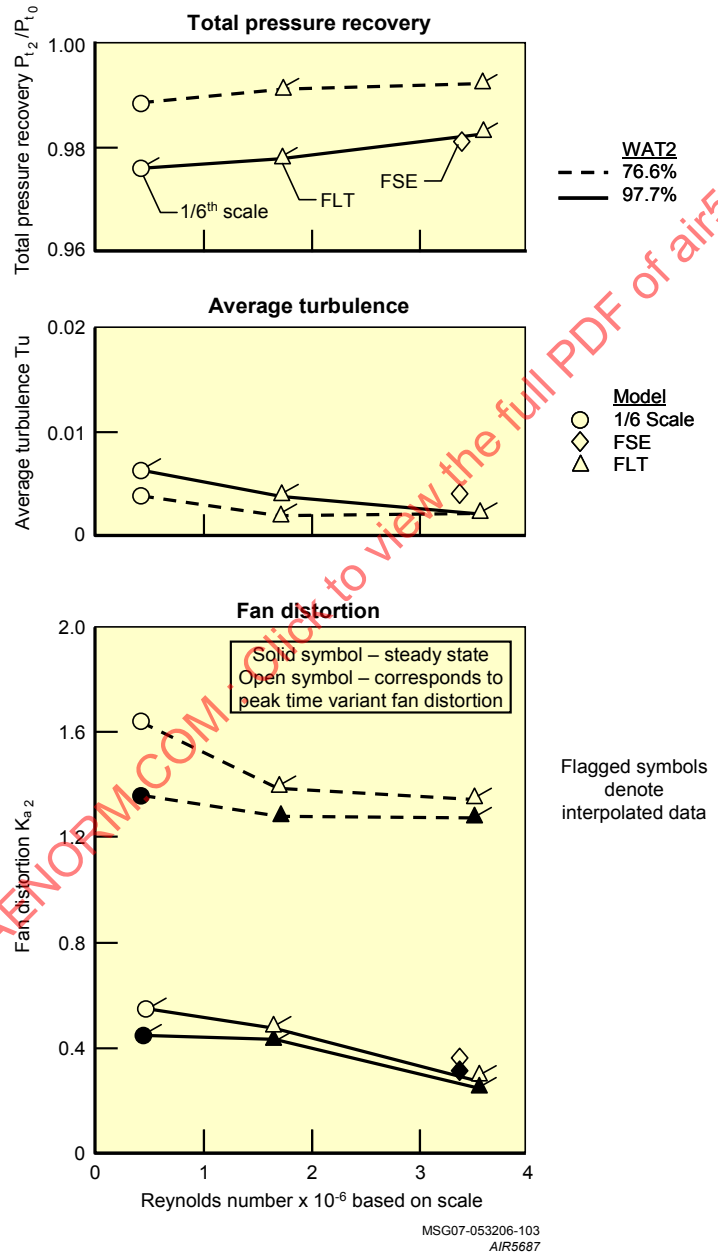

FIGURE 21 - REPRESENTATIVE EFFECT OF REYNOLDS NUMBER AT MACH 0.6, α = 4 DEG, β = 0 DEG

5.1.3.4.3 Frequency Content

The effect of low-pass filter cutoff frequency on turbulence and peak dynamic distortion was also evaluated. Filter cutoff frequencies used for full-scale data were 45, 100, 170, and 500 Hz resulting in 275-, 615-, 1040-, and 3070-Hz cutoff frequencies for 1/6th scale, respectively. As expected, the turbulence and calculated peak dynamic distortion increased with filter cutoff frequency in both scales. This was due to more local peaks being included as filter frequency increased, with an increased probability for higher absolute peaks. The combined effects of filter cutoff frequency and Reynolds number on peak time variant fan distortion and turbulence levels are shown in Figure 22. The data were consistent with Reynolds number and scale effects. As cutoff filter frequency was increased, the peak time variant fan distortion and turbulence levels increased.

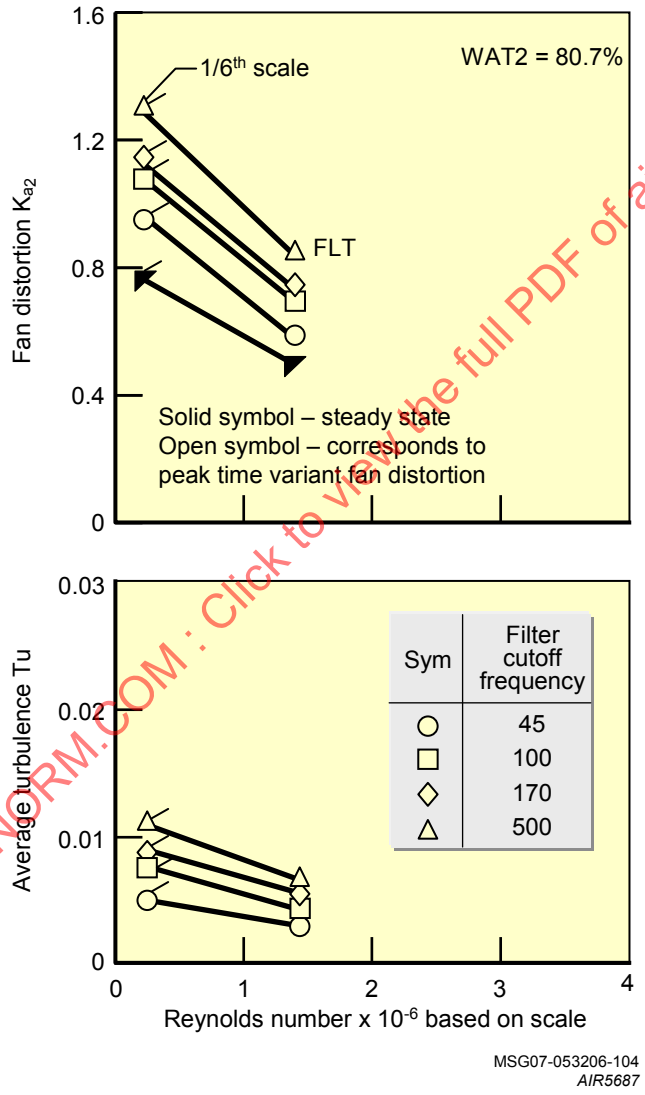

FIGURE 22 - EFFECT OF FILTER FREQUENCY ON INLET DATA AT MACH 1.8, α = -2 DEG, β = 0 DEG

5.1.3.5 Findings of the Original F-15 Study

The results of the original F-15 research indicated:

- Increasing Reynolds number and scale led to increasing pressure recovery, and decreasing turbulence and distortion.
- Increasing the filtering cutoff frequency led to increased magnitudes of turbulence, and distortion.
- The presence of an engine had small favorable influences on recovery, turbulence and distortion.
- Peak distortion obtained using a subscale model was representative of distortion obtained in flight.

5.1.3.6 S-16 Committee Observations of F-15 Data

Within the data examined here, there is evidence that increasing Reynolds number has a favorable effect on total-pressure recovery and distortion parameters. Further, examination of Figure 21 indicates the possiblility of turbulence and distortion becoming independent of Reynolds number when Re increases beyond a critical value (seen here to be approximately 2×10^6).

Examination of Figure 20 indicates that dynamic pressure distortion data obtained from ground tests of full-scale inlets without engines are marginally higher in magnitude than that which would be obtained when tested with an engine.

Scaling rules for the boundary-layer diverter standoff distance and bleed systems were successful for the F-15.

5.1.4 B-1 Case Study

The B-1 was developed in the 1970s to provide a replacement for the B-52. The B-1A was a variable sweep supersonic aircraft with podded nacelles in a wing-shielded installation. Each nacelle included two vertical ramp external compression inlets mounted back-to-back, feeding two engines. The initial bomber, subsequently given the B-1A designation, was to be a long-range vehicle capable of speeds up to Mach 2.2. The B-1A production program was cancelled in 1977, although flight testing continued into 1981. The B-1 was returned to development in 1981. A reduction in the maximum Mach number requirement for the aircraft permitted a simpler fixed inlet. The redesigned vehicle, designated the B-1B, will not be addressed in this report.

The B-1A had an extensive inlet test program, providing an opportunity to compare three different scale models with flight-test data. Initial inlet development tests were conducted using a 0.1-scale model in the Rockwell International 7- by 7-foot trisonic blowdown wind tunnel and at the AEDC's 16-foot transonic (16T) and supersonic (16S) wind tunnels. Following the development tests, a 0.2-scale model was tested in 16T and 16S. A full-scale model was then tested in 16T and 16S, both in a cold pipe mode and with an operating engine. The wind-tunnel testing was followed by a series of flight tests.

The data presented here are from the wind tunnel and flight tests for the B-1A configuration (References 2.2.18 and 2.2.19). Sketches of the aircraft and inlet are shown in Figure 23.

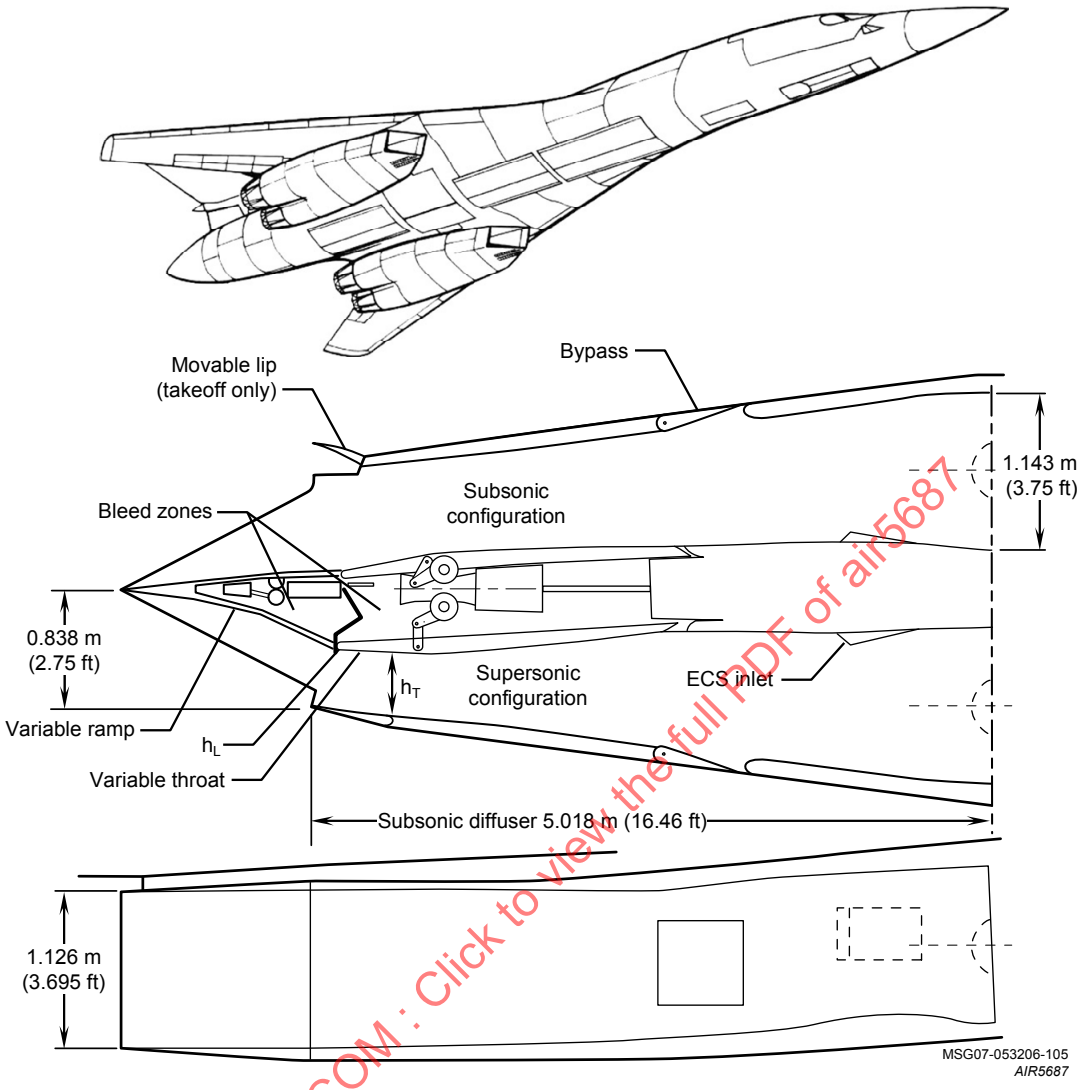

FIGURE 23 - B-1 AIRCRAFT AND INLET DETAILS

5.1.4.1 Test Article Configuration

The inlet for the B-1A propulsion system was a variable geometry, two-dimensional, multi-ramp, external compression design with provisions for engine airflow matching by use of a bypass system. The inlet duct was relatively straight, with a length-to-diameter ratio of 4.3, a butt line offset of 0.28, and a waterline offset of 0.13. The compression system consisted of one fixed ramp and two movable ramps followed by a variable throat (fourth) ramp. Boundary-layer control (BLC) was provided through porous surfaces on the third ramp, fourth ramp, and portions of the upper and lower endplates (i.e., sidewalls). The low-pressure air from the third ramp and endplates was discharged through fixed aft-facing louvers under the nacelle. The air from the throat ramp was discharged under the nacelle through doors that were open only at supersonic speeds. A movable lip was opened for takeoff and landing conditions to reduce losses due to separation at the cowl leading edge (Reference 2.2.20) and hence, to increase AIP total-pressure recovery.

All B-1A wind-tunnel inlet models were mounted on struts installed in the tunnel floor. The models were mounted in the inverted position to minimize strut interference, facilitate handling of bulky hardware, and simplify model configuration changes.

Both the 0.1- and 0.2-scale wind-tunnel models included a complete forward fuselage, a major portion of the wing, and a complete left-hand nacelle with both inlets (Figure 24 and Figure 25). The 0.2-scale model was designed specifically for use at AEDC and was as large as the shock rhombus in 16S would permit. This model was the major source for subscale inlet/engine compatibility data because its use in a continuous-flow tunnel provided the desired data sampling time, and because its size was favorable from the standpoint of data scaling, the installation of instrumentation, and the duplication of the boundary-layer bleed passages.

The 0.1-scale model had a nominal diverter height of 0.7 inches, with shims that could be installed or removed to change diverter height (Reference 2.2.21). No information was available about whether the diverter height was actually changed during any of the tests. For the 0.2-scale model, the diverter height was fixed at 1.4 inches (Reference 2.2.22). The full-scale model had a 3.8 inch diverter height.

MSG07-053206-106
AIR5687

FIGURE 24 - 0.1-SCALE B-1A IN AEDC TUNNEL 16S

MSG07-053206-107
AIR5687

FIGURE 25 - 0.20-SCALE B-1A INSTALLED IN AEDC TUNNEL 16S

The full-scale inlet wind-tunnel test article was actual flight hardware (Figure 26). Only the outboard inlet was functional. Because the model was so large, the full-scale portion of the wing necessary to duplicate the local flow into the inlet could not be installed in the wind tunnel. Instead, a wedge-shaped plate provided the correct local flowfield, with the design based on results from the 0.1-scale inlet wind-tunnel test (Reference 2.2.19). The size of the model precluded any ability to change model attitude, so the outboard inlet was tested at a fixed 2.67-degree angle of attack and 0.5-degree sideslip angle, approximating the nominal cruise flowfield. In the case where the full-scale inlet wind-tunnel model was tested with an engine, an XF101-GE-100 was used. While the inlet was mounted inverted, the engine was installed right side up. Sketches of all the models are shown in Figure 27.

MSG07-053206-108
AIR5687

FIGURE 26 - FULL-SCALE B-1A IN AEDC TUNNEL 16T

Each test article had a somewhat different arrangement of the AIP instrumentation. All wind-tunnel models and flight-test vehicles used a 40-probe ring/rake array (5 rings, 8 rakes) with steady-state and high-response total-pressure probes. The 0.1-scale inlet model had rakes evenly spaced at 45 degrees apart, with the whole array clocked 22.5 degrees from top dead center. The 0.2-scale inlet model had a rake array arrangement identical to the full-scale flight-test vehicle, but rotated by 1 degree clockwise looking aft. The full-scale wind-tunnel test article inlet array was integral with the engine front frame, with rakes positioned at 8, 44, 98, 134, 188, 224, 260, and 314 degrees from top dead center. Because the inlet was inverted on the full-scale wind-tunnel test, but the engine face frame installed right side up, this arrangement represents a 180-degree rake rotation for both the cold pipe and operational engine wind-tunnel tests relative to the flight-test aircraft (Reference 2.2.19).

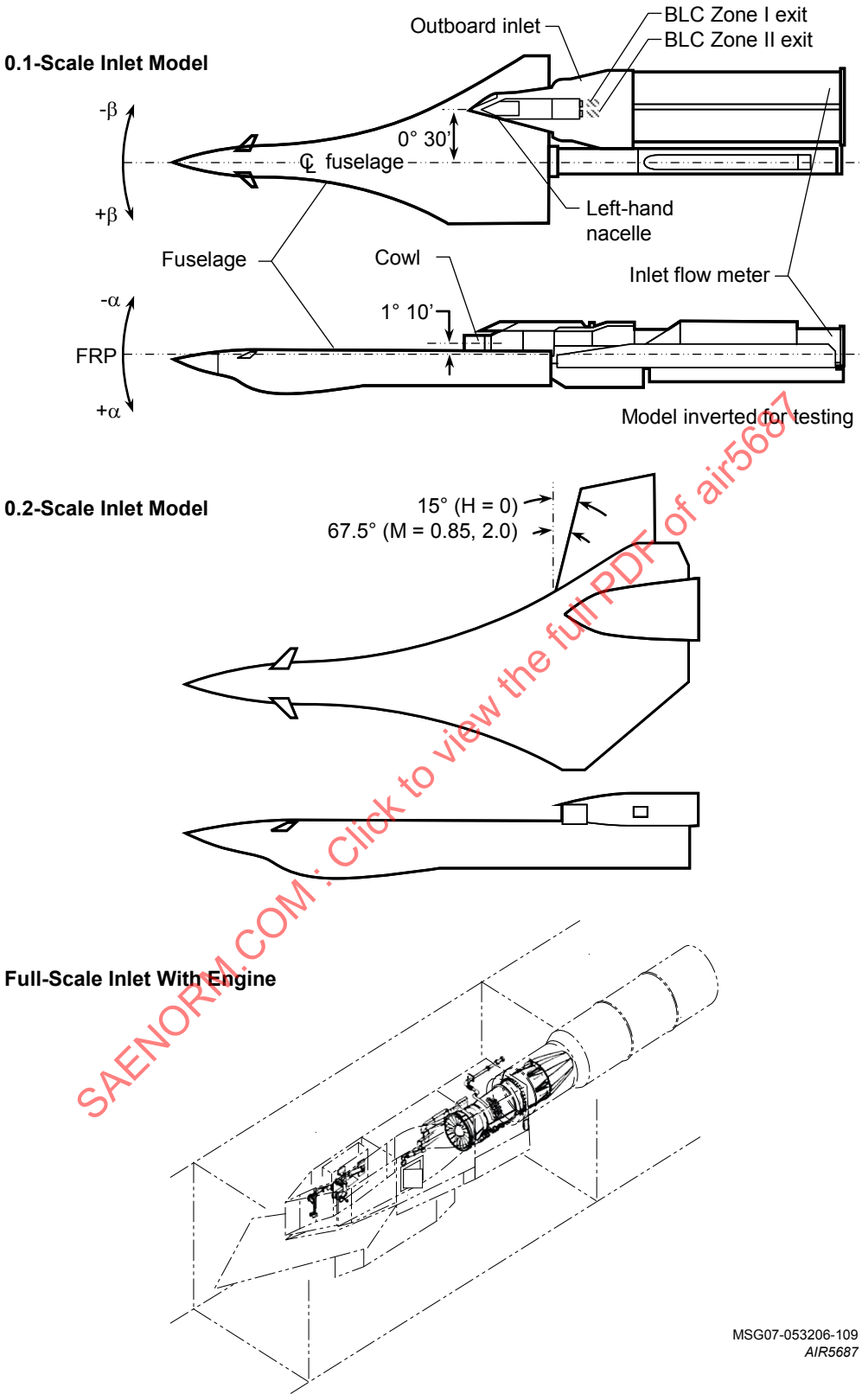

FIGURE 27 - DETAILS OF B-1A INLET WIND TUNNEL MODELS

The AIP probes for the wind-tunnel models were of a concentric design, with the high-response transducer centered inside the tube used to measure the steady-state pressure. The high-response transducer measured only the dynamic portion of the signal while the steady-state pressure was measured by a separate transducer.

The flight-test vehicle used a single high-response absolute transducer for each AIP probe to measure the instantaneous absolute pressure. The zero offsets and sensitivities of the flight-test high-response transducers changed with temperature, time, and turbulence level. To ensure valid data, the transducers were equipped with a system that allowed them to be recalibrated and re-zeroed as required. During a typical flight test, a calibration was performed about once a minute (Reference 2.2.19).

5.1.4.2 Test Conditions

The 0.1-scale inlet model was used for initial development and was tested primarily at the Rockwell International 7- by 7-foot trisonic wind tunnel. The 0.2-scale and the full-scale inlet wind-tunnel models were tested at AEDC 16T and 16S. Flight-test aircraft were designated A/C-1 and A/C-2. Comparison data were available for freestream Mach numbers of 0.0, 0.85, and 2.00. The Reynolds number (based on the length of the subsonic diffuser) varied with Mach number, ranging from 3.6 to 95.3 million (Reference 2.2.19).

5.1.4.3 Data Processing Effects

All dynamic pressure data were filtered at cutoff frequencies corresponding to full-scale frequency of 62.5 Hz, which was based on the time for one revolution of the engine at design RPM (Reference 2.2.18). Johnson (References 2.2.18 and 2.2.19) also documented the character of the dynamic data for the various models scales and the effect of data processing on the peak dynamic distortion testing. All of the dynamic data was found to be random and statistically stationary.

5.1.4.4 Results and Discussion

Data comparisons included inlet performance, and steady-state and dynamic distortion at nominal design airflow and inlet geometry. The distortion indices were calculated using methodology provided by GE (Reference 2.2.19).

5.1.4.4.1 Effect of Reynolds Number and Scale

The data in Figure 28 and Figure 29 show the effect of Reynolds number and test article scale on several inlet performance and compatibility indices. Data are shown for all model scales and from the aircraft flight tests at M = 0.85 in Figure 28. The data were interpolated to nominal airflow values. Except at the lowest Reynolds number, the effects of Reynolds number and wind-tunnel model scale were insignificant for most indices. IDC (circumferential distortion index) was slightly lower for the full-scale model, which had values close to that of the flight-test aircraft. The flight-test aircraft had slightly lower IDL (combined distortion index, the primary compatibility index for this vehicle), IDR (radial distortion index), and IDT (total distortion index) values than the wind-tunnel test models. The data at the lowest Reynolds number included an indicated scatter band. This scatter was due to nonrepresentative flow separation in the inlet duct because of the low Reynolds number. This indicated that there is a lower limit to the Reynolds number at which testing should be performed to ensure flow similarity.

Figure 29 indicates the effect of Reynolds number and scale for M = 2.0. Data from the 0.1-scale model were not available for this condition. The wind-tunnel full-scale test was analyzed at a Mach number of 2.2, but the closest flight-test data comparison point was at M = 2.0. The flight-test data were also acquired at slightly off-schedule inlet geometry. Data from the 0.2-scale inlet test were used to adjust the recovery for the difference in Mach number. An examination of these data also determined that there were no differences in recovery or distortion for a range of inlet geometries, so no adjustment was necessary to account for the effects of the off-schedule geometry. The results showed recovery increasing as Reynolds number increased. Distortion indices for the flight-test vehicle were generally within the range of the wind-tunnel values for the different models with no apparent trends.

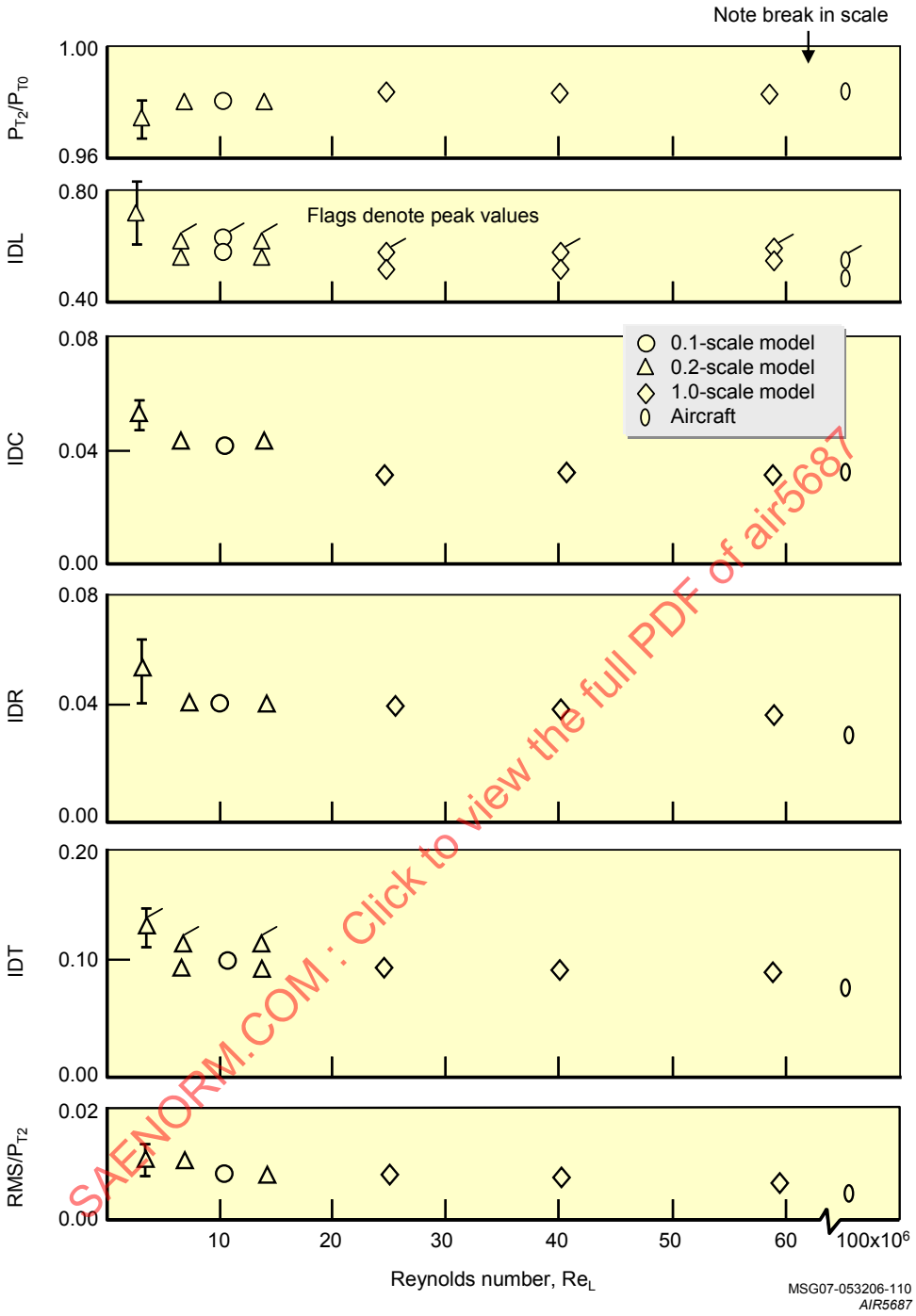

FIGURE 28 - EFFECT OF REYNOLDS NUMBER AND SCALE AT M = 0.85

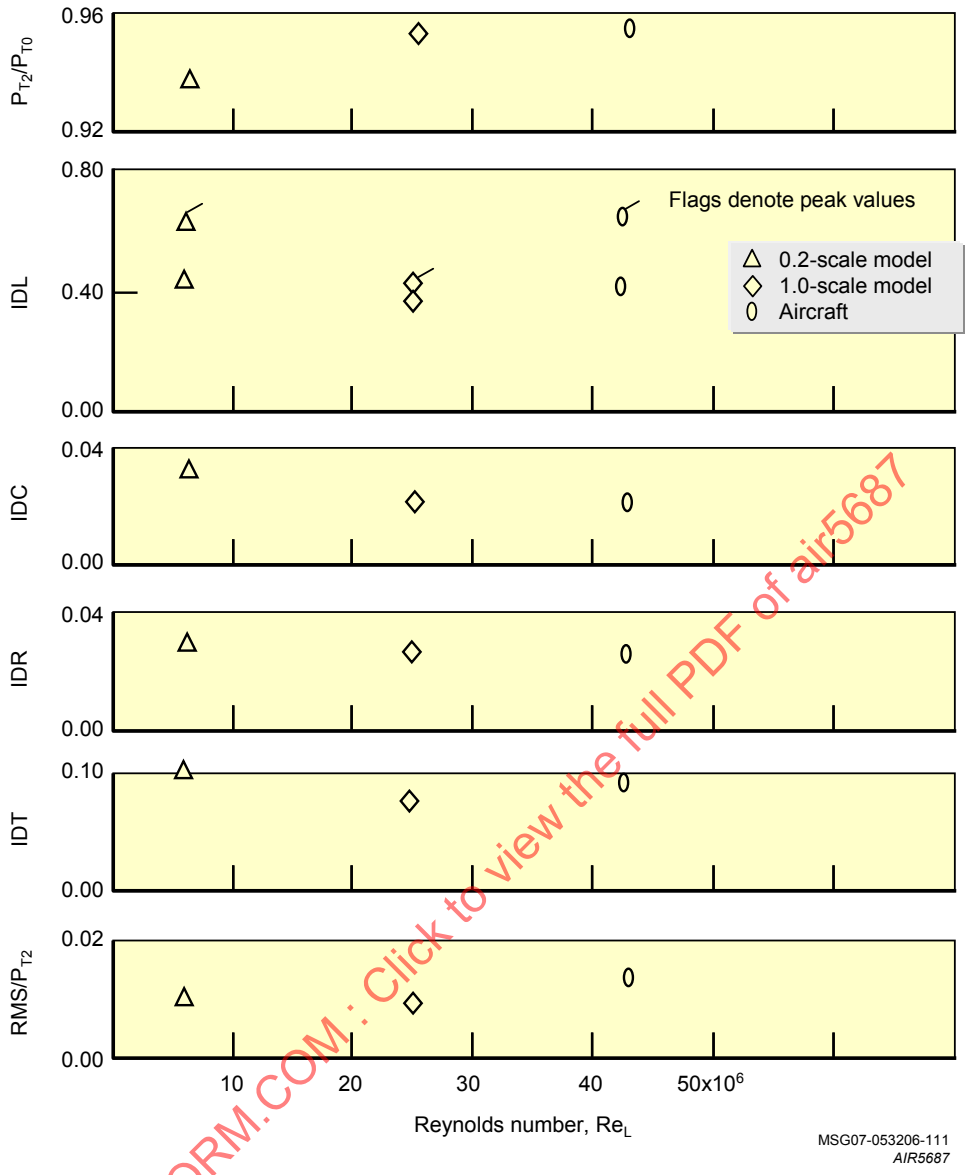

FIGURE 29 - EFFECT OF REYNOLDS NUMBER AND SCALE AT M = 2.0

Figure 30 contains the comparison of recovery and combined distortion between wind-tunnel model and flight tests at Mach numbers of 0.0, 0.85, and 2.0. The agreement at static conditions (M = 0) was very good. At M = 0.85, recovery was slightly higher and distortion slightly lower for the flight-test vehicle at both low and high angles of attack. At M = 2.0, the recovery for the flight-test vehicle was slightly higher than the full-scale wind-tunnel model and significantly higher than the 0.2-scale model. Flight-test distortion levels fell within the range of wind-tunnel test results at this Mach number (Reference 2.2.19).

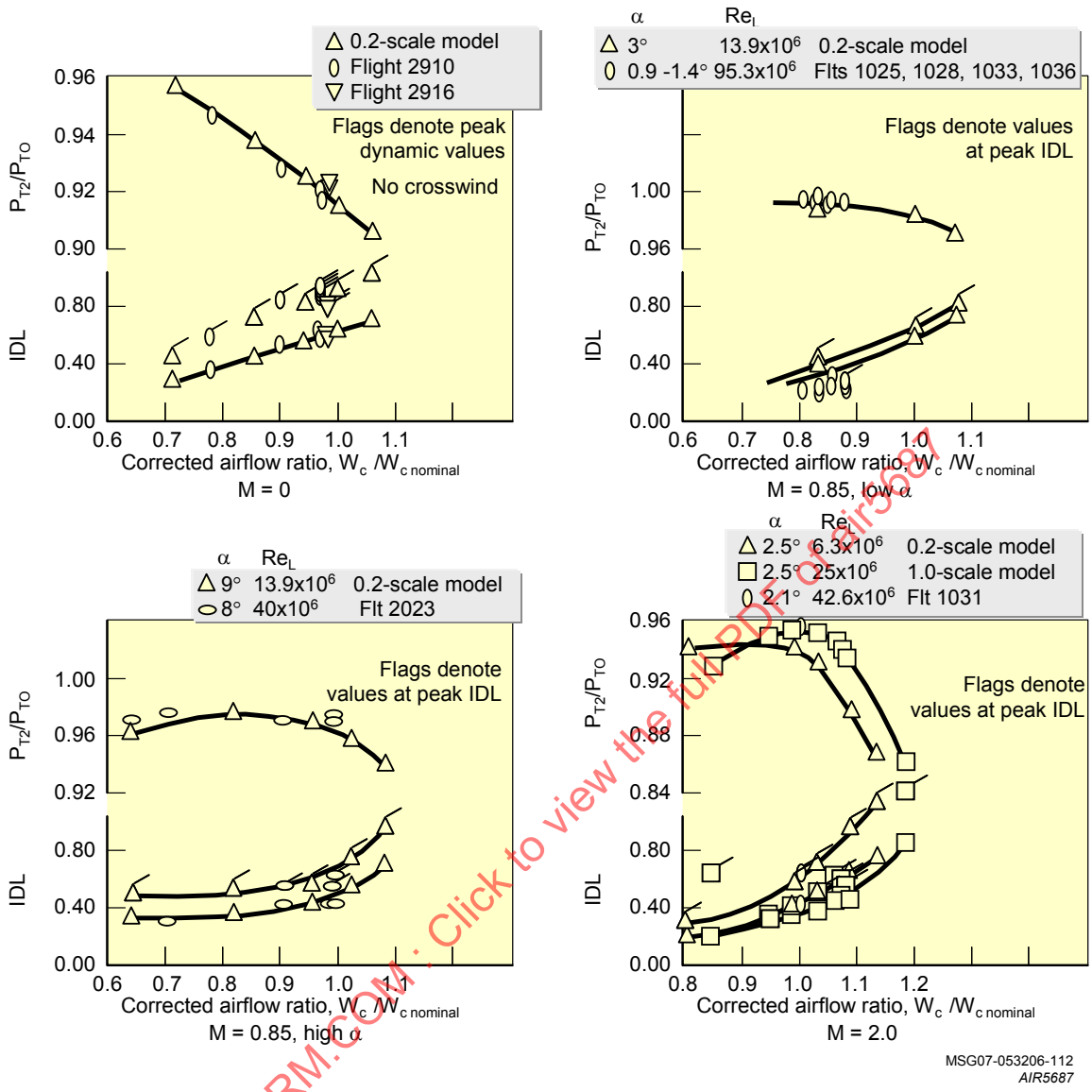

FIGURE 30 - COMPARISON OF FLIGHT TO WIND TUNNEL TEST

Other significant observations from Reference 2.2.19 are summarized in this paragraph. The effect of Reynolds number at constant model scale on distortion patterns was found to be negligible at Mach 0.85 and 2.0. The engine face turbulence patterns showed very little differences at various Reynolds numbers. The characteristics of the distortion time traces near the peak IDL value were similar. No significant differences were found in the power spectral densities at various Reynolds numbers. These results were also true for the effect of different model scales as well as the presence of the engine. The only case where these results were not true is when the Reynolds number was lowest and nonrepresentative flow separation occurred in the duct.

5.1.4.4.2 Effect of Engine Presence

The effect of engine presence was determined from the full-scale wind-tunnel inlet model, which was tested with a cold pipe and with the engine. Comparison data were available at Mach 0.0 (Figure 31) and Mach 2.2 (Figure 32). (Note that the supersonic flight-test data comparisons were at Mach 2.0, while these wind-tunnel data are at Mach 2.2.) In both cases, the difference between testing the inlet with a cold pipe and with an operating engine was negligible except for a small increase in total-pressure recovery with the cold pipe at static conditions (Mach 0.0). Static pressures around the circumference of the engine face hub and tip did not change significantly between the engine and the cold pipe.

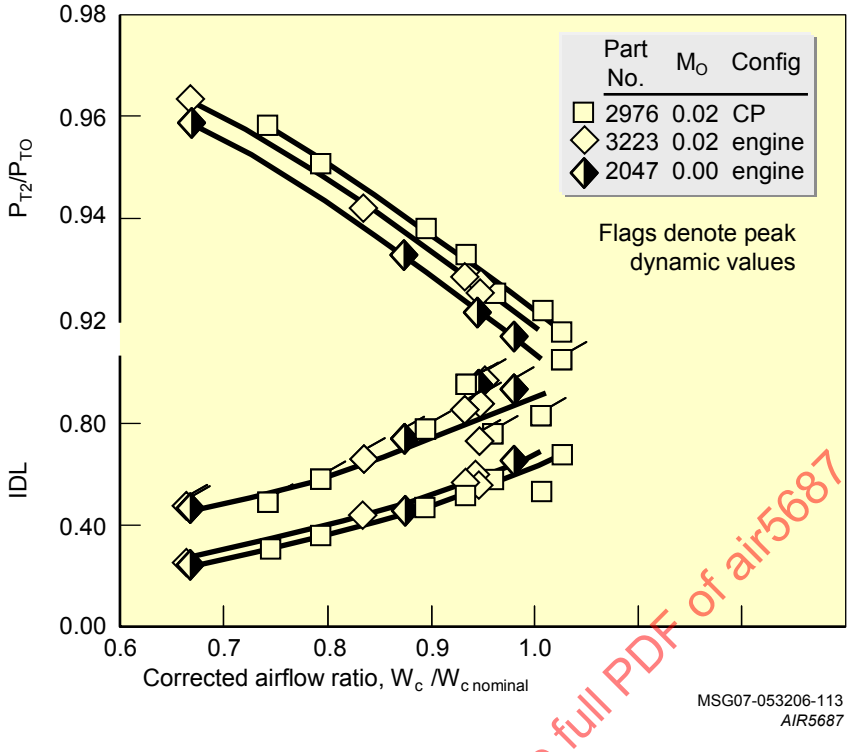

FIGURE 31 - ENGINE EFFECTS AT M = 0

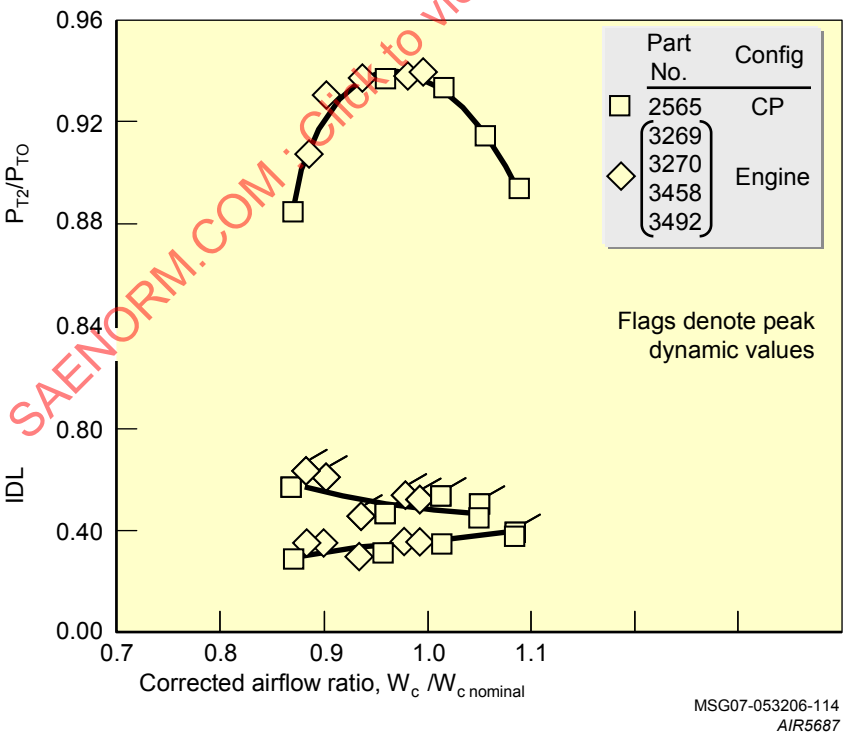

FIGURE 32 - ENGINE EFFECTS AT M = 2.2

5.1.4.5 Findings of the Original B-1A Study

The results of the original B-1A research indicated:

- Reynolds number effects due to model size or tunnel operating conditions were negligible at static conditions and Mach 0.85. The full-scale model and flight vehicle had higher pressure recovery and lower distortion at supersonic operating conditions.

- The presence of the engine in full-scale tests had no significant effect on engine face distortion or any other flow characteristic that was examined.

5.1.4.6 S-16 Committee Observations of B-1A Data

The data indicate that a threshold Reynolds number limit must be exceeded in order to have flow similarity. As seen in Figure 28, this threshold value is estimated to be about $Re_L \sim 5X10^6$. At Reynolds numbers below this value, duct separation may occur that is not representative of flow at realistic flight Reynolds numbers. For wind-tunnel tests, this implies a large model scale and sufficiently high freestream pressure.

Subsonic data correlate well between subscale wind-tunnel models, full-scale wind-tunnel test article, and flight-test vehicle. Supersonic data do not correlate as well as the subsonic data. The flight vehicle appears to pass higher airflow rates than the subscale model, a trend that has been noted for other vehicles and will be discussed further later.

5.1.5 F-18E/F Case Study

The F/A-18E/F is a fighter/attack aircraft designed to meet carrier-suitability, extended-range, high-maneuverability, and supersonic-dash requirements. The aircraft, powered by F414-GE-400 turbofan engines, has fixed-geometry waverider inlets located under each wing's leading-edge extension (LEX). Each inlet has two diverters, one located between the fuselage and inlet and the other between the LEX and the inlet. An ECS inlet is located within each subsonic duct. Steady-state and high-response total-pressure data were obtained during wind-tunnel and flight tests to assess inlet/engine compatibility. More detailed information may be found in Reference 2.2.23.

5.1.5.1 Test Item Configurations

The 17.6% scale integrated inlet/forebody wind-tunnel model (Model 404), seen in Figure 33, was representative of the F/A-18E aircraft back to the wing trailing edge. All external moldlines were geometrically scaled to the wing trailing edge with the exception of the wingspan, the boundary-layer diverter, and the inlet bleed system. The wing was truncated at 64% span. The diverter was scaled by boundary-layer thickness between a low-Reynolds-number flight condition and the nominal wind-tunnel condition. The inlet bleed system was simulated only on the port inlet. The bleed surfaces were located on the inboard and the upper compression ramps and the outboard cowl. The compression-ramp bleed surfaces were scaled between Model 404 and the flight vehicle by holding total porosity and hole length-to-diameter ratio constant. The port diffuser moldline was geometrically scaled to the AIP.

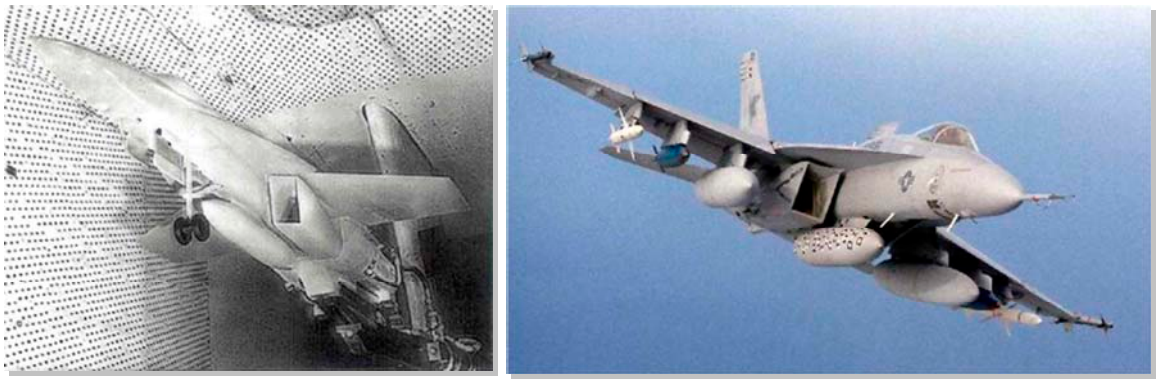

MSG07-053206-115
AIR5687

FIGURE 33 - F/A-18E INLET WIND TUNNEL MODEL 404 AND FLIGHT-TEST AIRCRAFT E2

The flight database was obtained using an Engineering and Manufacturing Development F/A 18E/F flight-test aircraft, designated E2, also seen in Figure 33. Although it was tested in various configurations, the data presented here represents that of a “clean” configuration (e.g., no external fuel tanks) with a flight-test nose boom.

5.1.5.2 Test Conditions

Wind-tunnel testing was accomplished in various facilities including Boeing’s Polysonic Wind Tunnel, the 11-foot Transonic Wind Tunnel at NASA Ames Research Center, and the Propulsion Wind Tunnel Facility at the AEDC. The data presented here were obtained in the early 1990s at AEDC’s Propulsion Wind Tunnels. Testing included a Mach number range from 0 to supersonic speeds beyond that of the flight aircraft, angles of attack and sideslip beyond that permissible by the flight aircraft, and inlet airflows from windmill to beyond maximum engine airflows. The test Reynolds number was nominally 2×10^6 per foot.

The inlet/engine performance and compatibility flight testing was conducted at the Naval Air Weapons Center – Aircraft Division, Patuxent River, Maryland, in the late 1990s. Data were obtained on the port inlet to compare with the wind-tunnel database, although the starboard inlet was also instrumented for efficiency in the flight-test program. Testing progressed from benign to aggressive flight conditions. Distortion data were acquired at roughly 500 points on about 60 flights using a fixed throttle with the aircraft attitude stabilized sufficiently long to obtain statistically significant sample sets. Flight speeds ranged from static to supersonic, and altitudes ranged from sea level to 45,000 feet.

5.1.5.3 Data Instrumentation, Acquisition, Processing, and Analysis

The AIP instrumentation was similar between the wind-tunnel model and the flight-test vehicle. Both were instrumented with 40 steady-state and high-response total-pressure probes located at centers of equal area in an eight-rake by five-ring arrangement. The wind-tunnel model had concentric steady-state and dynamic probes. The high-response output was digitally sampled for 6 seconds and summed to a reference pressure to arrive at an absolute pressure. The cutoff frequency for the high-response signals was determined from Strouhal scaling (further explained in Section 6.2) for the F414 engine and model scale.

The flight-test vehicle’s data-acquisition system was unique in that high-response absolute-pressure sensors were used. The probes were located to maintain similarity to the wind-tunnel model and were integrated into rakes mounted from the duct wall. The exposed length of the each probe was about 6.6 times its diameter. Each of the 40 probes was thermally stabilized at 225°F using an integral heater element. The probes had the required accuracy, and the result was a simple, low-cost instrumentation configuration for measuring both the steady-state and dynamic data. The overall pressure transducer/acquisition system had a flat response of ±1 dB over a frequency range of 0 to 225 Hz. Each probe’s signal was filtered, digitally sampled, and recorded on board for postflight processing.

The definitions and computation procedures used in assessing inlet/engine compatibility reflected a history of successful correlations of inlet-distortion effects for the F404 engine family. Inlet-performance parameters were computed using the steady-state and dynamic total-pressure measurands. These parameters included inlet recovery, circumferential and radial distortion, and planar wave indices. Definition of these indices may be found in Reference 2.2.24. For clarity here, the planar wave index, PWptp, was defined as

$$PWptp = \frac{\max\left[PT_{FAVk}\right]_{k=1,K} - \min\left[PT_{FAVk}\right]_{k=1,K}}{\overline{PT_{FAV}}}$$

where

k= Sample k of K total samples
K= Total samples
$\overline{PT_{FAV}}$ = Average Total-Pressure of AIP Probes
PT_{FAVk} = Instantaneous Spatial-Averaged Total-Pressure of AIP Probes

The data were screened to locate the maximum circumferential distortion index, $\overline{(\Delta PT/PT)}_{c_{max}}$, for adjacent ring pairs. The radial distortion, $\overline{(\Delta PT/PT)}_{r_{max}}$, corresponds to that present at the time of maximum circumferential distortion.

5.1.5.4 Results and Discussion

Recovery measured at transonic cruise speeds on the E-2 vehicle, as well as the Model 404, is found in Figure 34. Recovery is presented as a function of inlet airflow ratio. Inlet airflow ratio is defined as the ratio of the operating corrected airflow to the maximum corrected airflow of the wind-tunnel test data at that Mach number. Error estimates for the flight data are indicated. Good correlation between the flight-test data and the wind-tunnel data was found when the wind-tunnel data were interpolated to the flight-test conditions. Recovery is seen to drop off at lower airflows where it is observed that recovery is sensitive to angle-of-attack changes. At these low airflows, it appears that the flight and wind-tunnel recoveries have similar values.

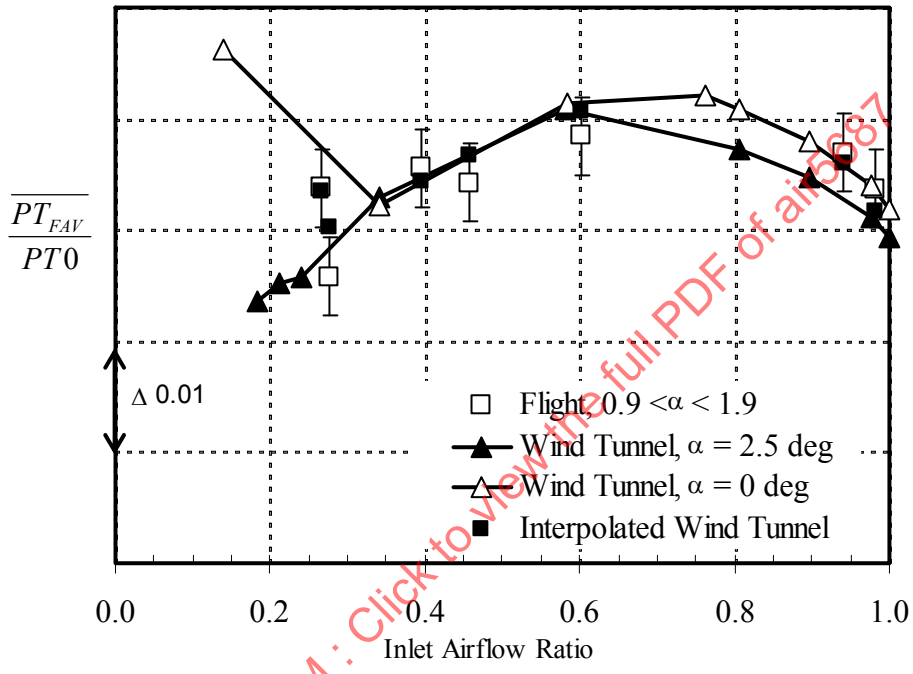

FIGURE 34 - INLET RECOVERY AT TRANSONIC CRUISE CONDITIONS

The variation of recovery with unit Reynolds number was measured in flight and the wind tunnel. The data were for cruise attitudes and engine power settings. The expected trends of increasing recovery with unit Reynolds number were found (Figure 35). The wind tunnel, flight and 1/7 power-law trend lines were well correlated. A correction of inlet recovery between wind tunnel and flight was warranted when correlated with Reynolds number.

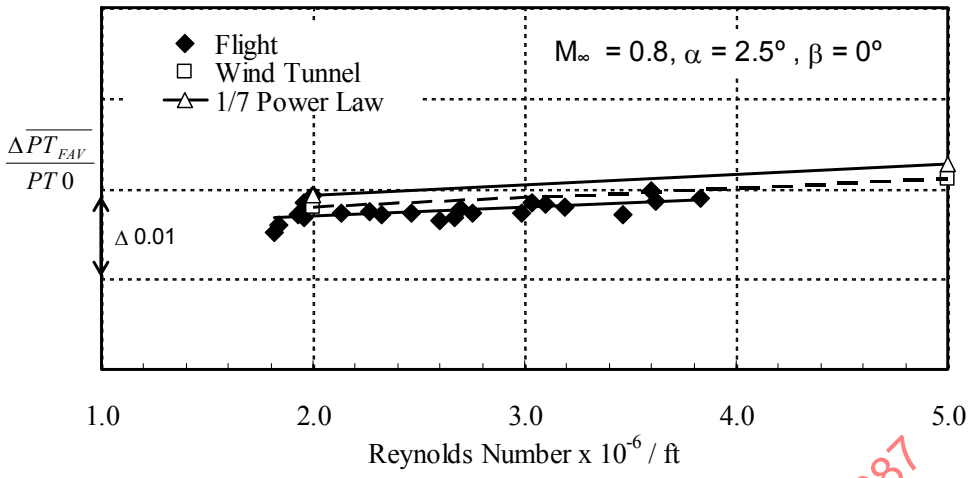

FIGURE 35 - INLET RECOVERY VARIATION WITH UNIT REYNOLDS NUMBER

At transonic cruise and maneuver flight conditions, distortion from the wind-tunnel tests correlated well with that found in flight. Magnitudes and trends in peak circumferential distortion with angle-of-attack correlated between wind tunnel and flight (Figure 36). The larger values of distortion were seen at cruise attitudes and decreased as the angle of attack was either increased or decreased. Circumferential distortion did not increase again until the angle of attack increased beyond 20 degrees or decreased beyond –3 degrees.

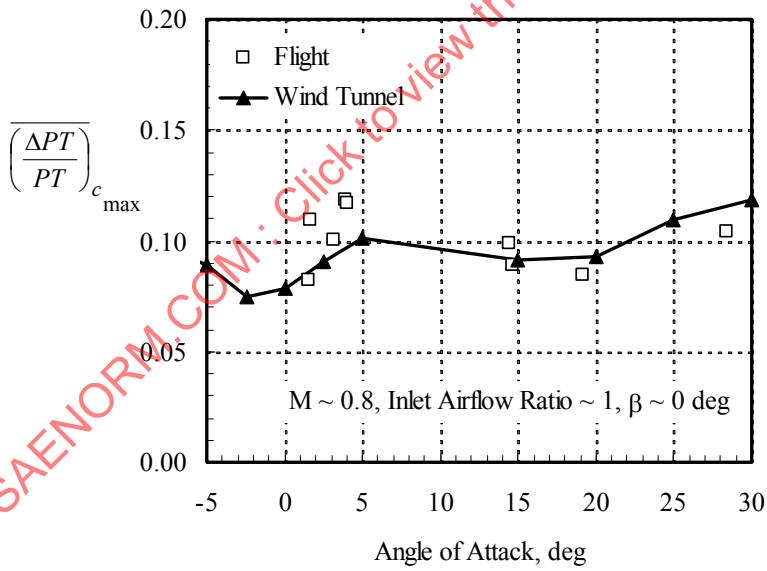

FIGURE 36 - PEAK CIRCUMFERENTIAL DISTORTION DURING MANEUVERS AT TRANSONIC SPEEDS

The peak radial distortion measured either in the wind tunnel or flight also correlated, Figure 37. Here, the largest values of peak radial distortion were measured about the cruise attitudes and decreased as angle of attack was either decreased or increased from there.

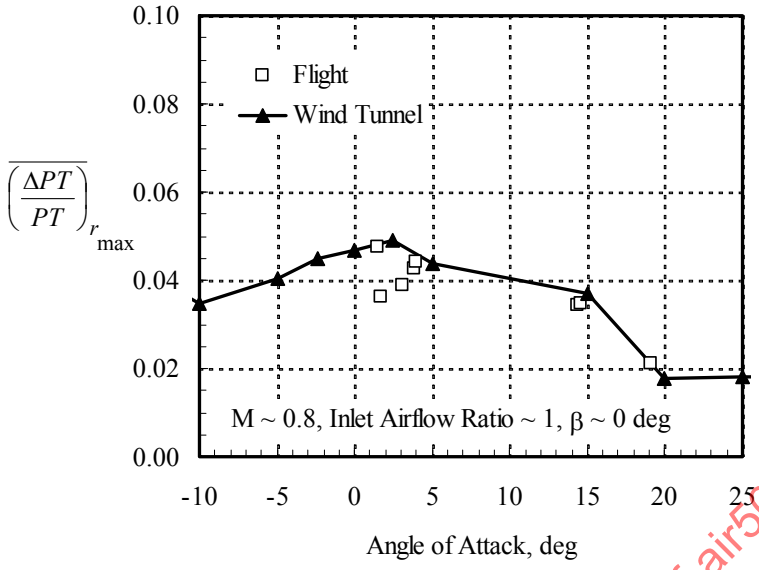

FIGURE 37 - PEAK RADIAL DISTORTION DURING MANEUVER AT TRANSONIC SPEEDS

High-response total-pressure patterns found in the wind tunnel and flight at the times of peak circumferential distortion may be seen in Figure 38. An instrumentation boom was on the flight vehicle but not on the wind-tunnel model. Flight-test booms as installed on the F/A-18E typically have minimal effect on total-pressure patterns at the AIP. The patterns presented were similar: a 180-degree one-per-revolution pattern having similar maximum and minimum pressures, with the wind-tunnel pattern being a good indication of that found later in flight. These patterns correspond to flight at M_∞ ~ 0.80 and α ~ 30 degrees with no sideslip.

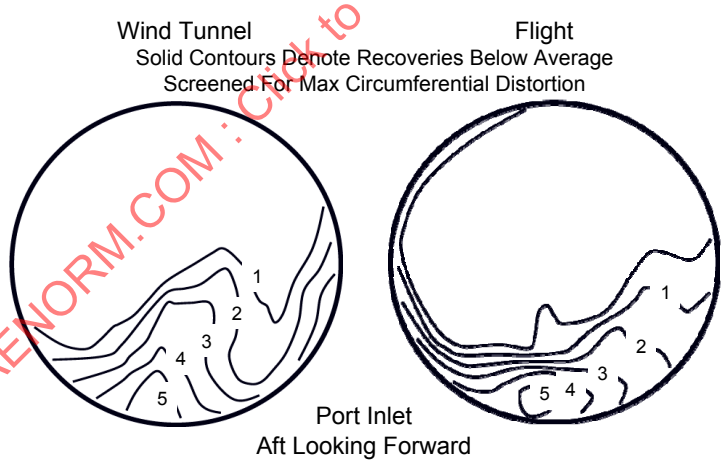

FIGURE 38 - PEAK TOTAL-PRESSURE PATTERNS DURING MANEUVER AT TRANSONIC SPEEDS

The planar wave content of the inlet flow found at transonic speeds in the wind tunnel was somewhat larger than that found in flight tests. As seen in Figure 39, planar wave content increased as the inlet airflow dropped below about an inlet airflow ratio of 0.6 in the wind tunnel. Sensitivity of planar wave content to model attitude was also found. In flight, similar increases were measured but at lower inlet airflow ratios.

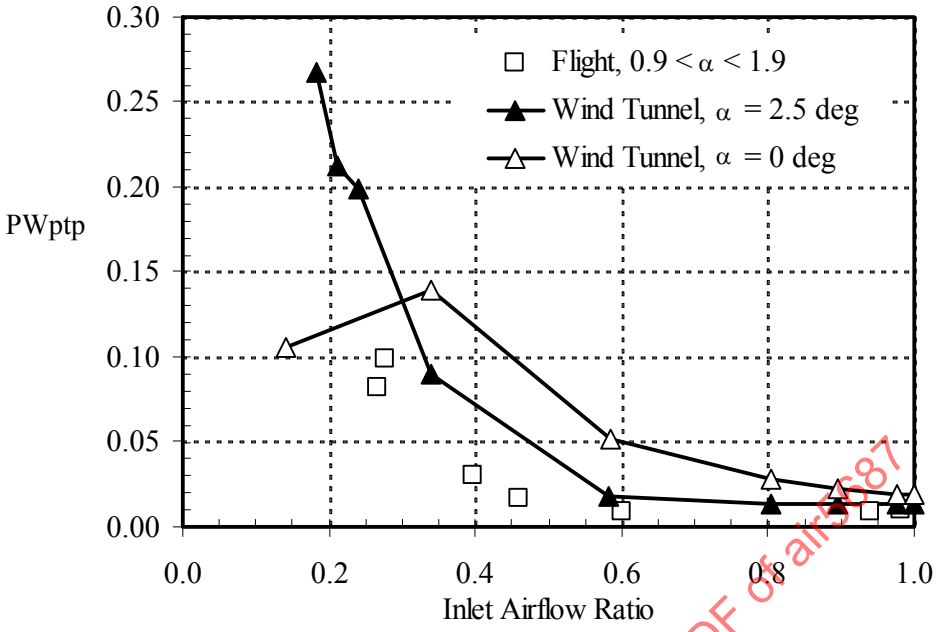

FIGURE 39 - PLANAR WAVE CONTENT AT TRANSONIC SPEEDS

At supersonic speeds the engine operates principally at high airflow. For high airflows, Figure 40, the recovery measured in flight correlates well with that found on the wind-tunnel model. The principal differences between the wind-tunnel and flight recoveries were found at reduced inlet airflows. Data analyses indicated that the bleed system of the flight vehicle passed more massflow resulting in higher recovery. As inlet airflow was reduced, the flow became unsteady, and it was difficult to determine, either in flight or wind tunnel, a steady-state total-pressure recovery. It should be noted that the acquisition of statistically stationary data is problematic when the inlet flow is unsteady.

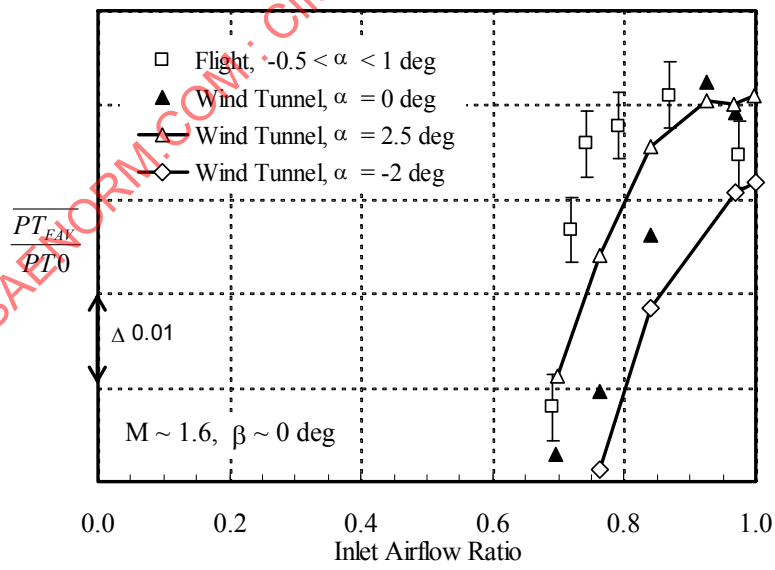

FIGURE 40 - INLET RECOVERY AT SUPERSONIC FLIGHT CONDITIONS

Peak circumferential distortion measured on the flight vehicle correlated well with that of the wind-tunnel model at high inlet airflows (Figure 41). However, as the inlet airflow was reduced, more pronounced differences between the flight and the wind-tunnel model were measured. This may be associated with unsteady flow at reduced airflows. From an overall standpoint, the values of the peak circumferential distortion index measured in the wind tunnel indicated that no operability issues should have been expected in flight, as indeed was the case. If anything, the wind tunnel provided a conservative estimate of peak circumferential distortion as compared with flight.

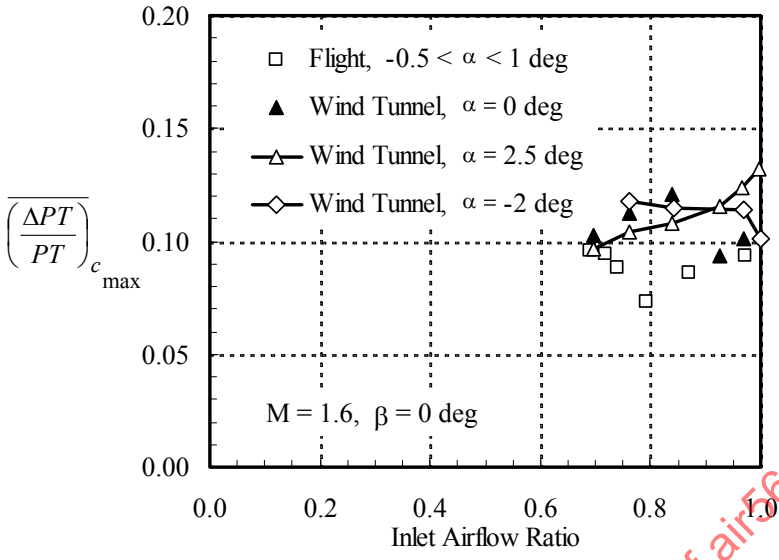

FIGURE 41 - PEAK CIRCUMFERENTIAL DISTORTION AT SUPERSONIC SPEEDS

In contrast to peak circumferential distortion, radial distortion measured in the wind tunnel was a good indicator of that found in flight (Figure 42). At high inlet airflows, the radial distortion of both the wind-tunnel model and the flight vehicle was predominately tip radial distortion. As inlet airflow was reduced, radial distortion transitioned to a hub radial pattern.

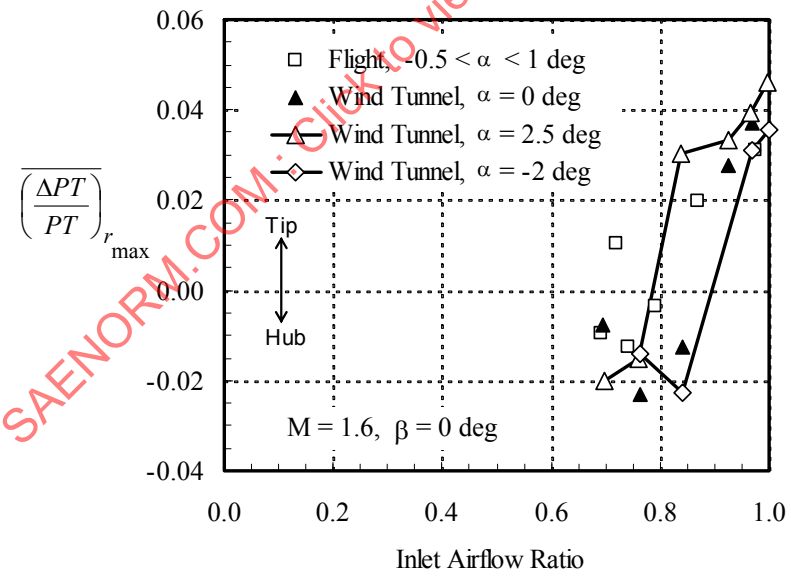

FIGURE 42 - PEAK RADIAL DISTORTION AT SUPERSONIC SPEEDS

The planar wave content of the flow measured on the wind-tunnel model provided a conservative indication of this type of distortion when compared with that found in flight (Figure 43). As inlet airflow is reduced, the planar wave content of the wind-tunnel model increased rapidly compared with that measured on the flight vehicle. Evidently, the test techniques used in the tunnel were inadequate in reproducing flows found at low inlet airflows in supersonic, high-Reynolds-number flight conditions.

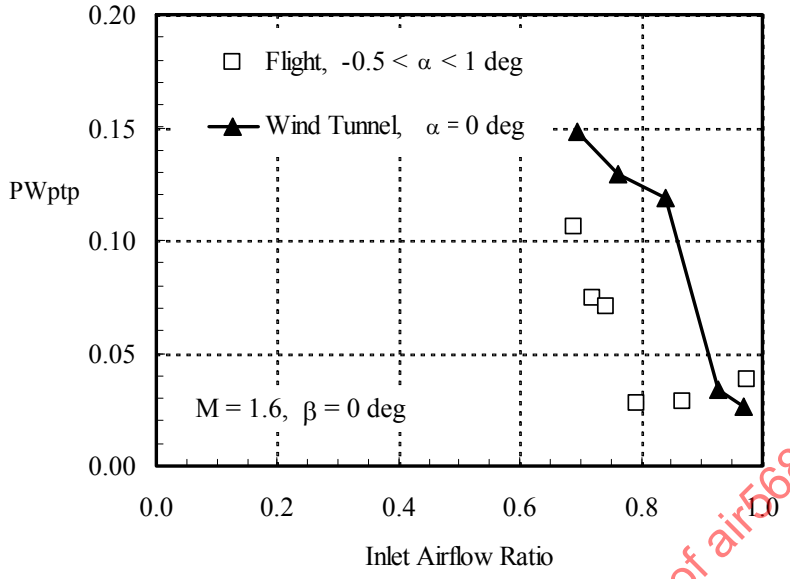

FIGURE 43 - PLANAR WAVE CONTENT AT SUPERSONIC SPEEDS

The total-pressure patterns at the AIP of the wind-tunnel model and the flight vehicle are similar in character. As seen in Figure 44, both sets of data indicate a total-pressure pattern that is predominately a 180-degree pattern. The wind-tunnel pattern is rotated roughly 60 degrees clockwise compared with the pattern measured in flight. However, the total-pressure pattern obtained in the wind tunnel provided correct guidance for an engine screen pattern.

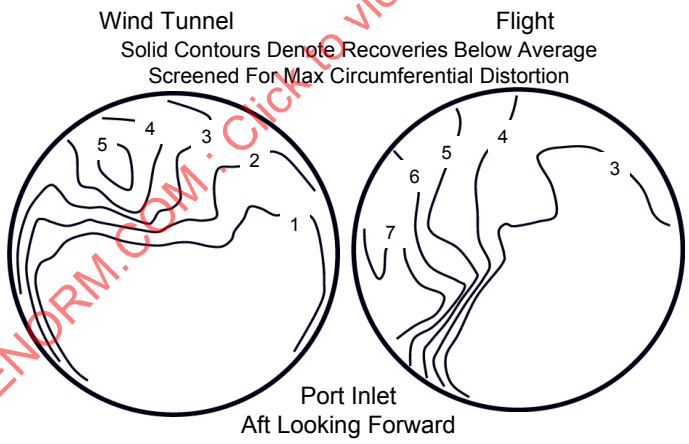

FIGURE 44 - PEAK TOTAL-PRESSURE PATTERNS AT SUPERSONIC SPEEDS

5.1.5.5 Findings of Original F/A-18E/F Study

The results of the F/A-18E/F research indicated:

The F/A-18E/F benefited from a coordinated wind tunnel to flight-test program that measured dynamic total pressures at the AIP. Overall, pressure recovery measured in the wind tunnel at high airflows correlated well with flight across the Mach numbers examined. At transonic cruise flight conditions, recovery correlated well with Reynolds number and would justify increments in recovery from wind tunnel to flight conditions. However, recovery measured at low airflows in the wind tunnel for M = 1.6 conditions was lower than obtained in flight.

Dynamic total-pressure distortion measured in the wind tunnel correlated well with flight data. Distortion levels and trends correlated with changes in inlet airflow, Mach number, and angles of attack. No basis was found for correcting the levels of distortion measured in the wind tunnel to those found in flight. Total-pressure contours measured at the AIP of the wind-tunnel model were similar to the contours measured in flight. In all cases examined, the type of pattern observed (i.e., one per rev or two per rev) was the same. Differences were observed in the pattern orientation.

At subsonic and supersonic speeds, the planar wave levels and trends measured at high inlet airflows in the wind tunnel were similar to those obtained in flight test. However, planar wave levels measured in the wind tunnel at reduced inlet airflows were higher than found in flight test.

The use of single-barreled, temperature-controlled, absolute-pressure probes for the flight-test AIP rake was successful. Use of these probes provided quality data at half the cost, hardware, and data processing. The flight data correlated well with data obtained in the wind tunnel.

5.1.5.6 S-16 Committee Observations of F/A-18E/F Data

The data presented here displays sensitivity of inlet recovery and distortion to angle-of-attack changes at low airflows for both transonic and supersonic flight. This may be a manifestation of a (1) Reynolds number effect of boundary-layer interactions with high pressure-gradient flows, and/or (2) nonstationary flows approaching and within the inlet. Further research into similar phenomena on future inlet systems is warranted.

Higher amplitude planar waves found in the wind tunnel may be due to the location of the acoustic reflection plane in the scale model as compared to the flight-test aircraft. In flight, the acoustic reflection plane was associated with the first rotor of the fan. In the model, the reflection plane was associated with the flow plug which was located downstream of the scaled-location of the first rotor. While the frequency content of the planar waves may be correlated between model- and full-scale using Strouhal scaling, the wave amplitude is related to the volume of the resonating duct and complex flow interactions within the duct.

The practices recommended by ARP1420, as implemented here, provided correct insight and understanding of inlet/engine compatibility and engine stability for the F/A-18E/F aircraft.

5.1.6 F-22 Case Study

The F-22 case study is the most recent instance of model to full-scale correlation. As a result, it is a good example of the planning and execution required to allow success performing the model to full-scale comparisons. Additionally, this case study includes lessons learned which provide guidance for future projects. For brevity, case study data presented in this section are a subset of material presented in a technical paper at the 2005 International Symposium on Air Breathing Engines, Reference 2.2.25.

5.1.6.1 Test Item Configuration

5.1.6.1.1 F-22 Engine Inlet Overview

The F-22 engine inlet, shown in Figure 45, was sized to accommodate the F119-PW-100 (F119) engine and employs a fixed external compression inlet with compression ramp bleed to maintain inlet shock stability during supersonic operations. Inlet bleed air exits a fixed-area bleed exit on the upper surface of the engine inlet. The fixed-area screened vent and actuated door were initially provided to increase bleed flow at high Mach numbers. However, part way through the flight-test program, the variable inlet bleed door was removed from the aircraft to reduce cost and weight without unduly sacrificing inlet performance or stability. The F-22 engine inlet uses a variable bypass system for inlet/engine airflow matching and to maintain stable inlet operation at supersonic conditions. The bypass is located approximately two engine-face diameters forward of the engine and dumps air overboard through the upper surface of the aircraft.

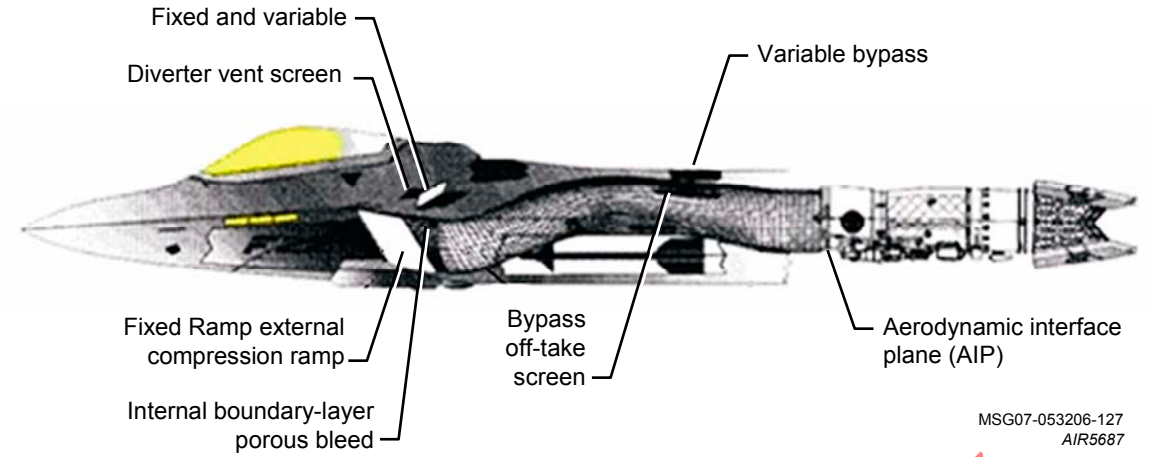

FIGURE 45 - FULL-SCALE F-22 INLET WITH FIXED AND VARIABLE BLEED

5.1.6.1.2 Inlet Development

The most recent wind-tunnel model tested in this program was the 0.14-scale IF3-2 model. This model was tested in the AEDC 16-foot Transonic and Supersonic wind tunnels (16T and 16S) in 1994 and was the fourth in a series of inlet models designed for the propulsion development program. Inlet development history includes the IF3-1 model, tested in AEDC tunnels 16T and 16S in 1992, the IF2 model, built for the YF-22A program, tested in the Ames Research Center 11-foot transonic and 9- by 7-foot supersonic wind tunnels in 1988, and the NIF1 model, built for the NATF program in 1990. Engine-inlet compatibility flight testing began in 1992 during the concept demonstration phase of YF-22A testing and concluded in 2001 with flight-testing of F-22 aircraft, which included 61 flights of engine-inlet compatibility testing.

5.1.6.1.3 Subscale F-22 Inlet Configuration

The IF3-2 model, shown in Figure 46, was a 0.14-scale representation of the aircraft external and internal duct and inlet duct geometry from the nose to the Aerodynamic Interface Plane (AIP). Duct mold lines reflect the production aircraft configuration with fully-modeled inlet bleed and bypass systems. The inlet diverter height was geometrically scaled and not adjusted for model-to-full-scale Reynolds number boundary-layer effects. Flow blockage associated with the F119 fan and fan nose cone were not simulated. All discussion included in this F-22 case study relates to testing the left-hand (port) engine and inlet.

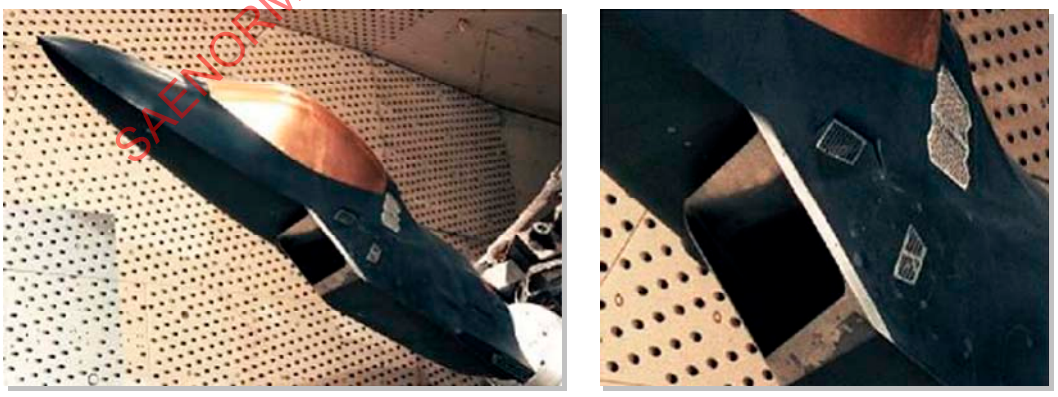

FIGURE 46 - SUBSCALE F-22 INLET TESTED IN THE AEDC 16-FT TRANSONIC AND SUPERSONIC WIND TUNNELS

Bypass doors were variable and were remotely operated. Inlet airflow was controlled by an independent, remotely operated, variable-exit area flow controller. Primary inlet auxiliary suction was provided by a high-pressure air-powered ejector system at Mach numbers below approximately 1.2 where ram pressure ratio was insufficient to provide the necessary flow rates.

5.1.6.2 Test Conditions

5.1.6.2.1 Wind Tunnel Test Conditions

Subscale inlet testing of the IF3-2 model was conducted at static conditions and at Mach numbers ranging from 0.18 to 1.5 in 16T and from 1.6 to 2.1 in 16S. Model angle-of-attack ranged from -20 to +90 deg at sideslip angles from ±30 degrees, depending on Mach number. Configuration variables included a simulated flight-test nose-boom assembly, nose landing-gear assembly, inlet ramp-bleed porosity, inlet ramp-bleed exit area, weapons bay doors, bypass exit area, air data probes, and a secondary air system.

5.1.6.2.2 Flight Test Conditions

F-22 engine and inlet compatibility testing included fixed and transient throttle movements during steady-state and dynamic maneuvers throughout the F-22 envelope. Time-dependent inlet-total-pressure data were continuously recorded at 800 samples per second during the maneuver sequences (maneuver entry, actual maneuver, and recovery). The high-speed compatibility testing was not considered to be traditional aircraft envelope expansion in that small Mach and altitude increments across the envelope were not used. In essence, high-speed testing was an inlet survey to validate the wind-tunnel predictions. High-speed testing was conducted by performing “maneuver blocks” at limited Mach and altitude combinations. These maneuver blocks consisted of 15 to 30 maneuvers and included incremental buildup to the maximum maneuver capability of the aircraft.

A more traditional approach to flight envelope expansion was used for low-speed inlet/engine compatibility testing. Low-speed compatibility testing consisted of three groups of tests: 1-g maneuvers at increasing angles of attack, zoom climb recoveries at increasing pitch angles, and elevated airspeed pull-up/push-over maneuvers to maximum and minimum angles of attack. Each group included: 1) a buildup to lower dynamic pressures and temperatures, 2) a buildup to the most severe inlet distortion, 3) a buildup in horsepower extraction, and 4) a buildup to the least-engine-stability-margin-remaining conditions, including throttle transients.

5.1.6.3 Data Acquisition, Processing, and Analysis

5.1.6.3.1 Wind Tunnel Data Acquisition and Processing

The F-22 project used a typical 40-probe wind-tunnel inlet instrumentation array for measuring inlet recovery and distortion. It consisted of eight equiangular-spaced rakes with five probes per rake located at the centers of equal areas. The number 1 rake for the IF3-2 model was located 22.5 deg counterclockwise from top dead center (forward looking aft).

The dynamic content of total pressure for the F-22 inlet is relatively small, thus motivating the separate measurement of the high- and low-frequency components of total pressure. For IF3-2 testing and flight testing, measurement accuracy was improved by tailoring transducer and signal-conditioning ranges to maximize resolution for each of the individual components. The IF3-2 model included 40 steady-state and 40 high-response total-pressure probes at the AIP, as shown in Figure 47.

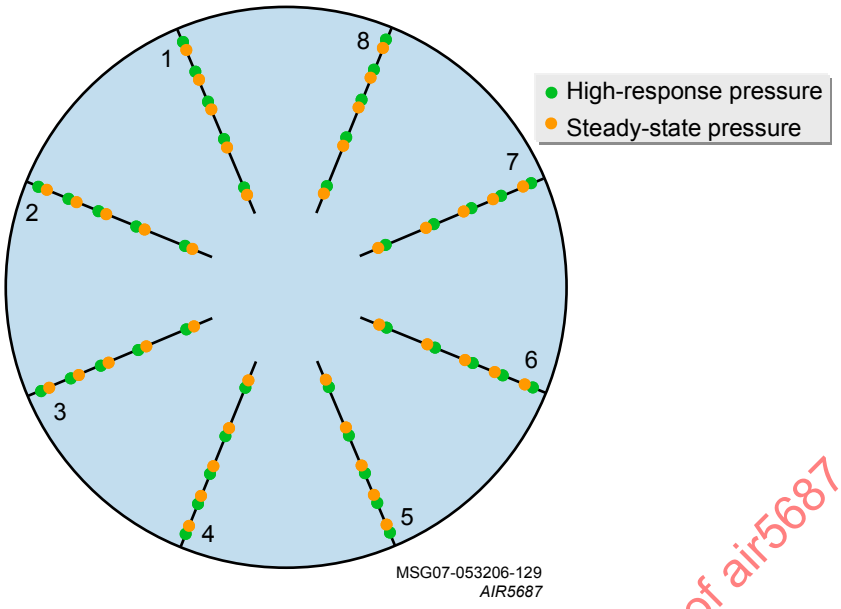

FIGURE 47 - WIND TUNNEL INLET RAKE GEOMETRY

High-response pressure measurements on the subscale IF3-2 model were acquired at the AIP using transducers located adjacent to the steady-state total-pressure probes. Analog Root-Mean-Square (RMS) meters with a low-pass cutoff filter of 4 KHz were used to determine the RMS total-pressure amplitude, or turbulence. Analog data were digitized and low-pass filtered to 1250 Hz to match the compression-system dynamic-response characteristics using four-pole (-24 dB/octave) Bessel filters. The sampling rate was 6250 samples per second. Data were screened during testing, and erroneous signals from the 40 high-response and 40 low-response steady-state probes at the AIP were replaced using analytical techniques based on adjacent probes. The 40 steady-state and high-response pressure measurements were combined, and the ARP1420 (Reference 2.1.1) spatial distortion descriptors were evaluated. Stability margin remaining for the F119 fan and compressor was calculated using sensitivities provided by the engine manufacturer. For specified conditions, selected data were also screened post-test for worst-case combinations of circumferential, hub-radial, and tip-radial distortion.

During wind-tunnel test operations, the requested Mach number was set and the computer-controlled data-acquisition cycle initiated. The model was positioned to the desired attitude and data were obtained at specified airflow values. Engine corrected airflow was then varied from the maximum value to the minimum value, or until inlet flow instability occurred. For certain pre-selected conditions expected to challenge engine stability, data were digitally acquired for five seconds and all peak distortion descriptors were computed and stored. On all other points, one second of data was acquired, and the data were screened only for minimum remaining engine fan or compressor stability margin. If the remaining stability margin for either the fan or the compressor was less than 1 percent at high airflow points, or 2 percent at lower airflows, an additional 5 seconds of data were recorded and processed. This process was repeated for a given test configuration until data had been acquired at all desired attitudes and Mach numbers.

5.1.6.3.2 Flight Test Data Acquisition and Processing

The flight-test rake configuration was located very close to the AIP and was integral with the inlet guide vanes of the F119-PW-100 engine. The rake consisted of eight instrumented struts with five ring locations and was incorporated into a modified engine-inlet case as shown in Figure 48. As seen, the leading edge of the engine guide vanes were modified with a small recessed area which housed the pressure and temperature instrumentation. The instrumentation included a total of 40 high-response pressure transducers, 40 low-response differential pressure transducers, one absolute reference pressure transducer, and 16 high-response thermocouples for armament gas ingestion testing, as shown in Figure 49.

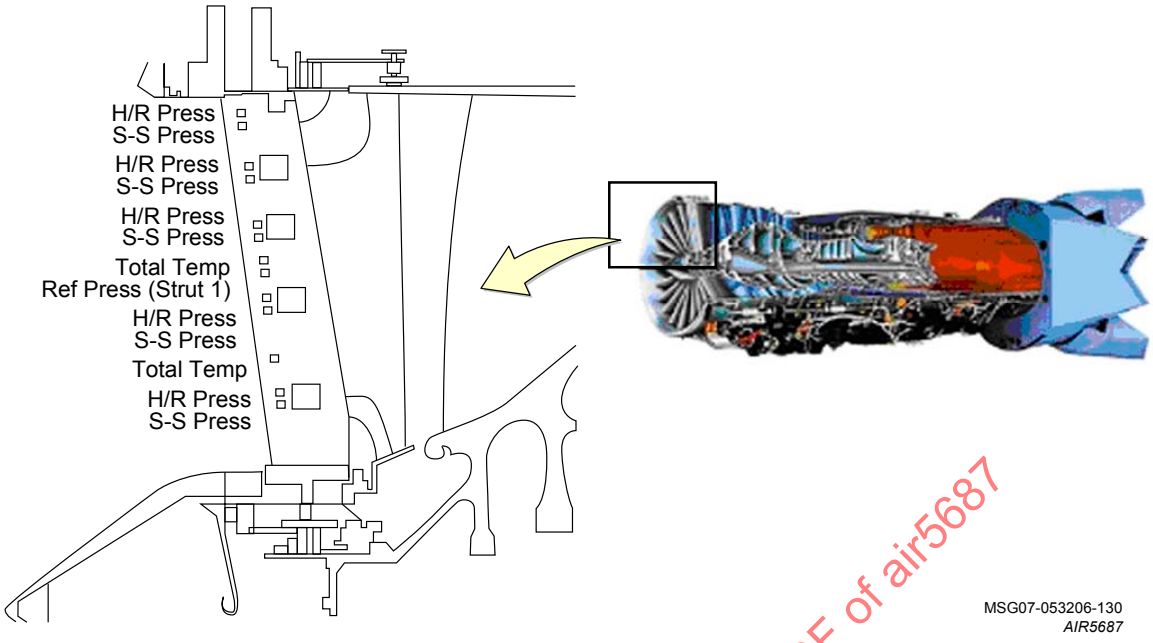

FIGURE 48 - F119-PW-100 FLIGHT TEST ENGINE-FACE RAKE

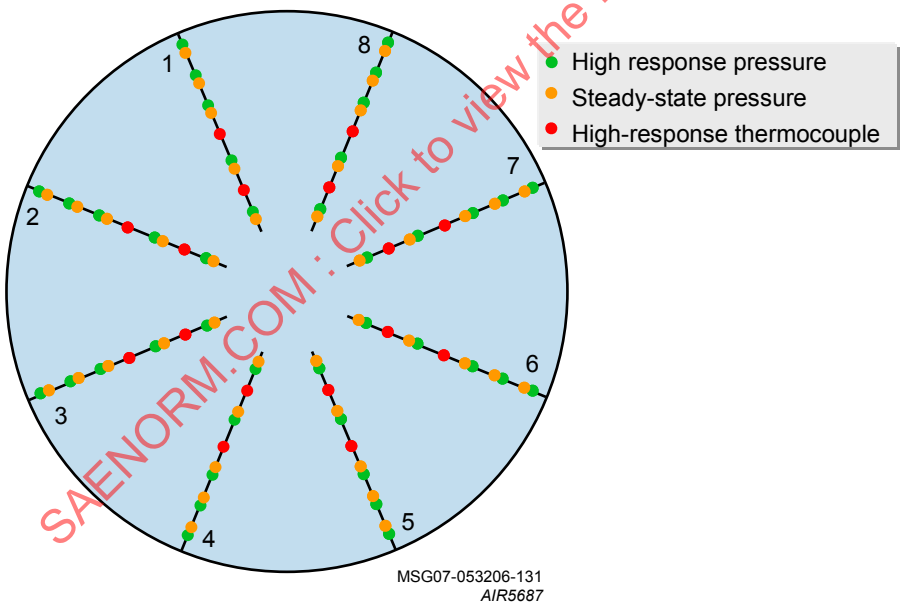

FIGURE 49 - FLIGHT TEST INLET RAKE GEOMETRY

Each instrumented strut contained five high-response pressure transducers and five total-pressure orifices and tubing leading to the low-response steady-state transducer scanning module. The absolute-pressure reference transducer was used in conjunction with a 48-channel scanning module to gather the low-response pressure data. Strut 1 was located 17 deg counter-clockwise from top dead center (forward looking aft) and incorporated an additional location between rings 2 and 3 for the reference pressure. It should also be noted since the flight-test rake was integral to the inlet guide vanes, the rake angles used resulted in slight variations from the wind-tunnel configuration which had eight equiangularly-spaced rakes.

To increase accuracy, the low-frequency response pressure measurements were made with a scanning module located in a remote, fuel-cooled environment. The scanner was mounted in a heated chamber, which was enclosed in a fuel-cooled box located in the engine bay in close proximity to the AIP rake. This fuel-cooled box was required to maintain near-constant temperature. The temperature inside the box was not monitored. The reference pressure transducer was located in a side weapons bay, well removed from the engine compartment, and close-coupled to the AIP scanner module. The plumbing required for the remote instrumentation resulted in a significant lag in the reference pressure measurement. This lag proved to complicate a number of measurement system and data processing activities including pretest calibrations, thermal corrections for the steady-state pressure measurements, instabilities in the digital filtering algorithms used to filter the high-response pressure measurements, and configuration control of the data analysis software. The effect of this lag was determined to be “self-compensating” since the steady-state differential pressures were all measured relative to the same reference pressure sensed by the close-coupled transducer. No time lag was introduced into the final computed results.

Data were acquired at pre-flight wind-off conditions to determine and account for day-to-day sensor drifts on the 40 steady-state differential pressure transducers, the steady-state reference pressure transducer, and the 40 high-response pressure transducers. High-response pressure measurements for flight test were digitally recorded at 800 samples per second (approximately 4.5 samples/cycle). High-response data were then band-pass filtered between 2 and 178 Hz to match the compression system dynamic response characteristics using a six-pole Butterworth filter. Initially, instabilities were seen in the digital filtering algorithms at frequencies between 0.20 and 1.00 Hz. As a result, the cutoff frequency was increased to 2 Hz to remove the observed instabilities from the filtered high-response pressure data. This band-passed high-response-pressure data were then combined with the steady-state reference and delta pressure data which had been low-pass filtered to 2 Hz. Data were screened during testing, and erroneous signals from the 40 high-response and 40 low-response steady-state probes at the AIP were replaced using the adjacent probes and Shepard’s inverse distance-weighted interpolation method (Reference 2.2.26) to account for slight variations in the probe locations at the AIP. The 40 steady-state and high-response pressure measurements were combined to compute the ARP1420 spatial distortion descriptors and the planar wave instability descriptors described in AIR5866 (Reference 2.1.3).

5.1.6.3.3 Model-to-Flight Correlation Analysis Techniques

A quantitative assessment of F119 engine performance and stability was performed at a number of selected conditions to assure inlet/engine compatibility. Test conditions from wind-tunnel and flight programs were defined in terms of inlet/engine interface conditions (airflow and total pressure), free stream Mach numbers, aircraft angles of attack and sideslip, total-temperature, ambient pressure, installation interfaces (e.g., customer bleed and power extraction), and engine operating conditions (e.g., engine power settings and service bleeds, including anti-ice and control trims). Inlet recovery and distortion levels were characterized primarily as a function of Mach number, angle of attack, angle of sideslip, bleed and bypass door positions, altitude, and engine airflow.

F-22 flight testing included 61 flights of inlet compatibility testing over a period of nearly four years (1999-2004) and produced a significant amount of test data. In general, secondary configuration variables (e.g., nose gear, weapons bay doors, and air data probes) had a minimal effect on inlet flow stability and performance. Bleed and bypass door angles were considered primary configuration variables even though the bleed door was removed early in the test program. With the simulated flight-test nose boom installed, reductions in inlet recovery and flow stability were seen during wind-tunnel testing at supersonic speeds and specific angles of attack and sideslip. All flight-test results presented are with the nose boom installed. Only limited amounts of wind-tunnel data were obtained with the nose boom installed, and as a result the wind-tunnel and flight data available for comparison are limited.

5.1.6.3.4 Inlet Total-Pressure Recovery Analysis Techniques

Computational Fluid Dynamics (CFD) was used to determine the magnitude of the Reynolds number effect on the wind-tunnel total-pressure recovery data. The CFD modeling was intended to determine only the internal duct effects attributable to wall flow scrubbing. No attempt was made to determine the Reynolds number effect on the external flow approaching and entering the inlet. Reynolds number effects on the fuselage boundary layer were not accounted for in the sub-scale Reynolds number total-pressure recovery correction. The change in recovery as a function of flight unit Reynolds number is shown in Figure 50 indicating the expected trend of increasing recovery as a function of increasing Reynolds number. The Reynolds number effects on total-pressure recovery range from one-tenth of one percent to eight-tenths of one percent. The wind-tunnel predictions (wind-tunnel data interpolated to flight-test conditions) and CFD approximation of the Reynolds number effects were used to sort out inconsistencies in the flight-test recovery.

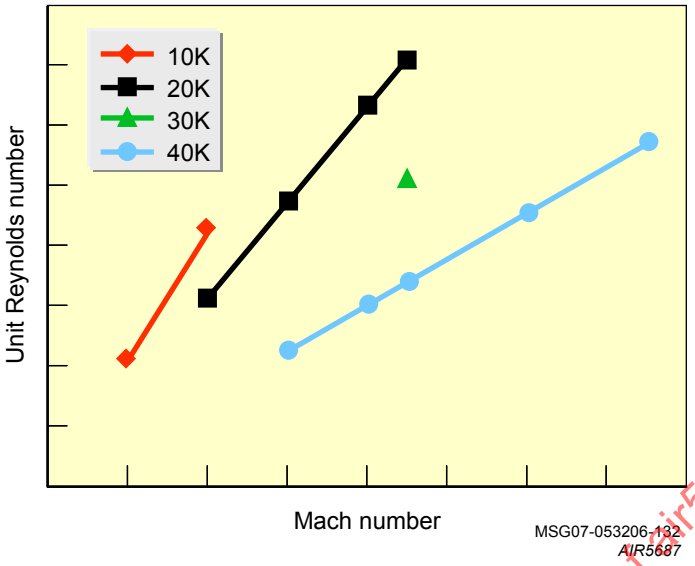

A) FLIGHT UNIT REYNOLDS NUMBER

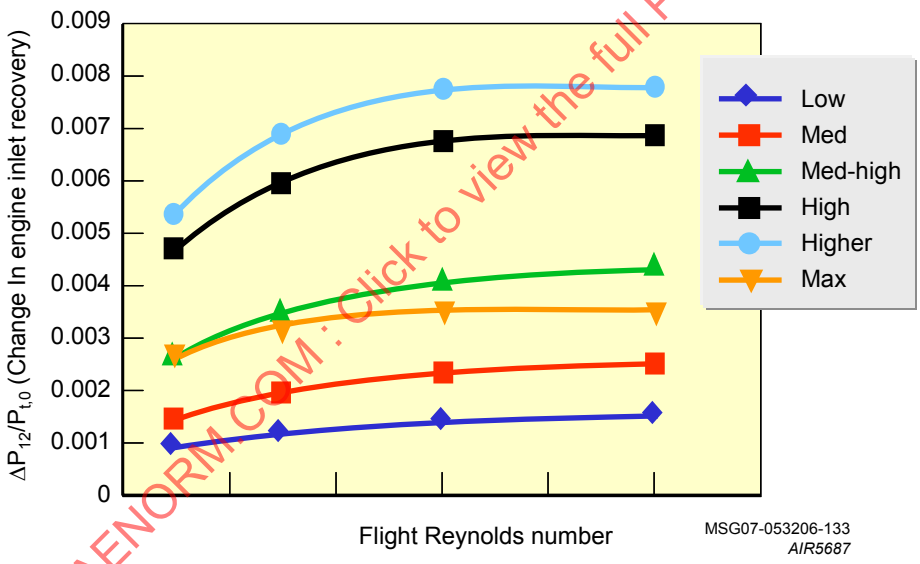

B) REYNOLDS NUMBER CORRECTION

FIGURE 50 - REYNOLDS NUMBER CORRECTION

5.1.6.3.5 Spatial Total Pressure Distortion Descriptor Analysis

Circumferential distortion was described for each instrumentation ring in terms of intensity, extent and multiple-per-revolution elements. The ARP1420 circumferential distortion for each ring is the difference between the ring average pressure and the ring low-pressure average, normalized by the ring average pressure. For the F-22 program, including the data presented herein, the circumferential distortion intensity (ΔPC/P) was defined as the average of the five-ring circumferential-distortion intensities. The ARP1420 radial distortion intensity (ΔPR/P) of a ring is defined as the difference between the engine-face-average pressure and the ring-average pressure divided by the face-average pressure where positive values reflect a ring-average pressure that is below the engine-face-average pressure. The radial-distortion intensity of a ring was set to zero if the intensity was less than zero. The tip-radial-distortion intensity $(\Delta PR/P)_{tip}$ was defined as the largest of radial-distortion intensities for the two outer rings, and the hub-radial distortion $(\Delta PR/P)_{hub}$ intensity was defined as the largest of the radial-distortion intensities for the two inner rings.

5.1.6.3.6 Planar Instability (Buzz) Total-Pressure Distortion Descriptor Analysis

Flow interactions in aircraft inlets may produce one-dimensional, unsteady pressure fluctuations at the engine face. These are often referred to as “planar waves,” “in-phase distortions,” “planar instabilities,” or “inlet buzz.” AIR5866 provides guidance for the calculation and assessment of Planar Waves (Reference 2.1.3).

Compression-system performance and stability response depend on the amplitude and frequency of the planar waves. Two different approaches to determining planar wave, designated “SUM40” and “Peak-to-Peak,” were used to characterize planar wave (or in-phase pressure fluctuations, “inlet buzz”) for F-22 inlet compatibility testing and to determine the minimum stable airflow for stable inlet operation. SUM40 is the RMS of the area-weighted average of the dynamic pressures divided by the average engine-face total pressure. Peak-to-Peak (one cycle) is calculated using the AC component of the dynamic engine-face total-pressure recovery. Local maxima (above zero) and minima (below zero) are used to determine the peak-to-peak one-cycle magnitude of the planar wave. The Peak-to-Peak (one cycle) approach is intended to be more sensitive than SUM40 to planar wave content. “RMS Turbulence” (the average compressor face turbulence normalized by the engine face total pressure) was also analyzed.

The analog RMS meters used during the wind-tunnel inlet tests incorporated resistor packs in the meters to provide a 4KHz, low-pass cutoff frequency. It was believed that the roll-off rate was equivalent to a 1-pole filter (-6 dB/octave). Differences between the wind-tunnel RMS meter determination of RMS turbulence and the digital filtering approach used with the flight-test data were believed to be the most significant factor associated with differences between wind-tunnel and flight-test RMS turbulence values.

5.1.6.3.7 Peak Total-Pressure Distortion Screening

With constant statistical properties and similar test conditions, data from subscale-wind-tunnel and flight tests were investigated for the effects of Reynolds number/scale effects, frequency content, and engine presence. CFD was not used in this study to quantify the magnitude of the predicted decrease in peak time-variant-distortion values and turbulence as a function of increasing Reynolds number/scale. The eleven screening parameters shown in Figure 51 were used post-test for the F-22 subscale wind-tunnel test for some test conditions, with the worst-case stability margin remaining for the fan and the compressor used on-line in real time for all the data. All screening parameters except the worst-case stability-margins remaining for the fan and the compressor were also used during flight testing. Fan and high-pressure compressor stability pressure ratio losses were calculated using sensitivities provided by the engine manufacturer. Key engine and aircraft parameters (including the 40 individual pressure measurements) were output at each of the worst-case conditions corresponding to each of the screening parameters. Only test results associated with the worst case circumferential, tip- radial, and hub-radial distortions are presented in Figure 51.

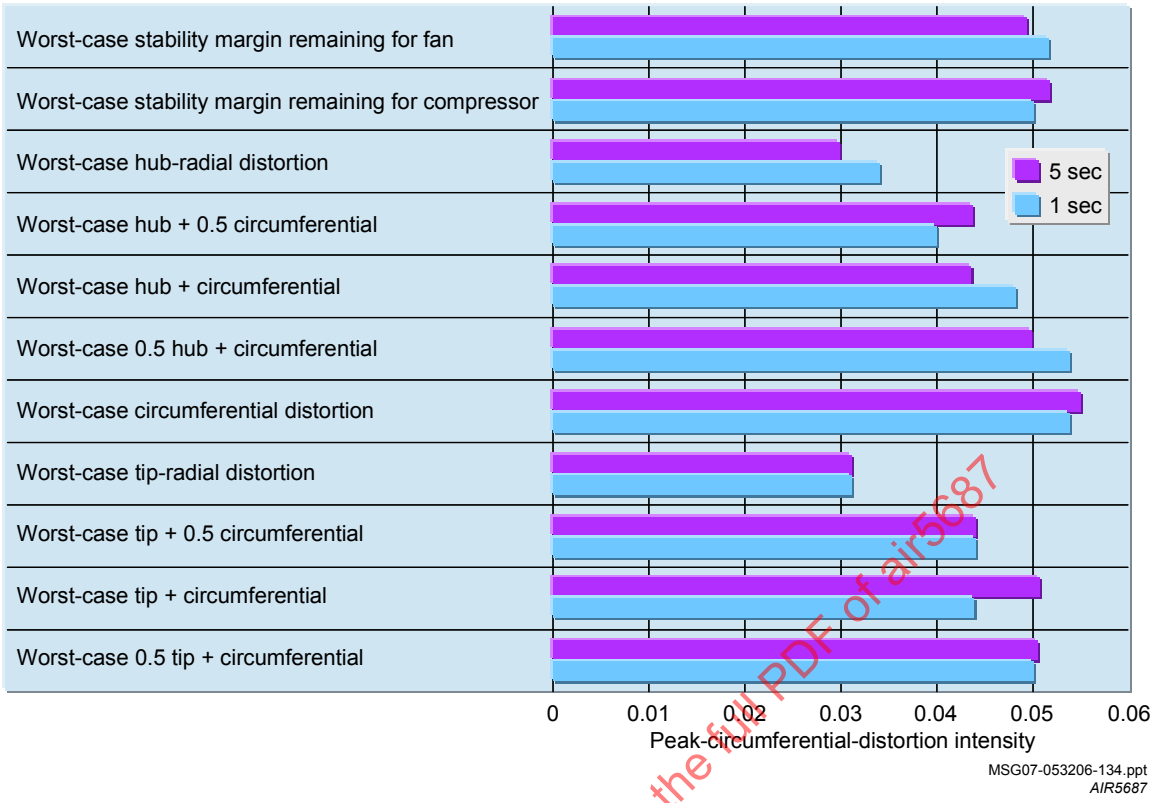

FIGURE 51 - STATISTICAL IMPACT OF SCREENING ONE SECOND VERSUS FIVE SECONDS OF DATA TO DETERMINE WORST CASE DISTORTION INTENSITY

Data comparisons necessary to evaluate peak distortion descriptors generally require that the samples of time-variant distortion data be statistically stationary. A sufficient volume of data was analyzed to verify the assumption of stationarity of the wind-tunnel and steady 1-g flight-test data. Wind-tunnel data were screened for one second at each condition and if during that period “stability-margin remaining” was within one percent of the limit at high airflows, then the maneuver was repeated for five seconds to increase statistical confidence of capturing peak distortion. As can be seen in Figure 51 some peaks occurred during the one second timeslice and some peaks occurred in the five second timeslice.

To make valid comparisons of peak circumferential- and radial-distortion intensities, the wind-tunnel and flight-test data were screened with consistent screening parameters. Screening parameters associated with the worst-case stability margin remaining for the fan and compressor changed throughout the developmental engine program. At Mach numbers below 1.5, most of the wind-tunnel data were screened primarily at “worst-case stability-margin remaining for the fan or compressor.” Engine-manufacturer stability audits for the F119 engine indicate that for flight conditions below Mach 1.5, the fan was twice as sensitive to stalling from elevated circumferential distortion as from radial distortion. As a result, the minimum-stability-margin point generally occurred with the maximum-circumferential distortion intensity, making the wind-tunnel “min-fan-stability-margin” screening parameter comparable to the maximum flight-test circumferential-distortion intensity. [S-16 Committee Observation: A common set of screening parameters needs to be used for both wind-tunnel and flight testing to ensure that the data obtained can be readily analyzed. When common screening parameters are not possible, raw dynamic-pressure data should be saved to allow re-processing if necessary to allow direct comparision between wind-tunnel and flight-test results.]

5.1.6.4 Results and Discussion

5.1.6.4.1 Model-to-Flight Correlation

Wind tunnel-to-flight correlations were made throughout the aircraft flight envelope for steady-state 1-g flight conditions. Wind-tunnel data were linearly interpolated as a function of Mach number, engine airflow, angle of attack, and angle of sideslip to match the specific flight conditions. Only two examples of the flight correlation results (Reference 2.2.25), one at low altitude/low-subsonic and another at mid altitude/high-supersonic trimmed-flight conditions, are presented here. Additionally, peak-distortion data encountered during dynamic flight-test maneuvers are also compared to wind-tunnel predictions from similar steady-state conditions.

For comparison purposes, the wind-tunnel total-pressure and turbulence contour plots presented in this section were visually altered to reflect the presence of the engine bullet nose, which was not present during subscale wind-tunnel testing. In this case, visually altering meant placing a blacked out circle on the center of engine-face contour plot; no pressures were translated in this process. Engine-face total-pressure contours presented here were not corrected for Reynolds number.

5.1.6.4.2 Model-to-Flight Correlation, 1-g Low Altitude and Low Subsonic Flight Conditions

At low altitudes and low subsonic 1-g flight conditions, the wind tunnel/flight-test correlation in the steady-state data was excellent, Figure 52, with the exception of the approximately 1-percent disagreement in total-pressure recovery at the higher airflows, Figure 52A. The excellent agreement was seen between the high- and low-pressure areas of engine-face total-pressure contour plots, Figure 52B, which were not corrected for Reynolds number, but have been interpolated for differences in wind-tunnel test conditions. The slight differences in the steady-state circumferential and radial distortion, Figure 52C and Figure 52D, were insignificant considering the low value of the distortion intensities. The peak circumferential-distortion intensities are of similar magnitude at the higher airflows, and the slight difference in magnitude, as well as the trend with airflow, may be attributable to the difference in peaks used for screening. The significant difference in the turbulence levels, Figure 52E, was attributed to the difference in the low-pass cutoff frequencies used for the RMS meters (nearly broadband) in the wind-tunnel tests and the digitized data in the flight tests. However, it is noteworthy that the location of the higher turbulence area is common to both data sets, Figure 52F.

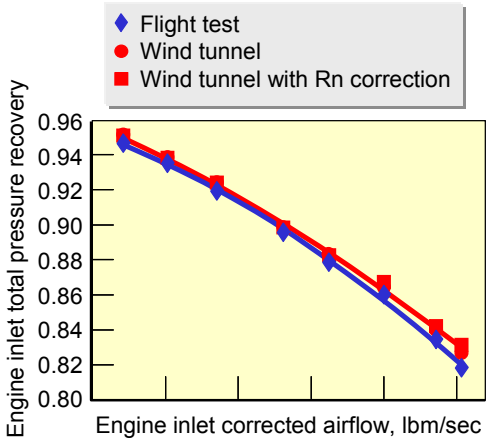

a) Total pressure recovery

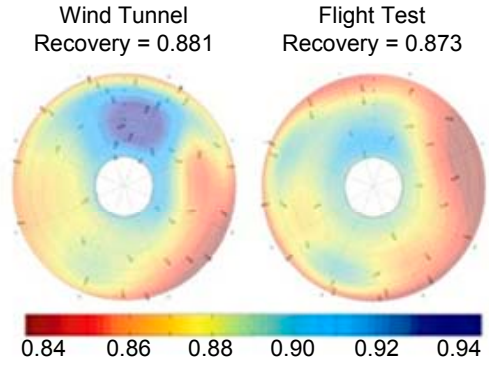

b) Total pressure contours

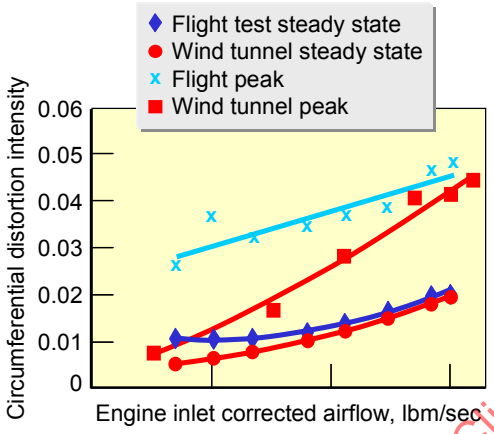

c) Circumferential distortion Intensity

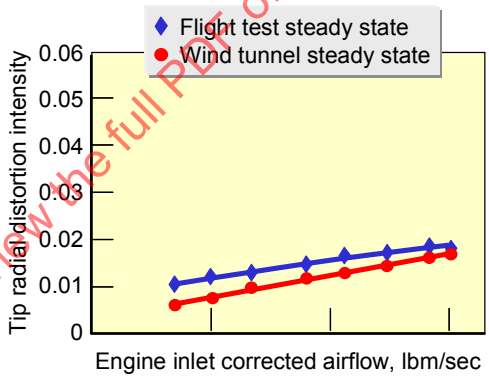

d) Tip radial distortion intensity

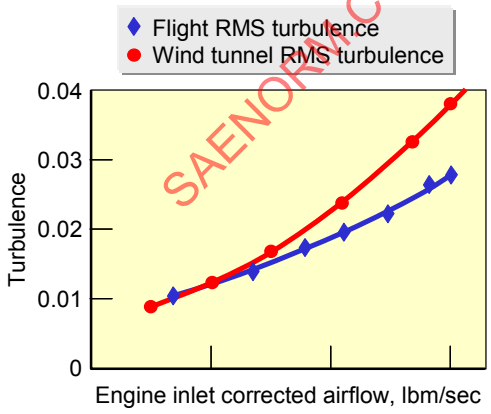

e) Turbulence

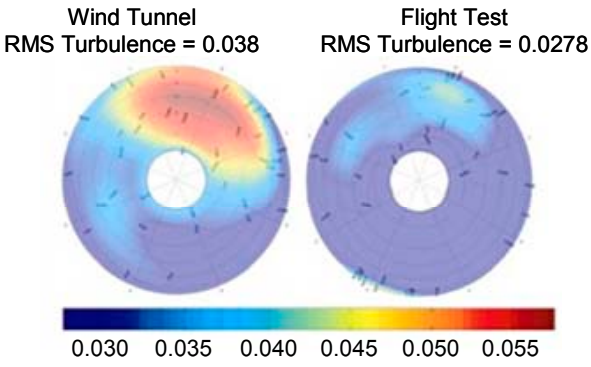

f) Turbulence contours

MSG07-053206-135.ppt
AIR5687

FIGURE 52 - WIND TUNNEL AND FLIGHT TEST CORRELATIONS AT 1-G TRIM FLIGHT, LOW ALTITUDES AND LOW-SUBSONIC FLIGHT CONDTIONS

5.1.6.4.3 Model-to-Flight Correlation, 1-g Mid Altitude and High Supersonic Flight Conditions

Flight-test recovery data at supersonic speeds are presented in Figure 53. Reynolds number-adjusted wind-tunnel recovery data were about one-half percent lower, Figure 53A, than the flight-test data at some of the airflow conditions. Wind-tunnel and flight-test engine-inlet total-pressure recovery contour plots at maximum airflow rates are shown in Figure 53B. Total-pressure recovery contour plots were not corrected for Reynolds number effects but were interpolated for differences in wind-tunnel test conditions. The distortion indices (steady-state and peak instantaneous) were within 0.01 of each other, Figure 53C and Figure 53D, but the flight circumferential-distortion data are lower than wind tunnel. The difference in the turbulence levels, Figure 53E, was attributed to the difference in the low-pass cutoff frequencies used for the RMS meters (nearly broadband) in the wind-tunnel tests and the digitized data in the flight tests. However, the higher turbulence area was common to both data sets as seen in Figure 53F. While there were some differences and inconsistencies in the wind-tunnel and flight-test data sets, at nominally steady conditions the wind-tunnel test did accurately simulate the flight-vehicle inlet performance.

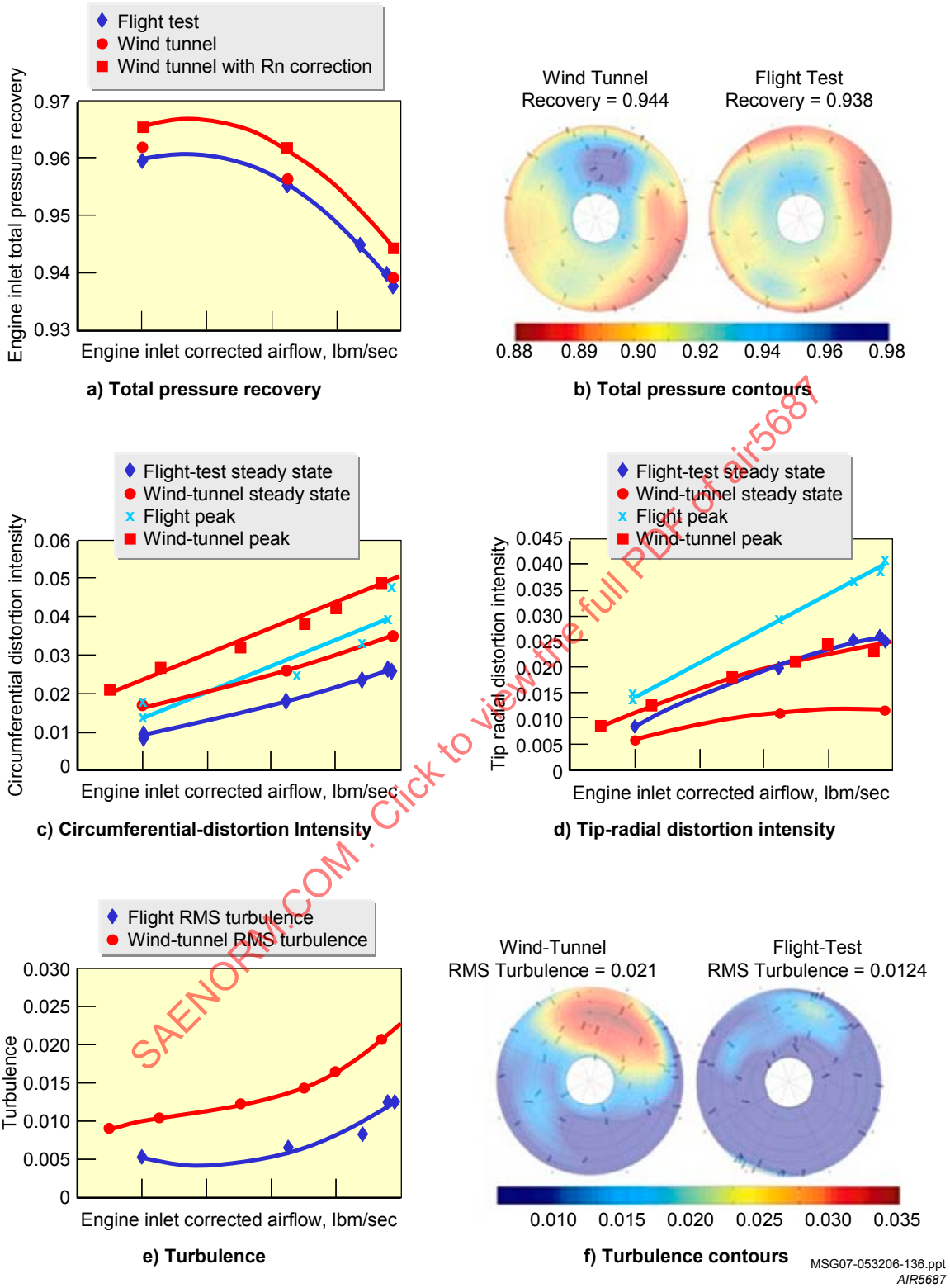

FIGURE 53 - WIND TUNNEL AND FLIGHT TEST CONDITIONS AT 1-G TRIM FLIGHT, MID-ALTITUDE AND HIGH-SUPERSONIC FLIGHT

5.1.6.4.4 Model-to-Flight Correlation, Aircraft Maneuvering

Peak-distortion data clouds from wind tunnel and flight test are presented in Figure 54 and Figure 55, and provide a summary of peak-circumferential- and radial-distortion intensities encountered at two ranges of flight conditions, one subsonic and one supersonic, respectively. In these peak distortion clouds, circumferential distortion intensity (ΔPC/P) was shown as a function of radial distortion intensity (ΔPR/P); however, positive values of radial distortion were shown as tip radial distortion, $(\Delta PR/P)_{tip}$, and negative values were shown as positive hub-radial distortion, $(\Delta PR/P)_{hub}$. Only data with the bleed door closed were included in the peak-distortion comparison plots. Individual data points denoted with a red triangle corresponded to the wind-tunnel data. Data points denoted with a blue diamond indicated the maximum distortion intensity experienced during the flight-test maneuver. Data points denoted with a black square corresponded to the maximum distortion intensity during the "on condition" portion of the maneuver (e.g., quasi-stable for 2-3 seconds at Mach 0.4 and 75 degrees angle of attack). Tolerances for "on-condition" data were ±1 degree of sideslip (AOS), ±1 degree of angle of attack (AOA), and ±0.05 in Mach number. Inlet distortion data shown are for a range of Mach numbers, angles of attack and sideslip, and airflows. Data shown in Figure 54 and Figure 55 were for wind-tunnel and flight-test results having similar geometric configurations and screening parameters.

For the positive AOAs at low-subsonic flight conditions, Figure 54, the flight-test and wind-tunnel results were in excellent agreement. Good agreement was also found between the flight-test and wind-tunnel data at negative angles of attack. However, the amount of flight-test data was too limited at negative angles of attack and at these Mach numbers to make a complete comparison.

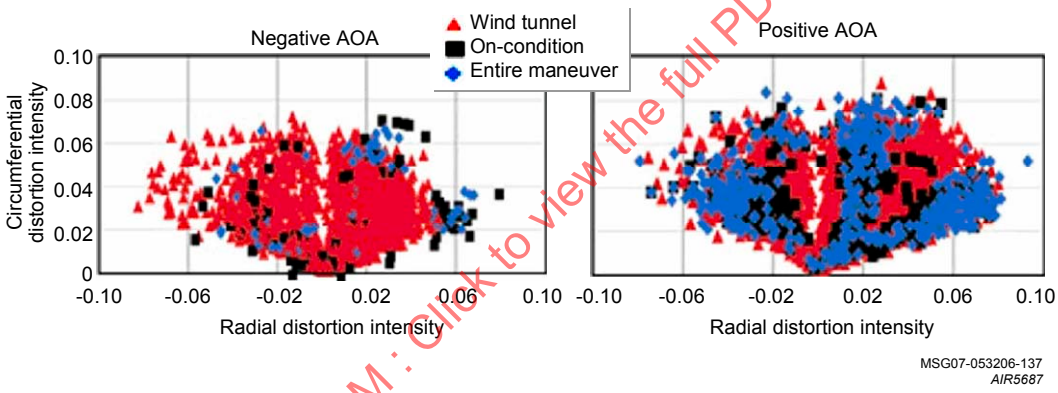

FIGURE 54 - DISTORTION SUMMARY AT LOW-SUBSONIC SPEEDS WITH NEGATIVE AND POSITIVE AOA

Peak distortion data for the mid- to high-supersonic flight conditions at both positive and negative angles of attack, Figure 55, show flight-test results were not within the bounds of predicted wind-tunnel results. A determination as to why these differences existed was not performed since there were no inlet compatibility concerns identified during F-22 flight testing. Speculation as to the cause included a) not accounting for sensor lag associated with varying line lengths on the steady-state pressure transducers, b) not accounting for the range of temperatures in which the pressure transducers were required to operate, c) impacts of flying with faulty dynamic pressure transducers and the substitution process using adjacent probes, or d) deficiencies in the wind-tunnel model (e.g., bleed system differences or diverter height scaling).

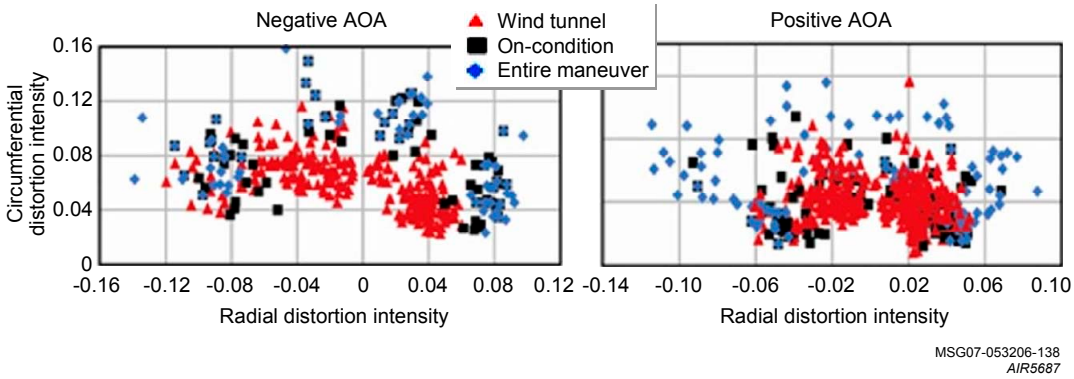

FIGURE 55 - DISTORTION SUMMARY, MID-TO HIGH-SUPERSONIC, NEGATIVE AND POSITIVE AOA

5.1.6.5 Findings of Original F-22 Study

The results of the F-22 research indicated:

- Steady-state and peak distortion intensities indicated by wind-tunnel data were representative of full-scale flight-test data.
- Sufficient technology exists to successfully predict inlet recovery and distortion intensities during the early phase of the inlet/engine development program based on sub-scale model testing.
- Use of analog RMS meters in the wind tunnel and digital filtering in the flight tests, and the different low-pass cutoff characteristics of each, were believed to be the most significant factor contributing to differences between wind-tunnel and flight-test RMS turbulence values. These differences prevented a quantitative comparison between wind-tunnel and flight-test of RMS turbulence values.
- Initial analysis of wind-tunnel and flight-test inlet total-pressure recovery data revealed inconsistencies in the flight-test data and, consequently, the algorithms used to calculate the steady-state pressure values. Sub-scale wind-tunnel data and CFD were used to resolve inconsistencies in the flight-test total-pressure recovery data. These inconsistencies were incorrectly presumed to be a result of temperature effects. Based on detailed analysis, the temperature compensation algorithms were eliminated, and another algorithm was used to eliminate the sensor bias during wind-off conditions.
- Challenges arose in the remote measurement of flight-test steady-state total-pressure data. The length of the pressure tubing resulted in a significant lag in the reference-pressure measurement. The overall effect of this lag was determined to be “self-compensating” since the steady-state pressures were all measured relative to the same reference pressure.

5.1.6.6 S-16 Committee Observations

Significant advances to the state-of-the-art resulted from the F-22 program. Key observations from this body of work include:

- Flight-test data should be translated from the measurement location at the engine face to the AIP location.
- Effort should be made to use an inlet rake in wind tunnel and flight test having the same rake geometry (rake angles and probe radial locations).
- The inlet rake should use total-pressure probes having an length-to-diameter on the order of ten, as opposed to placing the transducers in recessed areas on the leading edge of inlet guide vanes.
- RMS turbulence values should be determined digitally with the cutoff frequency recommended by the engine manufacturer.
- Wind-tunnel models should account for the engine bullet nose to improve predictions.
- Special care should be taken to assure that the thermal effect and/or other effects like zero shift on each pressure measurement are properly accounted. Vigilant data analysis will assure these instrumentation and calibration errors do not propagate into the final inlet compatibility evaluation. Pressure instrumentation available today, if properly implemented, should eliminate these problems (e.g., thermally-controlled environment for pressure transducers).
- Although flight-test analysis combines steady-state and dynamic pressures to calculate recovery and distortion, care should be taken to eliminate any time lag associated with steady-state pressure transducers caused by using varying line lengths. These differences may contribute to discrepancies between wind-tunnel and flight-test results.
- Filter instabilities were seen in the initial flight-test digital-filtering algorithms that were used to filter the high-response total-pressure measurements. This issue could have been addressed early in the inlet/engine development cycle (well before initiation of flight test) if the analysis software used was common (other than for scale factors) between test phases or was validated earlier in the inlet/engine development process.

- There is continuing debate over whether steady-state-pressure accuracy is improved by using smaller-range differential-pressure transducers with a varying reference pressure as opposed to slightly larger-range absolute transducers. It appears that the instrumentation capabilities have improved to the point that, for a well designed and maintained system, the latter scheme may provide sufficiently accurate data.

- A final lesson learned relates to screening the dynamic data for maximum distortion levels and determining RMS turbulence values. To put things in perspective, the high-response, subscale wind-tunnel data were acquired on the airframe-manufacturer's dynamic-data analysis system in the early 1990s, and four or five generations of computer processors and storage media had come and gone prior to initiation of inlet compatibility flight testing. During that same time, improvements were made to the fan and compressor hardware, and the fan and compressor stability margins and sensitivities to total-pressure distortion were better defined. As a result, the majority of the wind-tunnel data were screened during one-second test runs using only minimum F119 fan or core-stability-margin screening parameters. Flight-test data were screened on minimum-stability-margin remaining points, but these points had changed due to aerodynamic revisions in engine hardware. Flight-test data were also screened on worst-case circumferential and radial distortion; however, due to computing limitations in the wind tunnel, raw wind-tunnel data were not saved making it impossible to reprocess with additional screening parameters. Consistent screening parameters are required between wind-tunnel and flight test if model-to-full-scale correlations will be performed.

- Additionally, due to limited data-storage abilities during the wind-tunnel testing, raw high-response pressure data were not retained. As a result, RMS turbulence values could not be recalculated when it was determined that the RMS meters used during wind-tunnel testing had significantly different frequency cutoff characteristics.

- Based on the results of this case study, it is recommended that data processing tasks associated with inlet/engine compatibility testing be further automated to make the analysis more consistent between test phases. As can be seen, errors due to instrumentation calibration, filter stability and cutoff characteristics, as well as screening techniques, can result in similar test efforts ending up with non-comparable data. No matter what techniques are employed to make the sub- and full-scale data analyses more common, deliberate steps must be taken to assure the comparability of sub-scale wind-tunnel and full-scale inlet/engine compatibility test and evaluation programs and thus improve the data reliability and confidence.

- It should be both possible and cost effective to reduce the scope of the inlet-performance and inlet-engine compatibility portion of future flight-test programs to in-flight survey approaches, similar to that used during the F-22 flight-test effort. However, since the wind-tunnel distortion under-predicted flight-test distortion indices by 20 to 40 percent at higher Mach numbers, additional care should be taken to assure that inlet/engine compatibility has been demonstrated prior to considering developmental testing complete.

5.2 Case Studies Offering Key Observations

The case studies presented in the previous section offered insight into correlating inlet performance from wind-tunnel to flight-test results. There have been a number of other aircraft programs that did not provide wind-tunnel to flight correlations but still provided key lessons relating to using dynamic distortion in conducting inlet/engine compatibility assessments. Lessons from these programs are presented in this section.

5.2.1 F-16 Case Study

No high-response total-pressure rake data at the AIP were gathered during flight tests of the F-16 with production inlets. Thus, model-to-full-scale comparisons could not be made. However, the initial predictions of possible flight-test compatibility problems based on inlet model tests and engine tolerance to distortion were quite accurate. Stalls were encountered, as expected, during throttle transients in the upper left-hand corner of the flight envelope. Subsequent engine configuration and control system changes solved the problems.

There are two examples of correlation of model-scale data to flight-test data related to inlet buzz (planar wave instabilities) that are worth noting. These examples are discussed below.

5.2.1.1 Flight-Test Nose Boom

During flight testing of a change in the engine control-system logic for the F110-GE-129 engine, an unexpected incident of inlet buzz was encountered. The engine control was intentionally switched to the secondary control mode at a supersonic Mach number. The available wind-tunnel data indicated that no inlet buzz should occur even though the airflow would decrease. Significant buzz did occur at a higher airflow than expected.

Previous F-16 experience had indicated good correlation between buzz characteristics (freguency and amplitude) of the wind-tunnel scale-model and full-scale vehicle even though the wind-tunnel model did not acoustically duplicate the presence of the engine at the AIP with full fidelity (the choke plane was further aft than the effective location in the engine).

Because this buzz situation was unacceptable for a production aircraft, additional wind-tunnel testing was initiated to determine the cause of the unexpected inlet buzz. The cause was determined to be the use of the flight-test nose boom on the F-16 in the testing at Edwards AFB as opposed to the production nose boom. The added length of the flight-test nose boom caused increased thickness of the boundary layer on the aircraft lower surface near the center-line plane. This caused inlet buzz at a higher airflow than expected. The details of the investigation are well documented in Reference 2.2.27.

5.2.1.2 Total-Temperature Probes Ahead of Inlet

During the testing of the F-16 with Conformal Fuel Tanks at Eglin AFB, another incident of unexpected inlet buzz occurred. In this case, the aircraft was attempting to accomplish loads and control-system response tests at maximum dynamic pressure (test points on the right-hand side of the flight envelope). The sequence was to dive from high altitude (above 36,089 feet) to the maximum “q” point at a lower altitude. Because of the increase in ambient temperature at the lower altitude, the engine corrected airflow decreases at a constant power setting—maximum A/B, in this case. Based on previous flight testing and available inlet wind-tunnel-test data, this decrease in airflow should not cause inlet buzz. As the aircraft approached the desired test point, an aircraft “vibration” occurred. Because inlet buzz was not predicted, several other possible causes were investigated.

After several attempts at the test point with similar results, further discussions about the aircraft configuration ensued. In these discussions, it was discovered that, at Eglin, a camera to photograph external store separation was mounted in the location on the F-16 where the production total-temperature probe was normally located. The production probe was relocated on the test aircraft to a location about 18 inches ahead of the inlet along with a similar total-temperature probe used for test data. These probes have struts with a thin diamond cross section leading to a converging channel between the probes. This causes a normal shock, at supersonic speeds, ahead of the probe combination. It was speculated that this normal shock caused local boundary-layer separation that combined with the usual boundary-layer separation caused by the inlet normal shock at lower airflows, resulting in buzz at a higher airflow than normal.

This discovery occurred at the same time that an F-16 inlet model, Figure 56, was being tested at NASA Glenn at supersonic conditions. Taking advantage of this opportunity, total-temperature probes were fabricated and tested at this location on this model. The test data are presented in Figure 57. Note the slight increase in the buzz parameter, Sum40, starting at a corrected airflow of 195 pounds per second (pps). The level of the buzz parameter at the “slight increase” is below the level of 0.02 that is usually used as the buzz onset value. It is possible that this level of “buzz” would not be detected in flight at a low “q” condition, but at the high “q” condition it becomes noticeable. The buzz parameter stays at this slightly increased value until the usual large increase occurs. Based on this result, the total-temperature probes were relocated. No “vibration” was encountered at the desired test condition in subsequent flights, and the test program was able to continue. The overall Conformal Fuel Tank Test program including this incident is reported in Reference 2.2.28.

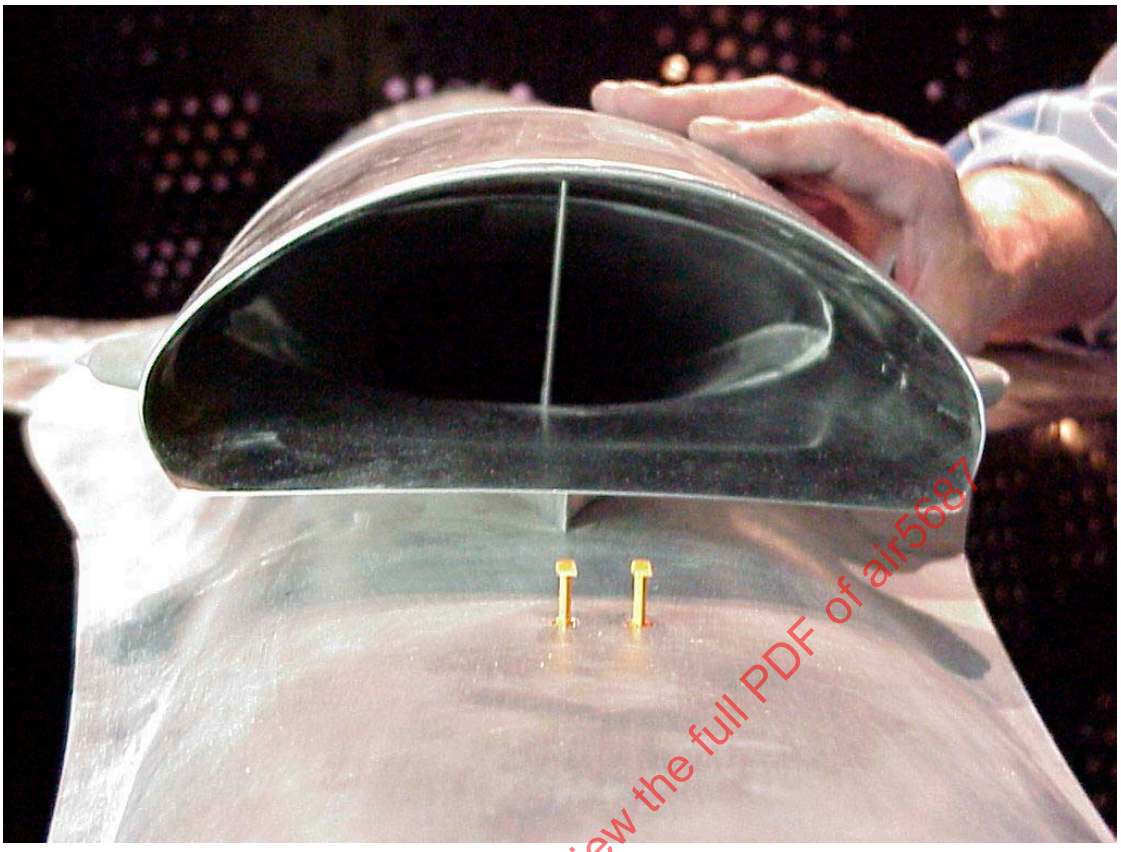

FIGURE 56 - F-16 INLET MODEL WITH SIMULATED PROBES

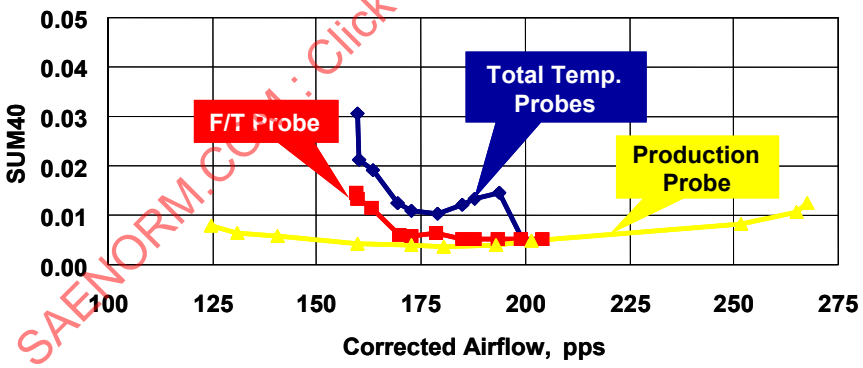

FIGURE 57 - F-16 INLET BUZZ TEST DATA

Several key lessons may be obtained from these experiences. Geometric similarity (e.g., for protuberances such as total-temperature probes or the difference between flight-test and production nose booms) must be maintained between the wind-tunnel model and the full-scale vehicle when using the wind-tunnel database. Additionally, these experiences highlight that planar wave instabilities are sensitive to boundary-layer properties.

5.2.2 B-2 Case Study

The B-2 air-induction system configuration is the result of an extensive inlet development program that included inlet/engine compatibility (IEC) and performance validation activities involving inlet/airframe wind-tunnel testing and analytical modeling (Reference 2.2.29). This was paralleled by the F118-GE-100 engine development program that included inlet-distortion-screen ground-engine testing. Before flight test, the results of these activities culminated in the successful completion of a comprehensive inlet/engine stability audit. “Classical” inlet/engine compatibility was established by the prediction of unrestricted engine throttle capability throughout the operational flight envelope of the B-2 following the guidelines outlined in SAE ARP1420 and AIR1419.

The B-2 inlets are integrated into the upper wing surface aft of the wing leading edge. Each inlet supplies flow to two engines. The main aperture is sawtooth shaped, has a sharp-lipped cowl, and blends into the upper wing surface at sharply angled inboard and outboard corners. The diffuser duct is highly offset, turning sharply down into the fuselage just aft of the main inlet aperture, where it bifurcates to supply flow to the inboard and outboard situated engines.

A diverter slot is incorporated into the lower surface just forward of the inlet and serves to remove low-energy boundary-layer flow developed over the wing upper surface aft of the leading edge. Flow through the diverter slot is diffused and channeled to various internal circuits collectively known as the secondary airflow system (SAFS).

During low-speed and ground operations, flow to the engines is augmented by four engine auxiliary-inlet doors (EAID) located on top of the inlet cowl and just forward of each engine face. Operation with the EAIDs open reduces the main inlet mass-flow ratio and hence, the associated sharp-lip turning losses. Total-pressure recovery to the engines is raised and inlet pressure-distortion levels are lowered, thus improving performance in low Mach flight regimes, particularly during takeoff.

5.2.2.1 Inlet/Airframe Model

The B-2 inlet/airframe integration model was tested in the mid-1980s at the AEDC's 16T wind-tunnel facility several times throughout the development cycle. The model was tested over a wide range of Mach numbers, angles-of-attack, angles-of-sideslip, and engine airflows that encompassed the vehicle and engine operating envelopes. Parametric diverter flow effects, particularly at maneuvering conditions, were also investigated. In addition, effects of asymmetric power settings, engine-out or windmilling conditions, and inlet low-flow planar-wave boundaries were examined. The auxiliary-inlet door system (for takeoff and landing) was also simulated and tested over its operating envelope.

The model was 12% scale and employed a 40-probe array of steady-state and dynamic pressure instrumentation at the aerodynamic interface plane. The primary factors considered in determining model scale were (1) required wingspan to provide the correct upper-wing flowfield to the inlet system, (2) wind-tunnel blockage consideration at maneuvering conditions in the AEDC 16T facility, and (3) AIP diameter large enough to install the array of required dynamic probes without significantly altering the local AIP flowfield. The key factor, required wingspan, was determined primarily from test experience with a smaller-scale inlet/airframe integration development model that was tested in the NASA Langley 16-foot Transonic Tunnel. In this earlier model, which was 8% scale, different wingspans were tested to assess their impact on inlet flowfield and inlet performance.

Only the left-hand inlet system was simulated on the AEDC model. This was based on test experience with the aforementioned NASA model. Analysis of the impact of left-hand inlet-mass-flow ratio effect on static pressure instrumentation from aircraft centerline to the right-hand inlet location saw little or no effect, therefore concluding there was little or no coupling of the left-hand/right-hand inlet flowfields. Once the decision was made that a right-hand inlet system was not required, the local geometry needed to be shaped to simulate the right-hand inlet flowfield. Related to the issue of flowfield simulation on the AEDC model was the performance of air-data-system sensor ports, particularly, the effect on inlet-mass-flow ratio. Data analysis showed little discrepancy between the inlet model with the truncated wing and the full-span smaller aero model, which suggests the flowfield simulation on the inlet model was fairly accurate.

The height of the boundary-layer diverter system on the AEDC inlet/airframe integration model was increased to account for the relatively thicker boundary layer on the scale model with the test Reynolds number. The adjustment was based on comparing boundary-layer conditions at a high-altitude/high-speed operating condition. The diverter height on the smaller scale NASA model was also adjusted to account for the model- to full-scale boundary-layer thickness discrepancy.

As previously mentioned, the SAFS boundary-layer diverter system of the B-2 consists of various internal circuits. The wind-tunnel-model internal circuits did not model the internal circuits of the air vehicle due to the complex geometry of the system. The simplified wind-tunnel model used two flow plugs to control mass flow and dumped the flow into a plenum. Because of wind-tunnel test matrix constraints, only limited high-percentage SAFS airflow sweeps were tested. As a result, flow phenomena for low or no SAFS airflow was missed, and this had a tremendous effect on inlet distortion.

Two calibrated flow plugs were used to set engine airflows in the left-hand-inlet systems. Additional calibrated flow plugs were used to set the airflow in the diverter system. High-pressure ejectors downstream of the flow plugs allowed testing of the model at AEDC over the total flight envelope including the static condition.

5.2.2.2 Flight Test Experience/Inlet Distortion

Propulsion flight tests with 40 steady-state and 40 high-response pressure probes located at the AIP of each inlet and instrumented engines on the left side of Air Vehicle 2 (AV-2) began in January 1993 with propulsion system performance and distortion survey testing. Early in testing, higher than predicted levels of inlet distortion (relative to wind-tunnel test results) were measured at various conditions within the flight envelope. This began a long period of extensive flight test and data analysis to determine the cause of the elevated distortion levels, reassess the engine distortion-handling capabilities, and evaluate the overall effect on B-2 system capability.

During flight test of AV-2, elevated distortion levels were measured at extreme attitudes that approached the B-2 angle-of-attack limits. The source of the high distortion was traced to the occurrence of flow separation on the wing surface forward of the inlet at high angles of attack and off the sharp lip of the outboard cowl with windward sideslip. This drives a “break” in inlet performance manifested by an abrupt increase in steady-state and dynamic distortion and inlet turbulence (see Figure 58). A major factor driving this characteristic was a lower than predicted SAFS pumping performance, which resulted in diverter flows below the range tested during inlet wind-tunnel model testing. As a result, the inlet “break” behavior was not evident before flight test. However, the risk associated with the SAFS design was recognized during early developmental testing of the ECS system. These test results led to design improvements in the SAFS that were incorporated into the B-2 aircraft beginning with AV-3 (modifications were identified too late to affect the first two air vehicles).

Although AV-3 and subsequent vehicles were not fully instrumented, analysis of engine data at high angles of attack has shown that the improved SAFS substantially improved inlet performance by delaying the inlet “break” to higher angle-of-attack conditions. All propulsion compatibility flight testing, however, was conducted on AV-2, which has the original SAFS design. Although no adverse engine behavior was experienced during inlet breaks on AV-2, a caution was established for all aircraft corresponding to the AV-2 angle of attack of the inlet break. This angle-of-attack boundary is a function of Mach number and is indicated to the pilot by the aircraft angle-of-attack indicator.

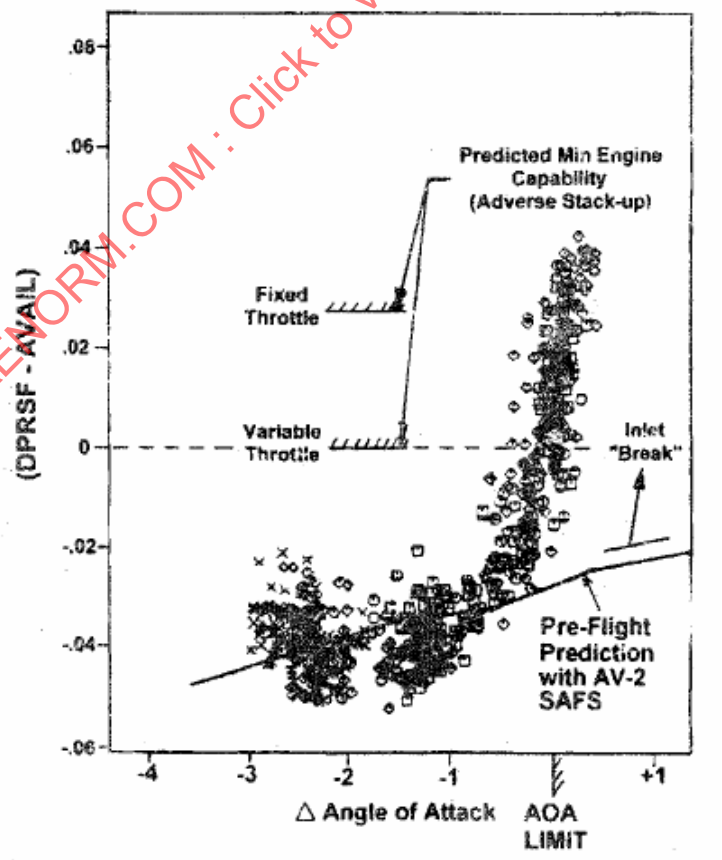

FIGURE 58 - EFFECT OF INLET BREAK ON CONSUMPTION OF FAN STABILITY PRESSURE RATIO

5.2.2.3 Summary and Conclusions

The evaluation of B-2 inlet/engine compatibility included the analysis of AV-2 IEC flight data as well as the demonstration of stall-free operation with several of the flight-test-aircraft extreme speed, altitude, angle-of-attack, and angle-of-sideslip conditions. During B-2 propulsion flight testing, an extensive body of inlet-distortion data was recorded and processed using classical engine-operability analysis methods. The results correlated with the wind-tunnel results at nominal conditions. However, at extreme aircraft angles-of-attack and angles-of-sideslip, in the “high” Mach regime, flight-measured inlet distortion and turbulence significantly exceeded levels measured in the wind tunnel. This was attributed to the loss of effectiveness of the SAFS (particularly in AV-2), resulting in inlet boundary-layer separation leading to extreme inlet distortion and turbulence. Under these conditions, the standard stability-audit approach failed to predict stable engine operation while under the conditions of large distortion and turbulence levels that were outside of the engine manufacturers’ distortion methodology, where flight tests repeatedly demonstrated stall-free engine operation with both fixed and variable throttle.

It is also important to emphasize that the lack of secondary airflow sweep testing played an important part in not determining the true flow phenomena for low or no SAFS airflows. These flow phenomena had a tremendous effect on inlet/engine distortion characteristics. As B-2 full-scale development progressed, it became apparent the SAFS was not operating as expected. By eliminating a few wind-tunnel test points, the program paid a heavy price in future years.

6. SIMILARITIES AND TEST TECHNIQUES

The following sections discuss methods of similarities and relevant test techniques with the goal of producing test and computational data that are representative of full-scale flight vehicle performance. This information incorporates lessons learned based on the case studies as well as current recommended practices.

6.1 Geometric Similarities

The question of accuracy in the approach outlined in ARP1420 consists of two separate issues:

a) Assessing the accuracy of the scaled-inlet-model wind-tunnel test in representing the engine-face spatial and time-dependent distortion of the full-scale vehicle in flight.

b) Determining the accuracy of the fan/compressor stability assessment as a function of distortion at the AIP in the true flight environment.

This document deals primarily with the first issue: wind-tunnel model- to full-scale correlation. Sources of error include mismatches in freestream conditions (Mach number, wind-tunnel turbulence, and Reynolds number), model geometry, angles of incidence, model primary- and secondary-flow rates, instrumentation, and data reduction. Several sets of data comparing model- to full-scale inlet distortion are available to make this assessment and were discussed in Section 5.

6.1.1 Moldline and Scaling

Acquisition of representative subscale data is predicated on accurate geometric scaling of the full-scale vehicle external and internal inlet duct contours—the outer and inner moldlines—with exceptions discussed below. Foresight in the choice of the scale and the configuration of the inlet model will result in large dividends in subsequent analysis and when comparing with full-scale data. Modeling techniques and guidelines discussed in the subsequent sections are used to achieve high-quality, consistent data from the subscale model.

6.1.2 Subscale Model

Wind-tunnel tests of subscale models are used to acquire data that validate the designs of air vehicles during their development cycle. Subscale inlet models can be used to provide adequate data to characterize inlet performance. Scale models are usually used early in program development and are modified and retested as the design progresses to a final configuration. Candidate designs are often evaluated with CFD to assess and refine the initial configuration before progressing to the wind tunnel.

Selection of the scale for a wind-tunnel model is influenced by several, sometimes competing, criteria. Typically, an inlet/airframe model is built as large as possible to allow the most accurate representation of the vehicle geometry. The process of scale selection begins with establishing the desired range of the test parameters: Mach number, q (dynamic pressure), AOA (angle of attack), AOS (angle of sideslip), inlet mass flow, and so on. Once these ranges are identified, existing hardware such as AIP instrumentation arrays, flow plug assemblies, and propulsion simulators (e.g., turbines and ejectors) is considered. Existing test hardware often is used to save the time and cost associated with designing, building, and calibrating new hardware. Other important factors in scale selection are the capabilities and blockage limitations of the test facilities that are under consideration. Scale selection due to blockage is influenced by the amount of the vehicle that needs to be simulated, the model angles of attack and sideslip required, the mass flow exiting the ejector, and the size of support system hardware and ejector/vacuum system apparatus.

Integrated airframe-inlet testing adds complexity to the scaling issues because the airframe influences the local inlet flowfield, resulting in significant changes to the inlet performance and operability characteristics. At all speed regimes, the vehicle forebody will produce variations in local Mach number and flow angularity at the inlet entrance. Moreover, the vehicle forebody develops a boundary layer that, depending on the design, may or may not enter the inlet. Inlet models should accurately represent the vehicle external moldline for those surfaces that influence the inlet flowfield. Computational methods may be used to make this determination provided internal inlet surfaces are accurately reproduced up to the AIP.

The model should be capable of accommodating design variations with adequate fidelity while maintaining structural integrity and shape. Parametric variations may include, but are not limited to, interchangeable lip shapes and variable geometry components (e.g., compression ramps, bleed doors, and auxiliary inlets). The parametric variations should be sufficiently broad to accommodate changes that may occur up to final moldline freeze.

The scale should be large enough to model any aircraft components that could have an effect on inlet performance. Some of the features and protuberances that should be considered for modeling are antennae, landing gear, gear doors, weapon bay doors, pylons, stores, air data probes, flight-test boom, refueling probe, wing slats/flaps, secondary inlets, engine nose cone, and vent exhausts. Some of these may be present throughout the flight regime; others may be only deployed during specific flight segments

Subscale models by their nature necessarily involve compromises in their ability to faithfully reproduce some features of the full-scale vehicle. An aerodynamic aspect needing consideration is boundary-layer growth and simulation of devices used for boundary-layer removal or control. For vehicle configurations with boundary-layer diverters, the diverter standoff height may need to be altered in the model to maintain proper boundary-layer characteristics relative to the inlet. At the lower Reynolds numbers of the subscale test, the forebody boundary layer will be proportionately thicker than full scale. The model diverter may be designed with more offset relative to the full-scale geometry in order to capture a larger portion of this thicker boundary layer. Thus, the flow entering the model inlet has the same ratio of diverter height to boundary-layer thickness as the full-scale aircraft. Some examples of diverter height scaling are given in the Case Studies, Section 5 (RA-5C, F-15, F-18E/F). However, it should be noted that the diverter can be scaled for only one condition, and at other conditions may be nonrepresentative.

Some configurations have removed the diverter from the design (the diverterless inlet, Reference 2.2.30). The test results must rely on extensive model- to full-scale corrections to achieve full-scale integrated airframe-inlet performance and distortion characteristics. These corrections would follow from extensive Reynolds number variation data acquired during the test; CFD analysis may also be considered. For diverterless inlet configurations, testing in high Reynolds number facilities is an option to be considered.

In addition to the thicker forebody boundary layer, testing at low Reynolds number will delay transition. An airframe-inlet configuration designed to operate with turbulent boundary layers in full scale will often exhibit major transonic/supersonic stability problems if the scale model boundary layer is laminar. To promote earlier transition in the model, boundary-layer tripping techniques should be considered. This is accomplished by applying nonscale roughness to the model surface in the form of grit or its equivalent (References 2.2.31 to 2.2.33). Even if the boundary layer is tripped to turbulent, the growth rate will still be larger than full scale. As was discussed above, the diverter offset height may need to be adjusted in the scale model. Techniques for boundary-layer tripping, such as epoxy dots, are described in Reference 2.2.34.

While geometric accuracy is desired, as features become small, they are more difficult to reproduce in subscale models. Overall outer moldlines are easy to duplicate, but details such as leading edge radii, boundary-layer bleed holes, and bleed plate thickness may be difficult to replicate in small scale. Even though the bleed-hole diameter and plate thickness may be difficult to simulate, the porosity of the perforated boundary-layer plate (screen) may be simulated.

The environmental control system (ECS) and other secondary flow systems should be modeled. As a minimum, the apertures should be accurately simulated. ECS systems should include flow metering devices so ECS flow may be varied as a test parametric. Testing of secondary flow systems should cover the full flow capability, including the range of intended operation. Depending on test requirements, it may be necessary to model most or all of the secondary ducting. During early development, boundary-layer bleed system ducts can be modeled in such a way that the flow through them can be varied to optimize the bleed system sizing. During later testing, when the inlet system is more developed, the internal bleed passages can be accurately modeled and routed to the exhaust location on the outer moldline of the model.

Surface finish is difficult to duplicate in model scale. Typical wind-tunnel models are made of aluminum and steel alloys, and more recently of stereolithography plastic. The general practice is to polish the surfaces to an acceptable surface roughness/waviness based on experience. However, the complication of instrumentation, assembly fasteners, steps, and gaps leave surface irregularities that proportionally exceed full-scale tolerances. Such features are usually smoothed with a filler material. Steps and gaps can generally be smoothed to a level consistent with the final step and gap criteria of the full-scale production vehicle.

6.1.3 Full-Scale Wind Tunnel Hardware

Some development programs choose to perform full-scale inlet/airframe testing with operating engines and/or with metered engine flow simulation devices (sometimes called cold pipe testing) similar to those used in subscale testing. This type of testing is performed primarily for risk reduction and developing subscale to full-scale correlations and is mostly used to acquire static and limited-maneuvering performance data and to optimize ramp and bleed scheduling. The amount of the vehicle that can and should be simulated in the tunnel varies greatly with the type of vehicle being tested (missile or aircraft). Tunnel blockage concerns and the apparatus needed to remove engine exhaust limit the angle of attack and angle of sideslip range relative to that achievable with the subscale model. Because the model is built to full scale, the manufacturing tolerances on such aspects as waviness, surface roughness, steps, gaps, and leading edge sharpness can be faithfully reproduced. Even in full-scale ground tests, boundary-layer simulation remains an issue that needs to be addressed due to lower Reynolds numbers and model completeness. Frequently full-scale complete forebodies introduce excessive blockage that restricts tunnel flow and, hence, desired test range capability. Therefore, forebodies may be required to be truncated and shaped differently from the real production fuselage (Figure 59) although they still must provide representative flow. Also, tunnel limitations may render actual flight Reynolds number unachievable for flight regimes of interest. This would make the boundary-layer growth on the model forebody different from that of the flight vehicle. Full-scale testing of large inlets was conducted in the 1970s; it is now more likely to be performed for missiles.

MSG07-053206-148
AIR5687

FIGURE 59 - FULL-SCALE F-15 INLET WITH MODIFIED FOREBODY